UNIVERSITY OF THE WITWATERSRAND

MASTERS DISSERTATION

A Study of Toeplitz Decorrelation Techniques for Direction of Arrival Estimation of Coherent Sources

---

Author:

Frans Shiwovanhu SHAFUDA

A dissertation submitted in fulfillment of the requirements for the degree of Master of Science in Engineering

in the

School of Electrical and Information Engineering

February 2019

Declaration

I, **Frans Shiwovanhu Shafuda**, declare that this dissertation titled, "**A Study of Toeplitz Decorrelation Techniques for Direction of Arrival Estimation of Coherent Sources**" and the work presented in it are my own. I confirm that:

- This work was done wholly or mainly while in candidature for a research degree at this University.
- Where any part of this thesis has previously been submitted for a degree or any other qualification at this University or any other institution, has been clearly stated.
- Where I have consulted the published work of others, this is always clearly attributed.
- Where I have quoted from the work of others, the source is always given. With the exception of such quotations, this dissertation is entirely my own work.
- I have acknowledged all main sources of help.

Signed:

Date: 07 February 2019

UNIVERSITY OF THE WITWATERSRAND

Abstract

Engineering and the Built Environment
School of Electrical and Information Engineering

Master of Science in Engineering

A Study of Toeplitz Decorrelation Techniques for Direction of Arrival Estimation of Coherent Sources

by Frans Shiwovanhu SHAFUDA

Supervisor(s): Prof. Anton VAN WYK, Mr. Andre MCDONALD and Prof. Jaco VERSFELD

The Direction of Arrival (DOA) is one of the features of propagating waves that is of interest in sensor array signal processing. Applications such as direction finding and source location make use of DOA estimation. A number of DOA estimation methods have been developed over time with special focus on achieving high resolution performance. Subspace-based, also known as eigenstructure-based; methods such as Multiple Signal Classification (MUSIC) and Estimation of Signal Parameters via Rotational Invariance Techniques (ESPRIT) are amongst the excellent and widely applied methods for DOA estimation. However, the performance of these methods is highly degraded in the presence of coherent or highly correlated incident sources caused by multipath propagation and electronic jamming. Conventional techniques such as spatial smoothing have been introduced to better the performance of these methods by removing correlation between coherent sources. However, this is attained at the expense of reduced array aperture (degree of freedom) and increased computational complexity. Of late, a variation of decorrelation techniques based on Toeplitz matrix theory gained much interest in overcoming the drawbacks of conventional decorrelation techniques. Based on a narrowband signal propagation model and a Uniform Linear Array (ULA) in the presence of white additive Gaussian noise, this study carried out an algebraic analysis of two Toeplitz decorrelation techniques. These are, the correlation Toeplitz (CTOP) and the average Toeplitz (AVTOP) decorrelation techniques. The techniques were studied for DOA estimation of coherent sources in conjunction with the MUSIC algorithm. The goal of the study is to provide an understanding of how and why these techniques work. Through the algebraic analysis the study found that, DOA information is perfectly preserved during decorrelation when retained as sums of individual sources of information (i.e. in a superposition form). This explains why the CTOP technique perfectly decorrelates coherent sources unlike the AVTOP technique. This is because decorrelation based on the CTOP technique retains superimposed sources' DOA information. Based on the assumption that the exact signal plus noise array covariance matrix is known, the MUSIC algorithm was applied algebraically in order to validate the findings from the analysis. A maximum of four array elements and three coherent narrowband sources were considered. The algebra becomes intractable when the ULA elements are more than four. The algebraic results have further shown that when the exact array covariance matrix is known, the noise variance has no influence on DOA information and DOA information can be accurately obtained using the MUSIC algorithm. Numerical simulations were also conducted in order to confirm the superiority of the CTOP decorrelation technique. Through numerical experiments, the performance of these techniques was evaluated in terms of Root Mean Square Error, standard deviation and probability of success in DOA estimation. The performance of the classic MUSIC algorithm was also evaluated to serve as a baseline for comparison. Regardless of the coherence among the sources, the CTOP MUSIC (CTOP technique applied in conjunction with the MUSIC algorithm) returns more accurate estimates even at low levels of SNR and minimum number of array sensors. The study has been able to provide an understanding of the working principles behind the two Toeplitz decorrelation techniques.

I dedicate this to my family and friends

for their support and encouragement during the entire duration of my study.

Acknowledgements

I would like to thank my main supervisor **Prof. Anton Van Wyk** for his mentorship, moral support and for giving me the opportunity to work under his supervision. Thank you for guiding me and steering my work into the right direction. I have learnt so much from you both academically and socially. I would also like to thank my co-supervisors **Mr. Andre McDonald** and **Prof. Jaco Versfeld** for their support and contribution to my work. To the support staff, academic staff and postgraduate students of the School of Electrical and Information Engineering, I acknowledge your good team work. Your support and friendliness made me feel welcome and being a part of you. I would like to thank my friends and family for believing in me. Finally I would like to acknowledge the full financial support of the **South African Radio Astronomy Observatory** (SARAO), which is a facility of the National Research Foundation, an agency of the Department of Science and Technology. I am very much grateful for your funding towards my studies at the University of the Witwatersrand.

Contents

List of Figures

List of Tables

Abbreviations

DOA	**D**irection **o**f **A**rrival
MUSIC	**Mu**ltiple **Si**gnal **C**lassification
CTOP	**C**orrelation **Toep**litz
ESPRIT	**E**stimation of **S**ignal **P**arameters via **R**otational **I**nvariance **T**echniques
AVTOP	**Av**erage **Toep**litz
AWGN	**A**dditive **W**hite **G**aussian **N**oise
EM	**E**lectro**m**agnetic
FSS	**F**orward **S**patial **S**moothing
FBSS	**F**orward conjugate **B**ackward **S**patial **S**moothing
BSS	**B**idirectional **S**patial **S**moothing
SNR	**S**ignal to **N**oise **R**atio
SINR	**S**ignal to **I**nterference-plus-**N**oise **R**atio
ULA	**U**niform **L**inear **A**rray
SVD	**S**ingular **V**alue **D**ecomposition
DMD	**D**ata-based **M**atrix **D**ecomposition
CVT	**C**ross-correlation **V**ector **T**oeplitz
HPBW	**H**alf **P**ower **B**eam **W**idth
RMSE	**R**oot **M**ean **S**quare **E**rror
PAA	**P**hased-**A**rray **A**ntenna
POS	**P**robability **O**f **S**uccess
CSDE	**C**orrelated **S**ignal **D**irection **E**stimate
DPE	**D**ifferential **P**hase **E**stimation

Publications

A paper in progress titled "**Algebraic Analysis of Toeplitz Decorrelation Methods for DOA Estimation of Coherent Sources with MUSIC Algorithm**" is being prepared for publication.

CHAPTER 1

Introduction

This chapter presents a brief background of the study, the identified research gap, research question, objectives and significance of the study. The last two sections of the chapter present the scope and delimitation of the study as well as the organisation of this dissertation.

1.1 Background of the Study

The Direction of Arrival (DOA) estimation, also known as direction finding, is a very crucial area of research in phased array signal processing. DOA estimation focuses on the acquisition and tracking of the angle of arrival of signals incident on an array of antennas, transmitted from radiating sources, using sophisticated array signal processing algorithms [1]. The theory of DOA estimation is applied in many areas [2, 3] such as astronomy, biomedicine, seismic event prediction, sonar, radar, wireless communication systems, rescue services and navigation.

Several DOA estimation algorithms have been developed and studied. They are widely classified into four different categories namely, **conventional**, **subspace-based** (sometimes referred to as **eigenstructure based**), **maximum likelihood** and **integrated algorithms** [4]. The most prominent algorithms are MUSIC [5], Root-MUSIC [6], ESPRIT [7], Bartlett and Capon's minimum variance [8]. The MUSIC algorithm, a subspace-based method, is the most studied and has been broadly applied for DOA estimation in applications such as location, radar, sonar and anti-jamming communications due to its superior resolution and stability [9, 10].

Analytical and computer simulation studies have shown that high-resolution DOA estimation methods like MUSIC have the ability to resolve closely spaced sources and are a promising solution to the DOA estimation problem. However, as stated in [11], there are many challenges prohibiting the applications of these methods to practical systems. These challenges include computational complexity and cost, model mismatch, robustness to system errors and higher resolution Signal-to-Noise Ratio (SNR) threshold. A major challenge which this study focused on is degradation in performance due to the presence of coherent (highly correlated) sources often as a result of multipath propagation of emitted signals [12, 13]. A description of coherence and coherent sources is given in Chapter 4.

In this study, the MUSIC algorithm has been used to estimate DOAs. In order to overcome the problems caused by coherent sources such as degrading of resolution and accuracy of subspace-based methods, several decorrelation techniques have been suggested for use as pre-processors of the MUSIC algorithm. These techniques are applied to the received array data before DOA estimation. **Spatial smoothing**, a conventional and popular decorrelation technique has been applied in [14–18] and other studies in literature, as a pre-processor of MUSIC to overcome the problem of coherence.

Spatial smoothing perfectly decorrelates coherent sources. However, the performance of this technique degrades as a result of reduced array aperture. It also increases the computation complexity and cost, simultaneously, it cannot differentiate signals in low SNR conditions [13, 19].

To overcome the drawbacks of conventional decorrelation techniques such as spatial smoothing, alternative techniques employing Toeplitz matrix theory have been proposed in [13, 19–23] and in other studies, for decorrelation of coherent sources. The techniques are known as Toeplitz decorrelation techniques. Decorrelation based on Toeplitz techniques does not reduce array aperture and yields better performance as opposed to conventional techniques.

In order to provide an understanding of the working principle behind these techniques, this study focused on the algebraic analysis of two Toeplitz decorrelation techniques proposed in [22, 23] for decorrelation of multiple coherent sources in conjunction with the MUSIC algorithm. The first technique is correlation Toeplitz (CTOP), a technique based on the reconstruction of a new Toeplitz covariance matrix using correlation sequences of the received coherent data. The second technique uses averages of diagonals of the coherent covariance matrix to reconstruct a new Toeplitz covariance matrix. It is referred to as average Toeplitz (AVTOP) technique.

A derivation of the array covariance matrix based on a DOA estimation scenario of two coherent sources was done. Thereafter, the two Toeplitz techniques were applied for decorrelation. This formed the basis of the analysis and also enabled the researcher to get a better understanding of how these techniques facilitate DOA estimation of coherent sources. The MUSIC algorithm was applied analytically in order to verify the findings from the analysis. Numerical simulations were also done to confirm the performance and superiority of the two techniques. The performance of the classic MUSIC algorithm was also evaluated and used as a baseline for comparison.

1.2 Problem Statement

The performance of the MUSIC algorithm severely degrades in the presence of coherent sources. Various studies in literature have proposed decorrelation techniques [13, 19–23] based on Toeplitz matrix theory, which offer a more promising solution to the coherent source problem. The problem is, many of these studies are numerically based and hence do not explicitly inform the reader about why and how these techniques work. A thorough understanding of the working principles behind these techniques is crucial for implementation in real-life applications.

In order to answer the research question below, this study carried out an analysis of selected Toeplitz decorrelation techniques, namely the CTOP and AVTOP decorrelation techniques [22, 23].

1.3 Research Question

- *What are the intricacies of the mathematics and working principles behind the CTOP and AVTOP decorrelation techniques?*

The following aspects about the selected techniques are investigated in order to find a solution to the research question above.

(a) How source DOA information is retained during Toeplitz matrix reconstruction without introducing spurious information.

(b) Why CTOP decorrelation technique results in better accuracy in DOA estimation than AVTOP decorrelation technique.

(c) The influence of noise power (variance) on DOA information.

1.4 Objectives

Overall objective:

- To carry out an algebraic analysis in order to develop an understanding of the working principles behind the selected Toeplitz decorrelation techniques.

Specific objectives:

(a) Derive the expression for an array covariance matrix based on a coherent DOA estimation scenario.

(b) Algebraically apply CTOP and AVTOP decorrelation techniques and analyse the resultant matrices.

(c) Develop an approach for applying the MUSIC algorithm analytically in order to verify the findings obtained from the analysis.

(d) Numerically evaluate the estimation performance of the CTOP, AVTOP and classic MUSIC algorithms.

1.5 Justification of the Study

The study provides an in-depth understanding of the Toeplitz methods, enabling easy use of these methods in real-life applications.

1.6 Scope and Delimitation of the Study

The study is intended to carry out an algebraic analysis of the CTOP and AVTOP decorrelation techniques in conjunction with the MUSIC algorithm. The DOA estimation problem considered is based on a ULA model where sources are assumed to be narrowband and the noise as additive white Gaussian noise. Other types of sources, array and noise models are not considered for the analysis in this study.

Numerical simulations are carried out to confirm the performance of CTOP and AVTOP decorrelation techniques. The classic MUSIC algorithm is used as a baseline for comparison. The numerical simulations are only conducted for scenarios involving coherent sources and non-coherent (mutually independent) sources. The degree of correlation between the sources is equal to one and zero for coherent and non-coherent sources respectively. Scenarios involving partially correlated sources are not critical or relevant for the purpose of the study.

1.7 Dissertation Organisation

The remainder of this dissertation is organised as follows. Chapter 2 presents a review of related work with a focus on eigenstructure-based methods. Chapter 3 outlines basic knowledge of DOA estimation and the approach derived for applying the MUSIC algorithm analytically. Chapter 4 presents a mathematical definition of coherence in a signal processing context. The effect of coherent sources on the MUSIC algorithm and a procedural description of the CTOP and AVTOP techniques are also presented in this chapter. Chapter 5 presents and discusses the results of the algebraic analysis of the CTOP and AVTOP techniques. Chapter 6 presents and discusses the results of numerical simulations carried out to confirm the performance of the two techniques. Chapter 7 concludes the study and recommends the areas of future work. The last part of this dissertation consists of appendices of additional information and the references list.

CHAPTER 2

Review of Related Work

This chapter consists of three sections. The first section covers a review of subspace-based methods and the major challenges encountered in the applications of these methods for DOA estimation. The second presents a review of pre-processing schemes developed to address the challenge of coherence in DOA estimation with subspace-based methods. The third presents a review of studies using an algebraic or analytic approach in analysing DOA estimation techniques.

2.1 Subspace-based Methods for DOA Estimation

2.1.1 Early development

The development of subspace-based methods began with the work of Schmidt in 1981 [24] and Bienvenu in 1979 [25]. These methods attracted a lot of interest because they seem to provide a fundamental approach to the problem of DOA estimation and are a promising solution among all other high-resolution methods [26]. Traditional beamforming based methods like Capon's minimum variance have a limitation in terms of resolution which is a result of the inability to fully utilise the input data model (presented in Section 3.3) structure. Schmidt and Bienvenu were the first to utilise the structure of a more precise data model for sensor arrays of an arbitrary form [4].

Schmidt first solved the DOA estimation problem by developing a geometric solution based on a noiseless case. The geometric concept was then extended to obtain a reasonable approximate solution in the existence of noise. The method developed by Schmidt is known as the Multiple Signal Classification (MUSIC) which is defined in [5]. MUSIC involves determining eigenvectors of the array covariance matrix. The eigenvectors of the covariance matrix can be classified into two groups: the eigenvectors that span the *signal subspace* (signal eigenvectors) and the eigenvectors that span the *noise subspace* (noise eigenvectors). The principle behind MUSIC DOA estimation is the orthogonality between the noise eigenvectors and the incident sources steering vectors. The orthogonality results in a peak in the MUSIC spatial spectrum at an angle corresponding to DOA of the incident source. The MUSIC algorithm has been widely studied since it was introduced [27].

Further modifications to the MUSIC algorithm were proposed to improve its resolution and to reduce the computational complexity. One such modification is the Root-MUSIC algorithm [6]. In Root-MUSIC, the DOA is estimated through the zeros of a polynomial to avoid spectral search of the conventional MUSIC algorithm hence reducing the computational complexity. However, Root-MUSIC is only applicable to uniform linear arrays. Another improvement is called Cyclic MUSIC proposed by Gardner in [28] which exploits the spectral coherence properties of the signal in order to better the performance of the normal MUSIC algorithm.

Other primary contributions to subspace-based methods include the Minimum-norm method by Kumaresan and Tufts [29] and the ESPRIT method proposed by Roy and Kailath [7]. The Minimum-norm constructs a polynomial (with special properties) from eigenvectors of the array data covariance matrix. The zeros of this polynomial give estimates of the DOA of incident sources. The ESPRIT method exploits the rotational invariance in the signal subspace which contains two arrays with a translational invariance structure. The DOAs are directly estimated in terms of eigenvalues instead of a spectrum search.

2.1.2 Challenges

The following are some of the challenges faced in the study of DOA estimation (direction finding) methods, particularly with the high-resolution subspace-based methods.

(a) Mutual coupling effect between array sensors

The DOA estimation methods based on ideal array response models, yield highly biased DOA estimates and results in a degraded performance. This is due to the effect of strong mutual coupling between the array elements. To avoid this, the methods should either be calibrated or modified in order to compensate for strongly interdependent behaviour. Ideal models assume that individual sensors responses can be independently expressed, which in practical sense fails to correctly model the exact response of the array, especially in circular arrays.

Zeytinogul et al. [30] derived alternative models of the array response based on array geometry and sensors electromagnetic features and calibrated DOA estimation models using the array output generated by these models. Two models were developed for a circular array, taking mutual coupling into consideration, based on the following two scenarios:

(a) The array operating above lossy ground.

(b) The array operating in free space.

The models developed based on the two scenarios above are referred to as the *lossy ground* and *free space* models. The simulated array response data from these models was then used to calibrate the MUSIC algorithm. The performance of MUSIC was evaluated in the presence of mutual coupling, and the results have shown that the calibrated MUSIC algorithm exhibits exemplary performance levels in resolving the DOA of incident sources as compared to the non-modified MUSIC algorithm.

Similar work can be found in [31–34] and many other studies done on DOA estimation algorithms in the presence of mutual coupling. Different array response models and approaches to compensate the effect of mutual coupling have been the focus of many studies.

(b) Model mismatch

In most DOA estimation applications it is assumed that the transmitting sources are situated in the array's far-field region. This assumption is only valid when the condition $d > \frac{2D^2}{\lambda}$ is satisfied, where d is the distance between the array and signal sources, D is the antenna array dimension and λ is the wavelength of the signals [35].

The far-field assumption forms the basis of most DOA estimation array models. However, signal reflections in the near-field of the antenna array are also received. As the distance of these reflections get nearer to the antenna array, the array model of these reflections differ from the far-field array model. When the source is in the near-field where the condition $d < \frac{2D^2}{\lambda}$ is satisfied, the EM waves received at the array are spherical and not plane waves as for the far-field assumption ($d > \frac{2D^2}{\lambda}$).

Elbir [36] investigated the difference between the far-field and near-field array models based on a particular ULA DOA estimation scenario. The difference was obtained by computing the norm difference of the near-field and far-field array steering vectors for different transmitter range, d, values. The results have shown that as the source distance d increases, the difference between the models decreases and the near-field array model converges to the far-field array model. For values of d less than $\frac{2D^2}{\lambda}$ the difference between the two models is very large resulting in a model mismatch between the two array models.

(c) Multipath

Another source of errors in DOA estimation applications with subspace-based methods is the multipath propagation of the source signal due to reflections from surfaces in the transmission path. The original and reflected signals from the source arrive at the antenna array from different directions. A multipath propagation scenario is shown in Figure 2.1, source [36].

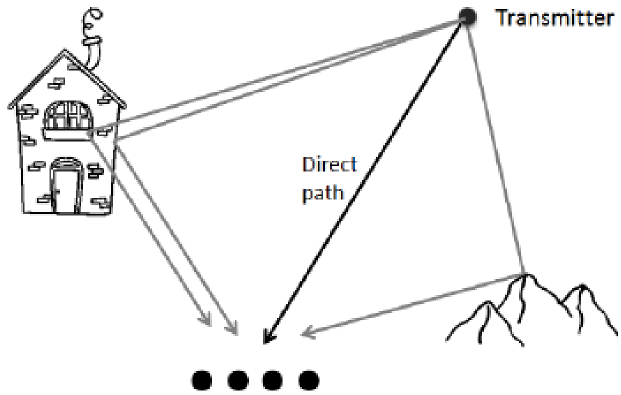

FIGURE 2.1: Multipath propagation.

In a multipath propagation environment, highly correlated (coherent) signals are received at the antenna array [37]. Coherent sources result in failure of several high-resolution estimation methods like ESPRIT and MUSIC. When the received signals are uncorrelated, the signal covariance matrix is non-singular and has full rank. However, when coherent sources exist, the signal covariance matrix suffers rank degradation and becomes singular. As a result, the performance of MUSIC and other subspace-based methods is severely degraded [38].

2.2 Addressing Coherence

To solve the problem of rank deficiency of the signal covariance matrix, a preprocessing technique also referred to as a decorrelation technique is needed to restore the rank. This study focused on pre-processing techniques, specifically Toeplitz based techniques. This section gives a review of several other decorrelation techniques including the Toeplitz based techniques. The following are some of the common techniques applied as pre-processors to DOA estimation methods in order to overcome the effect of coherent sources on DOA estimation.

2.2.1 Spatial smoothing

The Forward Spatial Smoothing (FSS) was first proposed by Evan et al. [39] for the case of a ULA. The purpose of this technique is to overcome the problem encountered in DOA estimation of coherent signal sources. It splits the array into overlapping subarrays and finds the averaged spatially smoothed covariance matrix by taking the mean of the subarray covariance matrices.

The spatially smoothed array covariance matrices are only full rank if the signal covariance matrix is non-singular. This is guaranteed when the number of subarrays is greater than or equal to the number of incident sources. The spatial smoothing technique guarantees the non-singularity property of the signal covariance matrix even when the signals sources are coherent. This is the key to successful DOA estimation with subspace-based methods.

In [40], Shan et al. carried out a complete analysis of the FSS technique and evaluated its performance in conjunction with the MUSIC algorithm. It was shown that it is possible to estimate the DOA of coherent sources irrespective of their degree of correlation.

The drawback of FSS is the reduction in array aperture. An array of M sensors can only detect a maximum of $M/2$ sources compared to a maximum of $M-1$ sources for normal DOA estimation of uncorrelated sources. To circumvent the problem of reduction in array aperture, Pillai and Kwon [41] proposed an improvement to FSS. It has been shown that by splitting the array into both forward overlapping subarrays and conjugate backward overlapping subarrays one can detect up to $2M/3$ sources. The technique is called Forward/conjugate Backward Spatial Smoothing (FBSS) which is also known as Bidirectional Spatial Smoothing (BSS).

Many studies including [10, 17, 42, 43] focused on the modification of the spatial smoothing technique in order to improve its performance in resolving the DOA of coherent sources. However, as stated in [16], spatial smoothing does not succeed in reducing the degree of correlation between sources with finite number of smoothing operations. It only realises rank restoration of the covariance matrix.

This results in the smoothed covariance matrix which is only full rank but not Toeplitz in structure, which degrades the performance of subspace-based methods like MUSIC.

2.2.2 Singular value decomposition

Most solutions to DOA estimation of coherent sources, such as spatial smoothing, are based on the modification of the array covariance matrix. Gao and Bao were the first to propose a method called Data-based Matrix Decomposition (DMD), which is based on Singular Value Decomposition (SVD) of the data covariance matrix [44].

Gao and Bao have shown that the singular-value structure of the data covariance matrix is independent of the correlation between the incident signals. Hence one can determine the signal-subspace via SVD even when the signals are perfectly correlated (coherent). The DMD method has been used in conjunction with MUSIC and has proven to be efficient in resolving the DOA of highly correlated sources.

Like spatial smoothing, decorrelation of coherent sources based on the SVD technique is also attained at the expense of loss in aperture size [45]. The SVD technique loses about half of the number of effective array elements. This results in reduced stability, resolution and a decline in the maximum number of sources that can be estimated [10, 46].

2.2.3 Correlated signal direction estimate

A Masters study by Wen Xu [47], proposed a scheme called Correlated Signal Direction Estimate (CSDE) to address the problem of multipath reflections in bathymetric sidescan sonar applications. The CSDE scheme is used to estimate DOAs and amplitudes of highly correlated signals using a multiple-row bathymetric sidescan sonar system configured in a ULA.

The scheme is specifically derived for a three-row bathymetric sidescan sonar. The derivation of CSDE is an extension of the conventional Differential Phase Estimation (DPE) method studied in [48], which only works for cases with a single directional source. A mathematical derivation of the CSDE estimator enabling resolution of two or more directional sources is fully presented by Wen Xu in his Masters thesis.

The proposed method was compared with the ESPRIT-based approaches for DOA estimation. The simulations results based on different data models and cases with two directional sources have shown that the CSDE method works well for correlated signals conditions in comparison to the ESPRIT-based methods. However its performance is limited in uncorrelated signal conditions. Thus the CSDE estimator derived its name from the fact that it is optimal for highly coherent or temporary correlated signals than for uncorrelated signals.

2.2.4 Toeplitz matrix reconstruction

It is known that, for the ideal case (i.e. when incident signals are not coherent), the received data covariance matrix of a ULA is non-singular and has a Toeplitz structure. However, in practice, due to a limited number of data snapshots, noise and multipath interference; the Toeplitz structure is often lost [46].

Toeplitz decorrelation is carried out to reconstruct a new covariance matrix from the coherent data covariance matrix. As a result, its rank and the non-singularity property are restored. The properties of an ideal covariance matrix are presented in Appendix A.1.2. There are different variations of Toeplitz decorrelation methods, of which some are discussed here.

In order to achieve decoherence, Zhou and Huang [46] used the eigenvectors corresponding to the largest two eigenvalues of the coherent data covariance matrix to construct two new matrices of Hermitian Toeplitz. Thereafter, the ESPRIT method was applied to estimate the DOA of coherent signals. The presented method was named T-ESPRIT. The T-ESPRIT was compared against

SVD-ESPRIT and has shown better resolution and robustness.

Prior to the work of Zhou and Huang, a similar Toeplitz reconstruction technique was proposed in [20] by Hu et al. This technique achieves decorrelation by constructing a new Toeplitz matrix using an eigenvector corresponding to the largest eigenvalue of the coherent data covariance matrix. The technique was applied with the MUSIC algorithm to give DOA estimates of highly correlated sources and it has shown better estimation precision and robustness in comparison to the SVD and spatial smoothing methods. However, this technique can only resolve DOA of coherent sources.

The Toeplitz techniques by Zhou and Huang and Hu et al. are both based on the principle that whether the sources are coherent or non-coherent, the eigenvector corresponding to the largest eigenvalue can be obtained by linearly combining all sources' steering vectors.

Other variations of the Toeplitz technique that do not involve reconstructing a Toeplitz matrix from the eigenstructure of the coherent data covariance matrix are also found in literature. These techniques only involve using the physical structure of the coherent covariance matrix to construct a new and decorrelated Toeplitz matrix.

One Toeplitz technique involves constructing a new Toeplitz matrix using the first row of the coherent data covariance matrix. This approach is found in several independent studies such as the study by Hui et al. [49], Bai et al. [23] and Goian et al. [22]. In all these studies the aforementioned approach is either referred to as cross-correlation vectors Toeplitz (CVT) technique, or correlation Toeplitz (CTOP) technique. Although these techniques are named or explained slightly different, they all involve reconstructing a Toeplitz matrix from the first row of the coherent data covariance matrix.

A study by Han and Zhang also constructs a Toeplitz matrix from the physical structure of the coherent data covariance matrix. In their study in [50], Han and Zhang mentioned that, any row of the coherent covariance matrix can be used to construct a new Toeplitz matrix. Studies mentioned above have however restricted themselves to using the first row in constructing a Toeplitz matrix.

A different Toeplitz technique, but still involving using the physical structure of the coherent data covariance matrix, is also found in [23]. This technique constructs a Toeplitz matrix using averages of the diagonals of the lower triangular part of the coherent data covariance matrix. It is referred to as average Toeplitz (AVTOP). The AVTOP technique can decorrelate coherent sources, however there is a great deviation in DOA estimation. The results of a simulation experiment comparing CTOP and AVTOP techniques have shown that CTOP yields nearer optimal angle estimates for both coherent and non-coherent sources.

More work on Toeplitz matrix reconstruction for decorrelation of coherent sources can be found in [21, 51–55]. In comparison to spatial smoothing and SVD techniques, Toeplitz decorrelation techniques offer powerful decorrelation ability without reduction of the array aperture. They provide highly precise estimates even at low SNR conditions and are less computationally intensive.

2.3 Analytical Approach to Analysis of DOA Estimation Methods

Most studies carried out on the analysis of DOA estimation methods and techniques are based on numerical simulations and experiments. Little attention has been paid to theoretical analysis of these techniques. Theoretical analysis is of great importance as it provides an in-depth understanding about the working principles behind these techniques.

A study based on an analytical approach was done by Pillai and Kwon [56]. Pillai and Kwon derived an expression of SNR threshold required to resolve the DOA of three sources in the presence of white noise using a MUSIC estimator for both coherent and non-coherent scenarios. This was made possible by first deriving parametric expressions for eigenvalues and eigenvectors for the array covariance matrix of each three-source scenario, and then use them to derive the required resolution threshold.

Another analytical study was done by Friedlander [57]. The study employed a first-order sensitivity analysis of the MUSIC algorithm to system errors. Assuming that the exact covariance matrix of a two-source scenario is known, a cost function based on the MUSIC spectrum function was derived in order to give DOA estimates of the two sources. The DOA estimates are provided by the location of the peaks in the spectrum. The locations of the peaks are characterised by the fact that the first derivative of the cost function is equal to zero at the peaks.

As the error is increased, the spectrum transitions from having two peaks to a flat single peak spectrum. Friedlander performed a first-order Taylor expansion of the cost function around true DOA to determine the peaks' shift when errors are introduced. From this study, a formula for computing the failure threshold of the MUSIC algorithm was derived and tested by simulation.

Other studies that involve an analytical analysis of DOA methods and techniques can be found in [58–62].

2.4 Summary

The development of subspace-based methods and challenges faced by these methods have been discussed. Studies proposing different solutions to the problem of coherence have been reviewed. A few studies employing an analytical approach to analysing methods and techniques in DOA estimation have been reviewed. An analytical approach similar to that in [57] was used in this study to analyse and understand the working principle behind the CTOP and AVTOP decorrelation techniques.

CHAPTER 3

Basic Knowledge of DOA Estimation

In this chapter, the basic knowledge of DOA estimation is outlined. The chapter briefly introduces phased arrays and basic array configurations. A DOA estimation data model based on a uniform linear array configuration is discussed. The chapter also presents a description of the MUSIC algorithm. The last section of the chapter introduces and demonstrates an approach for applying the MUSIC algorithm analytically.

3.1 Introduction to Phased Arrays

A Phased-Array Antenna (PAA) system has two or more radiating and/or receiving identical antenna elements in a uniform configuration [63]. In a typical antenna array system, individual or a group of array elements are connected to phase shifters and/or time delays. The relative phases and amplitudes of the signals feeding the array elements are electronically adjusted to produce a desired radiation beam pattern with more sensitivity or reinforced power in a desired direction, and suppressed in undesired directions (this is called beamforming).

Phased arrays are used to:

(a) Improve overall gain.

(b) Suppress interference from certain directions.

(c) Provide diversity reception.

(d) Increase array sensitivity in a particular direction.

(e) Obtain DOA estimate of the incident signals.

(f) Maximise Signal to Interference plus Noise Ratio (SINR).

The advantage of using Phased Array Antennas is that, they steer the main beam pattern rapidly (in milliseconds) without having to physically rotate the antennas. This helps to redress mechanical errors that are experienced when antennas are physically rotated. In addition, Phased Array Antennas can also be used to electronically control the array characteristics such as instantaneous beam position, half-power beam width (HPBW), position of amplitude nulls, level of radiated side lobes and antenna gain.

Possible Arrangements of Phased Arrays

The following are some of the most popular and simpler antenna array configurations. The detailed analysis and characteristics of each array arrangement can be found in [64, 65].

(a) Linear arrays

Linear arrays comprise of antenna elements arranged to form a straight line. In practical situations, linear antenna arrays are often realised with identical radiators equally spaced in a single dimension.

(b) Planar arrays

A planar array is a two-dimensional configuration where elements are arranged to lie on a plane. It can be thought of as a linear array of linear arrays. A planar array provides extra variables that can be used to control and shape the beam of the array. It is possible to scan the beam of a planar array toward any direction or point in space. They find applications in communications, searching and tracking radar.

(c) Circular arrays

A circular array, has elements arranged to form a circular ring. This type of configuration is of very practical interest. It is applied in air and space navigation, direction finding, sonar, radar and underground propagation.

This study is based on DOA estimation of signals incident on a uniform linear array. In practical systems such as navigation and wireless communication, DOA estimates can be used to steer the beamformer to capture signals in the direction of interest while rejecting signals from other directions.

3.2 Background of DOA Estimation

3.2.1 The DOA estimation system

DOA estimation is also known as spatial spectrum estimation. The spatial spectrum shows the incident signals' energy distribution in all spatial directions. Hence, when the spatial spectrum is known, the DOA of signals can also be obtained. The entire DOA estimation system consists of three stages: the target stage, observation stage and the estimation stage (see Figure 3.1 [66]).

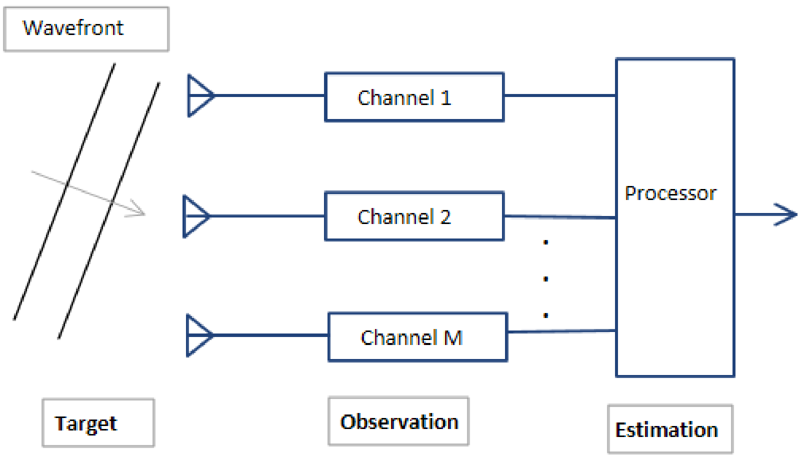

FIGURE 3.1: DOA estimation system structure.

The three stages are described below :

(a) **Target stage**

This stage consists of the incident signals parameters and the complex environment. The goal of the spatial spectrum estimation system is to estimate unknown parameters of the signals in a complex environment.

(b) **Observation stage**

The observation stage receives radiation signals from the target space. The obtained data may contain signal features (such as azimuth and polarisation) and space environment features (such as noise and interference), as a result of the complexity of the environment. The spatial array elements also have an effect on the received data due to features such as mutual coupling or channel inconsistency.

(c) **Estimation stage**

This is the stage that applies spatial spectrum estimation techniques to extract the parameters of signals from the received data. Extracting signal parameters is analogous to restoring the target stage. The restoration is influenced by several factors like array features and complexity of the environment.

3.2.2 Fundamental idea of DOA estimation

The front of the incident wave is taken as a plane if the received wave satisfies the far-field narrowband assumption. The angle between the array normal and the vector in the direction of the plane wave is known as the Direction of Arrival (DOA). It is also known as the Angle of Arrival (AOA) of the signal/wave.

The basic principle behind DOA estimation [66] is that when the signals are far and broad, there exists a wave-way difference when these signals impinge on distinct array elements. As a result, the array elements experience a phase difference among them. Therefore, the azimuth of the signal is estimated using this phase difference.

Figure 3.2 shows an array of two elements.

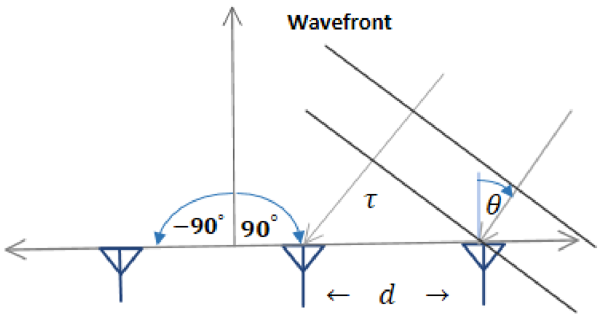

FIGURE 3.2: The theory of spatial spectrum estimation.

As shown, the signal arriving at the element on the left will take a delay τ due to the path difference, the delay is equal to

$$\tau = \frac{d\sin(\theta)}{c}, \tag{3.1}$$

where

(a) c is the speed of light.

(b) d is the array elements spacing.

(c) θ is the DOA of the incident signal.

Therefore the array elements experience a phase difference,

$$\psi = \exp(-j\omega\tau) = \exp(-\frac{j\omega d\sin(\theta)}{c}) = \exp(-\frac{j2\pi d\sin(\theta)}{\lambda f_0}f), \tag{3.2}$$

where λ is the wavelength and f_0 is the centre frequency of the incident wave. For narrowband signals the phase difference is

$$\psi = \exp(-\frac{j2\pi d\sin(\theta)}{\lambda}). \tag{3.3}$$

If τ (time delay) is known, then θ, the DOA of the incident wave can be found using Equation (3.1).

3.2.3 Data model assumptions

The data model for DOA estimation in this study is based on a ULA configuration and relies on the following assumptions [35].

(a) *Isotropic and linear transmission medium*: The transmission medium between the sources and the sensor array, through which the emitted signals travel, is assumed to be isotropic and linear. This means that the physical properties of the medium are uniform in all different directions and linear superposition of the signals is possible at any particular point.

(b) *Far-field assumption*: It is assumed that the array is situated in the far zone of the signal sources. This assumption guarantees that the sources generate planar wavefronts and each wavefront impinges on all array elements at the same direction of propagation.

(c) *Narrowband assumption*: The signals amplitudes and information-bearing phases change gradually with regard to the time required for the signals to propagate from a single sensor to the other. The narrowband assumption ensures that all array elements capture the signal at the same time.

(d) *AWGN channel*: The channel consists of additive white Gaussian noise with a common variance of σ^2 and uncorrelated at all array elements.

3.3 ULA System Data Model

The data model described here is applied to subspace-based algorithms for the estimation of DOA of signals incident on uniform linear array.

The following notation is used:

(a) Boldface uppercase letters are used to denote matrices, e.g. $\boldsymbol{R}$.

(b) Boldface small letters are used for column vectors, e.g. $\boldsymbol{a}$.

(c) Non-boldface letters represent scalar quantities, e.g. s.

(d) The superscripts $(.)^H$, $(.)^*$ and $(.)^T$ denote conjugate transpose, complex conjugate and transpose respectively.

(e) The operator $E\{\boldsymbol{a}\}$ denotes the expected value of the data represented by a vector $\boldsymbol{a}$.

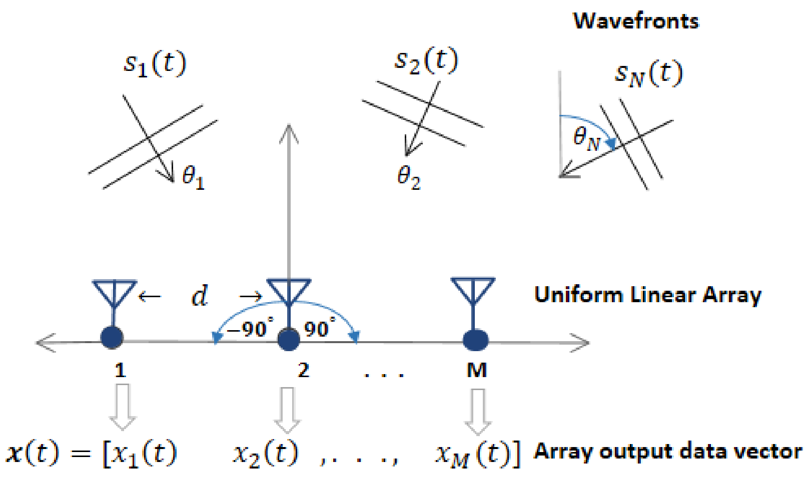

FIGURE 3.3: Data model.

Based on Figure 3.3, consider a ULA of M homogeneous omnidirectional elements, separated by an equal distance d. The sensors receive narrowband plane waves $s_n(t)$, $1 \leq n \leq N$, centered at frequency ω_0. If there are N, $(N < M)$ plane waves incident on the array from different DOAs θ_n, the data $\boldsymbol{x}(t)$ received by the array at any time t is obtained as a linear combination of the N received signals and noise [22, 67]. That is,

$$\begin{aligned} \boldsymbol{x}(t) =& \sum_{n=1}^{N} \boldsymbol{a}(\theta_n) s_n(t) + \boldsymbol{n}(t) \\ =& \boldsymbol{A}\boldsymbol{s}(t) + \boldsymbol{n}(t), \end{aligned} \tag{3.4}$$

where

$$\boldsymbol{x}(t) = [x_1(t), x_2(t), ..., x_M(t)]^T \ M \times 1 \text{ column vector;}$$
$$\boldsymbol{s}(t) = [s_1(t), s_2(t), ..., s_N(t)]^T \ N \times 1 \text{ column vector;}$$
$$\boldsymbol{n}(t) = [n_1(t), n_2(t), ..., n_M(t)]^T \ M \times 1 \text{ column vector;}$$
$$\boldsymbol{A} = [\boldsymbol{a}(\theta_1), \boldsymbol{a}(\theta_2), ..., \boldsymbol{a}(\theta_N)] \ M \times N \text{ Matrix.}$$

The quantity $x_m(t), (m = 1, 2, ..., M)$, is the combined output signal of the mth element, $\boldsymbol{a}(\theta_n)$, θ_n, $s_n(t)$, $(n = 1, 2, ..., N)$ are the steering vector, DOA of the nth source, and complex amplitude respectively. The additive white Gaussian noise at the mth element is represented by $n_m(t)$. The power of all signals is assumed to be uniform.

The $M \times 1$ steering vector is expressed as

$$\boldsymbol{a}(\theta_n) = \left[1, ..., \exp(-\frac{j2\pi(M-1)d\sin(\theta_n)}{\lambda})\right]^T. \tag{3.5}$$

From Equation (3.5), the array steering matrix is therefore given by

$$\boldsymbol{A} = \begin{bmatrix} 1 & 1 & \cdots & 1 \\ e^{-j\gamma_1} & e^{-j\gamma_2} & \cdots & e^{-j\gamma_N} \\ e^{-j2\gamma_1} & e^{-j2\gamma_2} & \cdots & e^{-j2\gamma_N} \\ \vdots & \vdots & & \vdots \\ e^{-j(M-1)\gamma_1} & e^{-j(M-1)\gamma_2} & \cdots & e^{-j(M-1)\gamma_N} \end{bmatrix}, \tag{3.6}$$

where $\gamma_n = \frac{2\pi d\sin(\theta_n)}{\lambda}$ is the electrical angle and θ_n is the mechanical angle (angle of arrival) of the nth source. It can be observed that the steering matrix $\boldsymbol{A}$ is of the form:

$$\boldsymbol{V}(v_1, v_2, ..., v_N) = \begin{bmatrix} 1 & 1 & \cdots & 1 \\ v_1 & v_2 & \cdots & v_N \\ v_1^2 & v_2^2 & \cdots & v_N^2 \\ \vdots & \vdots & & \vdots \\ v_1^{M-1} & v_2^{M-1} & \cdots & v_N^{M-1} \end{bmatrix},$$

hence $\boldsymbol{A}$ and $\boldsymbol{V}$ are Vandermonde matrices. The $M \times M$ covariance matrix of the data vector $\boldsymbol{x}(t)$ in Equation (3.4) is derived as

$$\begin{aligned} \boldsymbol{R} =& E[\boldsymbol{x}(t)\boldsymbol{x}^H(t)] \\ =& \boldsymbol{A}E[\boldsymbol{s}(t)\boldsymbol{s}^H(t)]\boldsymbol{A}^H + E[\boldsymbol{n}(t)\boldsymbol{n}^H(t)] \\ =& \boldsymbol{A}\boldsymbol{R}_{ss}\boldsymbol{A}^H + \sigma_n^2\boldsymbol{I}. \end{aligned} \tag{3.7}$$

The matrix $\boldsymbol{R}_{ss}$ is the signal covariance matrix, while $\boldsymbol{I}$ and σ_n^2 denote the $M \times M$ identity matrix and variance of the additive white Gaussian noise respectively. In practice the covariance matrix $\boldsymbol{R}$ is approximated by taking K samples of data vector $\boldsymbol{x}(t)$ and averaging. The approximate covariance matrix is denoted by $\hat{\boldsymbol{R}}$ which is given as

$$\hat{\boldsymbol{R}} = \frac{1}{K}\sum_{i=1}^{K} \boldsymbol{x}(t_i)\boldsymbol{x}(t_i)^H. \tag{3.8}$$

The subspace-based algorithms utilise the eigenstructure of the data covariance matrix derived in Equation (3.7) and (3.8) in order to estimate DOAs of the received signals. These algorithms are also referred to as eigenstructure-based algorithms. Important properties of covariance matrices are given in Appendix A.1.2.

3.4 The MUSIC Algorithm

The method was first put forward by Schmidt [5], to determine the parameters of multiple wavefronts impinging on an array of antennas by using the data measured from the signals captured at the array elements. MUSIC algorithm can be implemented to give a fair estimate of signal parameters such as direction of arrival, number of signals, signal strengths and cross-correlations among incident wavefronts, polarisation and strength of interference/noise.

These capabilities made MUSIC algorithm more suitable for applications such as

(a) Conventional interferometry,

(b) Monopulse direction finding and

(c) Multiple frequency estimation.

A full derivation of the MUSIC algorithm is given in Appendix A.3. The algorithm can be summarised into the following steps:

(a) Approximate the covariance matrix by taking K samples of the input data $\boldsymbol{x}(t)$ as given by:

$$\hat{\boldsymbol{R}} = \frac{1}{K}\sum_{i=1}^{K}\boldsymbol{x}(t_i)\boldsymbol{x}(t_i)^H. \tag{3.9}$$

(b) Carry out the eigendecomposition of $\hat{\boldsymbol{R}}$

$$\hat{\boldsymbol{R}}\boldsymbol{V} = \boldsymbol{V}\boldsymbol{\Lambda} \tag{3.10}$$

where $\boldsymbol{\Lambda}$ is a diagonal matrix whose diagonal elements are the eigenvalues, that is, $\mathrm{diag}\{\lambda_1, \lambda_2, ..., \lambda_M\}$, $(\lambda_1 \geq \lambda_2 \geq ... \geq \lambda_M)$ and $\boldsymbol{V} = [\boldsymbol{v}_1, \boldsymbol{v}_2, ..., \boldsymbol{v}_M]$, is a matrix whose columns are the corresponding eigenvectors of $\hat{\boldsymbol{R}}$.

(c) Evaluate the number of incident signals, $\hat{N}$, by using the multiplicity K of the smallest eigenvalue and the relation

$$\hat{N} = M - K. \tag{3.11}$$

(d) Form the matrix $\boldsymbol{V}_{\mathrm{n}} = [\boldsymbol{v}_{N+1} \boldsymbol{v}_{N+2}, ..., \boldsymbol{v}_{M}]$ using the eigenvectors corresponding to the $M - \hat{N}$ smallest eigenvalues and compute the MUSIC spectrum as

$$P_{\mathrm{MUSIC}}(\theta) = \frac{1}{\boldsymbol{a}^H(\theta)\boldsymbol{V}_{\mathrm{n}}\boldsymbol{V}_{\mathrm{n}}^H\boldsymbol{a}(\theta)}. \tag{3.12}$$

(e) Find the estimate DOAs of the incident signals by locating θs corresponding to the $\hat{N}$ largest peaks in the MUSIC spectrum.

The working principle behind the MUSIC DOA estimation is that the eigenvectors that form the matrix $\boldsymbol{V}_{\mathrm{n}}$ (known as noise eigenvectors) are orthogonal to the sources steering vectors. Allowing the MUSIC spectrum to be expressed as in Equation (3.12). The orthogonality between $\boldsymbol{V}_{\mathrm{n}}$ and $\boldsymbol{a}(\theta)$ results in peaks in the MUSIC spectrum at θs corresponding to DOAs of the incident sources.

In this study the MUSIC algorithm has been employed for DOA estimation of incident signals. The MUSIC algorithm is also frequently used in the field of spectral estimation to determine frequencies of multiple signals [68]. Other subspace based methods such as the ESPRIT method are also used in spectral estimation.

The spectral estimation problem

The spectral estimation problem can be stated as follows [69]: From a finite-length record $\{y(1), ..., y(N)\}$ of a second-order stationary random process determine an estimate $\hat{\phi}(\omega)$ of its power spectral density $\phi(\omega)$, for $\omega \in [-\pi, \pi]$. The desired result would be having $\hat{\phi}(\omega)$ as close to $\phi(\omega)$ as possible.

The DOA and spectral estimation problems have the same formulation and solution. A formulation of the spectral estimation problem as well as the derivation of the MUSIC algorithm for frequency estimation is given in the textbook on "Spectral analysis of signals" [69] by Stoica and Moses. The book also presents other state-of-the-art spectral estimation methods and cases of frequency estimation of correlated and uncorrelated sources.

Other studies such as [68, 70] also investigated the application of MUSIC algorithm in the field of spectral estimation.

3.5 Applying MUSIC Analytically

Most studies involving the application of MUSIC algorithm are based on numerical simulations. This study however has analytically applied the MUSIC algorithm in order to verify the findings or observations made from the algebraic analysis in Chapter 5. This section thus describes the analytical application of the MUSIC algorithm.

Consider the MUSIC spectrum given in Equation (3.12) which is presented here again for the purpose of explanations:

$$P_{\mathrm{MUSIC}}(\theta) = \frac{1}{\boldsymbol{a}^H(\theta)\boldsymbol{V}_{\mathrm{n}}\boldsymbol{V}_{\mathrm{n}}^H\boldsymbol{a}(\theta)}. \tag{3.13}$$

As previously mentioned, $\boldsymbol{a}(\theta)$ is the array steering vector and $\boldsymbol{V}_n$ is the matrix of noise eigenvectors. According to the MUSIC algorithm, for all θ corresponding to DOA of the incident signals the denominator $\boldsymbol{a}^H(\theta)\boldsymbol{V}_{\mathrm{n}}\boldsymbol{V}_{\mathrm{n}}^H\boldsymbol{a}(\theta) = 0$. Based on this knowledge, the analytic approach involves algebraically deriving the following cost function

$$J(\phi, \gamma) = \boldsymbol{w}^H(\phi)\boldsymbol{V}_{\mathrm{n}}(\gamma)\boldsymbol{V}_{\mathrm{n}}^H(\gamma)\boldsymbol{w}(\phi), \tag{3.14}$$

where γ is the electrical angle of the incident signal. Note that $\gamma = 2\pi(d/\lambda)\sin(\theta)$, where θ is the DOA or mechanical angle. The vector $\boldsymbol{w}(\phi)$ has the same form as $\boldsymbol{a}(\theta)$. Hence, $\boldsymbol{w}(\phi)$ is a continuum of all possible steering vectors. The only difference between the two vectors is that, the variables ϕ and θ denote any possible direction in terms of electrical and mechanical angles respectively.

The objective of this approach is to find the values of ϕ for which $\boldsymbol{w}(\phi)$ is orthogonal to the matrix $\boldsymbol{V}_{\mathrm{n}}(\gamma)$. In the case of a single incident source, this occurs at a point where the cost function $J(\phi, \gamma)$ has a global minimum. When there are multiple incident sources, $J(\phi, \gamma)$ has multiple global minima corresponding to the number of incident sources.

As shown in this section, the global minima occur at points where $\phi = \gamma_i$ for $i = 1, ..., N$ where N is the number incident signals. The minimum points are found by the minimisation of $J(\phi, \gamma)$ as shown in the following equation

$$\frac{\partial J(\phi, \gamma)}{\partial \phi} = 0. \tag{3.15}$$

Assuming that the exact array covariance matrix is known, the DOA of incident sources can be analytically estimated by deriving the cost function $J(\phi, \gamma)$. Then by minimisation of the cost function, find the values of ϕ for which the cost function has global minima. These values of ϕ corresponds to the electrical angles of the incident sources. A similar method of estimating DOAs analytically by cost function minimisation has been used by Friedlander [57] in his study on the sensitivity analysis of the MUSIC algorithm.

Construction of matrix $\boldsymbol{V}_{\mathrm{n}}(\gamma)$

In order to come up with an expression of the cost function $J(\phi, \gamma)$ for a particular DOA estimation scenario, the eigenvalues and eigenvectors of the array covariance matrix are algebraically derived. The matrix $\boldsymbol{V}_{\mathrm{n}}(\gamma)$ is then constructed from eigenvector(s) corresponding to the smallest eigenvalue(s) (also known as the noise eigenvalues). Since the exact array covariance matrix is known (not approximated), the noise eigenvalues are exactly equal to noise variance σ^2. This is simply a single eigenvalue repeated K times. Where K is its algebraic multiplicity. The value K is given by:

$$K = M - N \tag{3.16}$$

where N is the number of signal sources and M is the array size.

3.5.1 Analytic MUSIC demonstration

In order to appreciate the analytic approach for DOA estimation with MUSIC, a single source DOA estimation problem is used to demonstrate the approach. For this purpose, consider the following scenario:

(a) Assume a narrowband plane wave $s(\kappa, t) = pe^{j(\omega_0 t + \vartheta(\kappa))}$ with electrical angle γ is incident on a ULA.

(b) The noise at ULA is an additive white Gaussian with variance σ^2.

To simplify the problem, consider the signal amplitude p to be unity. The above scenario is used in the following three examples to demonstrate the analytic DOA estimation approach. The first example uses a ULA of two elements, then three and four array elements for the second and third examples respectively. For these three examples, the signal covariance matrix $\boldsymbol{R}_{ss}$ is given by:

$$\begin{aligned}
\boldsymbol{R}_{ss} &= \mathrm{E}\{s(.,t)s(.,t)^H\} \\
&= \mathrm{E}\{e^{j(\omega_0 t + \vartheta(\kappa))} e^{-j(\omega_0 t + \vartheta(\kappa))}\} \\
&= e^{j(\omega_0 - \omega_0)t} \mathrm{E}\{e^{j(\vartheta(\kappa) - \vartheta(\kappa))}\} \\
&= 1
\end{aligned}$$

Example 1: Two elements ULA

The array covariance matrix for a two elements ULA is derived as

$$\begin{aligned}
\boldsymbol{R} &= \boldsymbol{A}\boldsymbol{R}_{ss}\boldsymbol{A}^H + \sigma^2 \boldsymbol{I}_{2\times 2} \\
&= \begin{bmatrix} 1 \\ e^{-j\gamma} \end{bmatrix} \begin{bmatrix} 1 \end{bmatrix} \begin{bmatrix} 1 & e^{j\gamma} \end{bmatrix} + \sigma^2 \boldsymbol{I}_{2\times 2} \\
&= \begin{bmatrix} 1 & e^{j\gamma} \\ e^{-j\gamma} & 1 \end{bmatrix} + \begin{bmatrix} \sigma^2 & 0 \\ 0 & \sigma^2 \end{bmatrix}
\end{aligned}$$

$$= \begin{bmatrix} 1+\sigma^2 & e^{j\gamma} \\ e^{-j\gamma} & 1+\sigma^2 \end{bmatrix} \tag{3.17}$$

where the array steering matrix $\boldsymbol{A}$ is a 2×1 column vector. The noise eigenvalue and corresponding eigenvector of $\boldsymbol{R}$ are derived as

$$\lambda = \sigma^2, \quad \boldsymbol{v} = \begin{bmatrix} -e^{-j\gamma} \\ 1 \end{bmatrix}.$$

The eigenvector $\boldsymbol{v}$ forms the matrix $\boldsymbol{V}_{\mathrm{n}}(\gamma)$ and for a two elements ULA, $\boldsymbol{w}(\phi) = \begin{bmatrix} 1, & e^{-j\phi} \end{bmatrix}^T$. Therefore using the $\boldsymbol{V}_{\mathrm{n}}(\gamma)$ and $\boldsymbol{w}(\phi)$ the cost function is derived as

$$\begin{aligned} J_{21}(\phi,\gamma) &= \boldsymbol{w}^H(\phi)\boldsymbol{V}_{\mathrm{n}}(\gamma)\boldsymbol{V}_{\mathrm{n}}^H(\gamma)\boldsymbol{w}(\phi) \\ &= (e^{j\gamma} - e^{j\phi})(e^{-j\gamma} - e^{-j\phi}) \\ &= 2 - 2\cos(\gamma - \phi). \end{aligned} \tag{3.18}$$

By taking the partial derivative of the cost function $J_{21}(\phi,\gamma)$ with respect to ϕ and equating to zero, it follows that

$$\begin{aligned} &\frac{\partial}{\partial\phi} J_{21}(\phi,\gamma) = -2\sin(\gamma - \phi) \\ &-2\sin(\gamma - \phi) = 0. \end{aligned} \tag{3.19}$$

It can be observed from Equation (3.19) that $J_{21}(\phi,\gamma)$ has a global minimum when ϕ is equal to the target direction γ. In order to graphically visualise the cost function and its derivative, assume that the electrical angle $\gamma = 0.6981$ radians $(40°)$ (the same assumption is used in the next examples). The cost function and its derivative are plotted for values of ϕ from 0 to 2π radians as shown in Figure 3.4.

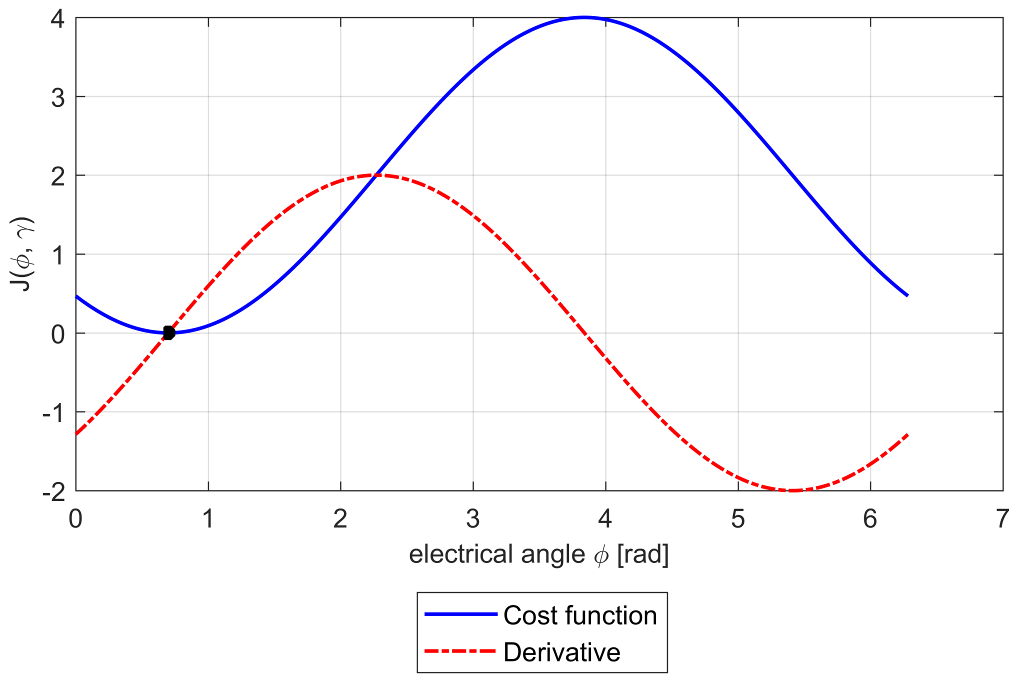

FIGURE 3.4: One source and two elements ULA.

Example 2: Three elements ULA

For this case the array covariance matrix is a 3×3 derived as

$$\begin{aligned}
\boldsymbol{R} &= \boldsymbol{A}\boldsymbol{R}_{ss}\boldsymbol{A}^H + \sigma^2 \boldsymbol{I}_{3\times 3} \\
&= \begin{bmatrix} 1 \\ e^{-j\gamma} \\ e^{-j2\gamma} \end{bmatrix} \begin{bmatrix} 1 \end{bmatrix} \begin{bmatrix} 1 & e^{j\gamma} & e^{j2\gamma} \end{bmatrix} + \sigma^2 \boldsymbol{I}_{3\times 3} \\
&= \begin{bmatrix} 1 & e^{j\gamma} & e^{j2\gamma} \\ e^{-j\gamma} & 1 & e^{j\gamma} \\ e^{-j2\gamma} & e^{-j\gamma} & 1 \end{bmatrix} + \begin{bmatrix} \sigma^2 & 0 & 0 \\ 0 & \sigma^2 & 0 \\ 0 & 0 & \sigma^2 \end{bmatrix} \\
&= \begin{bmatrix} 1+\sigma^2 & e^{j\gamma} & e^{j2\gamma} \\ e^{-j\gamma} & 1+\sigma^2 & e^{j\gamma} \\ e^{-j2\gamma} & e^{-j\gamma} & 1+\sigma^2 \end{bmatrix}. \qquad (3.20)
\end{aligned}$$

The noise eigenvalues and corresponding eigenvectors of $\boldsymbol{R}$ were derived as,

$$\lambda_1 = \sigma^2, \ \boldsymbol{v}_1 = \begin{bmatrix} -e^{j\gamma} \\ 1 \\ 0 \end{bmatrix}$$

$$\lambda_2 = \sigma^2, \ \boldsymbol{v}_2 = \begin{bmatrix} -e^{j2\gamma} \\ 0 \\ 1 \end{bmatrix}.$$

The noise eigenvalue has an algebraic multiplicity of 2 and the two noise eigenvectors $\boldsymbol{v}_1$ and $\boldsymbol{v}_2$ form the matrix $\boldsymbol{V}_{\mathrm{n}}(\gamma)$ as shown below

$$\boldsymbol{V}_{\mathrm{n}}(\gamma) = \begin{bmatrix} -e^{j\gamma} & -e^{j2\gamma} \\ 1 & 0 \\ 0 & 1 \end{bmatrix}.$$

For a three elements ULA the vector $\boldsymbol{w}(\phi) = \left[1, \ e^{-j\phi}, \ e^{-j2\phi}\right]^T$, therefore the expression for the cost function is derived as

$$\begin{aligned} J_{31}(\phi,\gamma) &= \boldsymbol{w}^H(\phi)\boldsymbol{V}_{\mathrm{n}}(\gamma)\boldsymbol{V}_{\mathrm{n}}^H(\gamma)\boldsymbol{w}(\phi) \\ &= (e^{j\gamma} - e^{j\phi})(e^{-j\gamma} - e^{-j\phi}) + (e^{j2\gamma} - e^{j2\phi})(e^{-j2\gamma} - e^{-j2\phi}) \\ &= 4 - 2\cos(\gamma - \phi) - 2\cos\left[2(\gamma - \phi)\right]. \end{aligned} \tag{3.21}$$

The following result is obtained by taking the derivative of the cost function with respect to ϕ and then equate to zero,

$$\begin{aligned} \frac{\partial}{\partial\phi} J_{31}(\phi,\gamma) &= -4\sin\left[2(\gamma-\phi)\right] - 2\sin(\gamma-\phi) \\ - 4\sin\left[2(\gamma-\phi)\right] &- 2\sin(\gamma-\phi) = 0. \end{aligned} \tag{3.22}$$

It is evident from Equation (3.22) that when $\phi = \gamma$, the cost function $J_{31}(\phi,\gamma)$ has a global minimum. Assuming that the source has an angle of arrival of $\gamma = 0.6981$ radians, the cost function and its derivative are plotted as shown in Figure 3.5

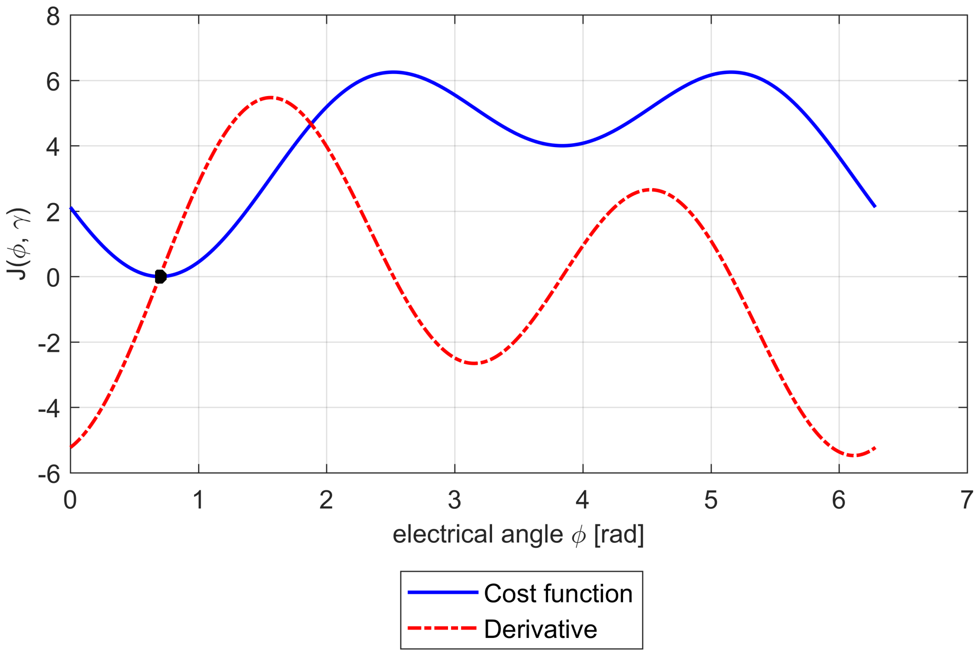

FIGURE 3.5: One source and three elements ULA.

Example 3: Four elements ULA

The array covariance matrix for a four elements ULA and one source is derived as follow

$$\begin{aligned}
\boldsymbol{R} &= \boldsymbol{A}\boldsymbol{R}_{ss}\boldsymbol{A}^H + \sigma^2\boldsymbol{I}_{4\times4} \\
&= \begin{bmatrix} 1 \\ e^{-j\gamma} \\ e^{-j2\gamma} \\ e^{-j3\gamma} \end{bmatrix} \begin{bmatrix} 1 \end{bmatrix} \begin{bmatrix} 1, & e^{j\gamma}, & e^{j2\gamma}, & e^{j3\gamma} \end{bmatrix} + \sigma^2\boldsymbol{I}_{4\times4} \\
&= \begin{bmatrix} 1 & e^{j\gamma} & e^{j2\gamma} & e^{j3\gamma} \\ e^{-j\gamma} & 1 & e^{j\gamma} & e^{j2\gamma} \\ e^{-j2\gamma} & e^{-j\gamma} & 1 & e^{j\gamma} \\ e^{-j3\gamma} & e^{-j2\gamma} & e^{-j\gamma} & 1 \end{bmatrix} + \begin{bmatrix} \sigma^2 & 0 & 0 & 0 \\ 0 & \sigma^2 & 0 & 0 \\ 0 & 0 & \sigma^2 & 0 \\ 0 & 0 & 0 & \sigma^2 \end{bmatrix} \\
&= \begin{bmatrix} 1+\sigma^2 & e^{j\gamma} & e^{j2\gamma} & e^{j3\gamma} \\ e^{-j\gamma} & 1+\sigma^2 & e^{j\gamma} & e^{j2\gamma} \\ e^{-j2\gamma} & e^{-j\gamma} & 1+\sigma^2 & e^{j\gamma} \\ e^{-j3\gamma} & e^{-j2\gamma} & e^{-j\gamma} & 1+\sigma^2 \end{bmatrix}.
\end{aligned} \tag{3.23}$$

The derived noise eigenvalues and eigenvectors for the covariance matrix $\boldsymbol{R}$ are as given below,

$$\lambda_1 = \sigma^2, \quad \boldsymbol{v}_1 = \begin{bmatrix} -e^{j\gamma} \\ 1 \\ 0 \\ 0 \end{bmatrix}; \quad \lambda_2 = \sigma^2, \quad \boldsymbol{v}_2 = \begin{bmatrix} -e^{j2\gamma} \\ 0 \\ 1 \\ 0 \end{bmatrix} \text{ and } \lambda_3 = \sigma^2, \quad \boldsymbol{v}_3 = \begin{bmatrix} -e^{j3\gamma} \\ 0 \\ 0 \\ 1 \end{bmatrix}.$$

In this case, the noise eigenvalue has an algebraic multiplicity of 3 and the matrix $\boldsymbol{V}_{\mathrm{n}}(\gamma)$ is a 3×3 matrix whose columns are the noise eigenvectors as shown below

$$\boldsymbol{V}_{\mathrm{n}}(\gamma) = \begin{bmatrix} -e^{j\gamma} & -e^{j2\gamma} & -e^{j3\gamma} \\ 1 & 0 & 0 \\ 0 & 1 & 0 \\ 0 & 0 & 1 \end{bmatrix}.$$

Using $\boldsymbol{w}(\phi) = \begin{bmatrix} 1, & e^{-j\phi}, & e^{-j2\phi}, & e^{-j3\phi} \end{bmatrix}^T$ and $\boldsymbol{V}_{\mathrm{n}}(\gamma)$ the cost function is derived as:

$$\begin{aligned} J_{41}(\phi, \gamma) =& \boldsymbol{w}^H(\phi)\boldsymbol{V}_{\mathrm{n}}(\gamma)\boldsymbol{V}_{\mathrm{n}}^H(\gamma)\boldsymbol{w}(\phi) \\ =& (e^{j\gamma} - e^{j\phi})(e^{-j\gamma} - e^{-j\phi}) + (e^{j2\gamma} - e^{j2\phi})(e^{-j2\gamma} - e^{-j2\phi}) \\ & + (e^{j3\gamma} - e^{j3\phi})(e^{-j3\gamma} - e^{-j3\phi}) \\ =& 6 - 2\cos(\gamma - \phi) - 2\cos[2(\gamma - \phi)] - 2\cos[3(\gamma - \phi)]. \end{aligned} \tag{3.24}$$

The cost function is minimised by taking the partial derivative with respect to ϕ and then equate to zero. The following result is obtained:

$$\begin{aligned} \frac{\partial}{\partial \phi} J_{41}(\phi, \gamma) &= -6\sin[3(\gamma - \phi)] - 4\sin[2(\gamma - \phi)] - 2\sin(\gamma - \phi) \\ & - 6\sin[3(\gamma - \phi)] - 4\sin[2(\gamma - \phi)] - 2\sin(\gamma - \phi) = 0. \end{aligned} \tag{3.25}$$

It is again evident that when $\phi = \gamma$, Equation (3.25) goes to zero, meaning the cost function $J_{41}(\phi, \gamma)$ has a global minimum at $\phi = \gamma$. This is confirmed by plotting the cost function and its derivative. Assuming that the target direction $\gamma = 0.6981$ radians, the plot in Figure 3.6 is obtained.

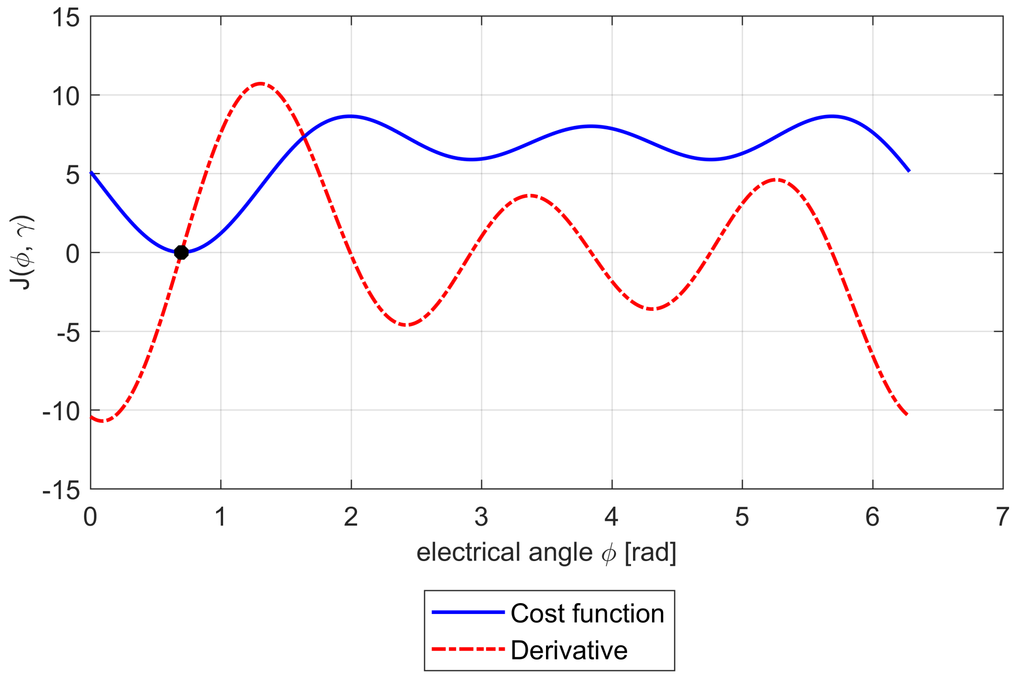

FIGURE 3.6: One source and four elements ULA.

3.5.2 Discussion

The cost functions and their derivatives plotted in Figures 3.4, 3.5 and 3.6 were derived. This was done in order to demonstrate the ability to estimate target directions by applying the MUSIC algorithm analytically. The results in each plot show that the cost function has a global minimum only at a point where $\phi = \gamma = 0.6981$ radians which corresponds to the electrical angle of the incident source. The cost function and its derivative intersect at this point. This is indicated by a dot on each plot. The following insights are worth taking note of:

(a) Global minimum

The value of the cost function at the point where a global minimum occurs is zero, that is $J(\phi, \gamma) = 0$. This is because when $\phi = \gamma$, $\boldsymbol{V}_n(\gamma)$ is orthogonal to the vector

$\boldsymbol{w}(\phi)$. Thus, $\boldsymbol{w}^H(\phi)\boldsymbol{V}_n(\gamma) = 0$. This corresponds to an infinitely high peak in the MUSIC spectrum because the denominator is zero. In general, the number of global minima is always equivalent to the number of signal sources and occurs at $\phi = \gamma$, the electrical angle of the signal source.

(b) Local minima

The cost functions in Figures 3.5 and 3.6 have local minima. The number of local minima is determined by the number of signal sources and the size of the array. It has been observed that in a scenario of N signal sources and M array elements the cost function can have a maximum of $(M - N) - 1$ local minima. In addition, the position of a local minimum around the global minimum is always deterministic.

The local minimum observations from the above Figures (3.4, 3.5 and 3.6) are presented below

Figure 3.4: The cost function has zero minima, since there are two array elements and one source, $(M - N) - 1 = (2 - 1) - 1 = 0$.

Figure 3.5: In this case, there is one signal source and three array elements. Hence, there is one local minimum, $(M - N) - 1 = (3 - 1) - 1 = 1$. For this particular scenario, it was found that for any target direction, γ, the local minimum always occurs at

$$\phi = \gamma + \pi \tag{3.26}$$

for $\gamma = 0.6981$ radians the local minimum is at $\phi = 0.6981 + \pi$ radians.

Figure 3.6: There are four array elements and one source in this case. Therefore, the maximum number of local minima is $(M - N) - 1 = (4 - 1) - 1 = 2$. The two local minima are always 0.58π radians apart. It was found that one of the local minima occurs at

$$\phi = \gamma + \frac{\pi}{\sqrt{2}} \tag{3.27}$$

and the second local minimum occurs at

$$\phi = \gamma + \frac{\pi}{\sqrt{2}} + 0.58\pi \tag{3.28}$$

3.6 Summary

The chapter introduced and discussed phased arrays and basic array configurations. A DOA estimation system and a ULA data model, on which this study is based, have been presented. In addition, the MUSIC algorithm has been introduced and an approach to applying MUSIC analytically was derived. Based on a single source DOA estimation scenario, three examples were used to demonstrate the ability to estimate source directions using the derived approach.

CHAPTER 4

Coherence and Decorrelation

This chapter provides a mathematical definition of the degree of coherence between two coherent sources in a signal processing context. The effect of coherent sources on the performance of the MUSIC algorithm and the procedures of the CTOP and AVTOP decorrelation techniques are also discussed.

4.1 The Concept of Coherence

According to Marple and Marino [71], the concept of "coherence" and coherent signal originated from literature on electromagnetic spectrum of light. It was later introduced in the signal processing community. However, it was only defined for narrowband EM waves. The term is now common in modern signal processing yet it is not clearly defined for the broadband case.

Coherence is a two-signal metric which, according to the current literature, is given as a cross spectral density between the signals normalised by the product of the individual signals auto spectral density. However, this is only applicable to narrowband stochastic processes. This motivated Marple and Marino in their work to provide various coherence definitions and metrics to handle the more sophisticated broadband (wideband) case.

Marple and Marino disagree with researchers who believe that coherence can also be defined as a single-signal attribute, such that, if a signal preserves its phase and amplitude, it is said to be coherent. They argue that this definition is erroneous. A simple condition for coherence states that for two signals to be coherent, their phase must either be identical or must have a constant difference. From the signal processing literature, the phase is the most common attribute associated with coherent signals.

In this study, the signal sources are assumed to be narrowband stochastic processes. Hence, the mathematical definition of coherence based on a narrowband assumption is considered. To be more specific, a general mathematical definition of coherence by Gardner [72] in terms of probabilistic definition of the correlation coefficient between two zero mean random variables is used as the basic definition of coherence in this study. Advanced key concepts on coherence and coherence metrics can be found in Gadner, and Marple and Marino's studies.

4.2 Degree of Coherence

Based on a statistical theory, the degree of coherence of two zero-mean, random variables $\boldsymbol{x}$ and $\boldsymbol{y}$ is given by the magnitude of their correlation coefficient $\underset{\sim}{\rho}$, where

$$\underset{\sim}{\rho} \triangleq \frac{E\{\boldsymbol{x}\boldsymbol{y}^*\}}{\sqrt{E\{|\boldsymbol{x}|^2\}E\{|\boldsymbol{y}|^2\}}} = \frac{\underset{\sim}{\boldsymbol{R}}_{xy}}{\sqrt{\underset{\sim}{\boldsymbol{R}}_{xx}\underset{\sim}{\boldsymbol{R}}_{yy}}} \tag{4.1}$$

and $E\{.\}$ is the expectation. By the Cauchy-Schwarz inequality it is true that $0 \leq |\underset{\sim}{\rho}| \leq 1$. In practice, the actual degree of coherence is computed using an ensemble of the random sample values $\boldsymbol{x}[n]$ and $\boldsymbol{y}[n]$ as

$$|\hat{\underset{\sim}{\rho}}| \triangleq \frac{|\hat{\underset{\sim}{\boldsymbol{R}}}_{xy}|}{\sqrt{\hat{\underset{\sim}{\boldsymbol{R}}}_{xx}\hat{\underset{\sim}{\boldsymbol{R}}}_{yy}}}, \tag{4.2}$$

where

$$\hat{\underset{\sim}{\boldsymbol{R}}}_{xy} \triangleq \frac{1}{N}\sum_{n=1}^{N}\boldsymbol{x}[n]\boldsymbol{y}^*[n] \tag{4.3}$$

and n is the ensemble index.

In a multiple signals environment, the following three different signal source scenarios may exist [73]:

(a) The sources may be uncorrelated (mutually independent), where $|\underset{\sim}{\rho}| = 0$.

(b) The sources can also be partially correlated, where $0 < |\underset{\sim}{\rho}| < 1$.

(c) The last scenario occurs when the sources are coherent (highly correlated), where $|\underset{\sim}{\rho}| = 1$.

In general, the degree of coherence is a measure of a degree of linear dependence. The variables that are less linearly dependent exhibit a low degree of coherence and vice-versa.

4.3 The Coherent Source Scenario

As mentioned in the subsequent sections, the coherent scenario is a result of multipath propagation, where a direct path signal and a reflected path signal from the same source arrive at the array from different directions. The exact type of coherence on which this research work is based is referred to as "Phase-coherence". Two signals are said to be phase-coherent when they:

(a) have the same frequency and

(b) a constant relative phase i.e phase difference is constant at all instances in time [74, 75].

The phase-coherent signal data model based on two multipath components is given in Section 5.1 and it is shown that when the above conditions are satisfied, the correlation coefficient between the two signals is equal to one, i.e $|\underset{\sim}{\rho}| = 1$. It should be noted that having the same frequency does not qualify two signals to be phase-coherent.

The concept of phase-coherent signals is described in the Application Note on "Signals Source Solutions for Coherent and Phase Stable Multi-Channel Systems" [74] by Agilent Technologies. Many studies on DOA estimation of coherent sources can be found in literature (of which some are cited in this thesis), but they do not explicitly describe the exact type of correlation considered, except that it is due to multipath propagation. Hence the term "phase-coherent" is not popular in this particular area. However the terms "constant relative phase", "same phase", "fixed phase difference" etc., as the main factor causing coherence (100% correlation) in multipath signal scenarios has been highlighted in some studies such as [22, 75–77].

4.4 MUSIC in the Presence of Coherent Sources

In a real-life environment, the problem of coherence occurs as a result of multipath propagation and electronic jamming. The detection and estimation of coherent sources became a very crucial research direction of DOA estimation [17]. The performance of MUSIC and other subspace-based methods degrade severely in a coherent or highly correlated signal environment.

It is required that for the MUSIC algorithm to successfully estimate DOAs of incident signals, the signal covariance matrix $\boldsymbol{R}_{ss}$ should be non-singular. The non-singularity property of $\boldsymbol{R}_{ss}$ is only guaranteed if the incident signals are not coherent (highly correlated) [4]. Under non-coherent signal conditions, the rank of $\boldsymbol{R}_{ss}$ is equal to the number of sources N. Coherence among incident signals results in a rank degradation of the signal covariance matrix, where $\text{rank}(\boldsymbol{R}_{ss}) < N$.

When eigendecomposition of the coherent data covariance matrix $\boldsymbol{R}_{C}$ is performed, the number of large eigenvalues will also be fewer than the number of sources N. This means that, the signal subspace dimension will be smaller; resulting in the noise subspace being not orthogonal to the array steering vector of coherent sources. As a result, the MUSIC algorithm fails to produce peaks at the DOA location of the highly correlated sources in the spatial spectrum. To compensate for rank deficiency in the signal covariance matrix caused by coherence interference, a pre-conditioning scheme is needed for decorrelation (decoherence) purpose.

Various types of pre-conditioning schemes have been reviewed in Section 2.2 of the literature review. The next section is dedicated to the CTOP and AVTOP decorrelation techniques.

4.5 Decorrelation using CTOP and AVTOP Techniques

The CTOP and AVTOP decorrelation techniques are of much interest in this study. Therefore, it is important to explain and understand the decorrelation procedure of each technique before further investigation is done. For this purpose, assume a $M \times M$ coherent array covariance matrix denoted by $\boldsymbol{R}_C$, which is given as:

$$\boldsymbol{R}_C = \begin{bmatrix} r[1,1] & r[1,2] & \cdots & r[1,M] \\ r[2,1] & r[2,2] & \cdots & r[2,M] \\ \vdots & \vdots & \ddots & \vdots \\ r[M,1] & r[M,2] & \cdots & r[M,M] \end{bmatrix}. \tag{4.4}$$

The matrix $\boldsymbol{R}_C$ is used to explain the decorrelation procedure of each technique.

4.5.1 Average Toeplitz(AVTOP)

This technique is presented in [23]. To reinstate the rank of the covariance matrix, the AVTOP technique constructs a new Toeplitz matrix $\boldsymbol{R}_T$ using a vector $\bar{\boldsymbol{r}}_{AVTOP} = \left[\bar{r}[1],\ \bar{r}[2],\ ...,\ \bar{r}[M]\right]$ whose elements are obtained by taking an average of the entries in each of the slanting diagonals of the lower triangular part of the correlated array covariance matrix $\boldsymbol{R}_C$. The procedure is summarised in the following equation

$$\bar{r}[i] = \frac{1}{M-i+1}\sum_{m=i}^{M} r[m, m-i+1], \quad i = 1, 2, ..., M. \tag{4.5}$$

The Toeplitz matrix constructed using $\bar{\boldsymbol{r}}_{AVTOP}$ is of the form

$$\boldsymbol{R}_T = \begin{bmatrix} \bar{r}[1] & \bar{r}^*[2] & \cdots & \bar{r}^*[M] \\ \bar{r}[2] & \bar{r}[1] & \cdots & \bar{r}^*[M-1] \\ \vdots & \vdots & \ddots & \vdots \\ \bar{r}[M] & \bar{r}[M-1] & \cdots & \bar{r}[1] \end{bmatrix}. \tag{4.6}$$

Subspace-based methods such as MUSIC can then be applied to $\boldsymbol{R}_T$ to estimate DOA of the coherent signals.

4.5.2 Correlation Toeplitz (CTOP)

The correlation Toeplitz technique is presented in [22, 23, 49]. The technique uses the array received data vector $\boldsymbol{x}(t) = [x_1(t), x_2(t), ..., x_M(t)]$ to form a vector $\boldsymbol{r}_{CTOP} = \big[r[1], r[2], \cdots, r[M]\big]$, by taking the cross-correlation between each sensor output and the reference sensor output. Taking the first element of the array as the reference, the cross-correlation sequence is generated as

$$r[i] = x_1(t)\boldsymbol{x}_i^H(t) \quad i = 1, 2, ..., M. \tag{4.7}$$

The vector $\boldsymbol{r}_{CTOP}$ is basically equivalent to the first row of the coherent covariance matrix $\boldsymbol{R}_C$ that is, $\boldsymbol{r}_{CTOP} = \big[r[1,1], r[1,2], \cdots, r[1,M]\big]$. The correlation-sequence $\boldsymbol{r}_{CTOP}$ is then used to construct a new Toeplitz matrix of the form

$$\boldsymbol{R}_T = \begin{bmatrix} r[1] & r[2] & \cdots & r[M] \\ r^*[2] & r[1] & \cdots & r[M-1] \\ \vdots & \vdots & \ddots & \vdots \\ r^*[M] & r^*[M-1] & \cdots & r[1] \end{bmatrix}, \tag{4.8}$$

where the MUSIC algorithm or any other subspace-based method can be applied to estimate DOA information of the incident sources.

The correlation Toeplitz technique can be summarised as follows:

(a) Obtain the received data vector $\boldsymbol{x}(t) = [x_1(t),\ x_2(t),\ ...,\ x_M(t)]$ and the first array element response $x_1(t)$.

(b) Compute the cross-correlation sequence using $x_1(t)$ and $\boldsymbol{x}(t)$ to form vector $\boldsymbol{r}_{CTOP}$.

(c) Construct the Toeplitz matrix $\boldsymbol{R}_T$ using the correlation sequence vector $\boldsymbol{r}_{CTOP}$.

(d) Find DOAs of coherent sources by applying MUSIC algorithm to $\boldsymbol{R}_T$.

According to Bai et al. [23], the CTOP method provides more accurate estimates. Whereas, the averaging of the diagonal elements of the coherent matrix results in deviation from the true DOA.

4.6 Summary

This chapter presented a mathematical definition of coherence in a signal processing context. The chapter also explained the exact type of coherence on which this study is based and also outlined the effect of coherence on the MUSIC algorithm and other subspace-based methods. The last section presented the decorrelation procedures of the CTOP and AVTOP decorrelation techniques.

CHAPTER 5

Algebraic Analysis

This chapter presents an algebraic analysis of the CTOP and AVTOP decorrelation techniques. Based on a given coherent signal data model a symbolic expression of a coherent array covariance matrix was derived and the two Toeplitz decorrelation techniques were applied to reconstruct new Toeplitz matrices from the coherent covariance matrix. From the investigation of the structures of the derived coherent array covariance matrix and the Toeplitz reconstructed matrices, a claim is made about the principle behind the performance of the two techniques. This provides an understanding of why the CTOP technique has an unbiased and more accurate estimation performance and why the AVTOP technique results in deviations from true DOA. The results from this analysis were verified using scenarios involving up to a four element ULA and a maximum of three narrowband sources, based on the assumption that the noise at the array is additive white Gaussian noise.

5.1 Coherent Signal Source Data Model

Consider a multipath propagation scenario caused by reflective objects in the transmission path. In this scenario the signals from the same source become coherent. Assume that $s_1(\kappa, t)$ is a direct signal and $s_2(\kappa, t)$ is a reflected signal emitted from a narrowband source, and

$$s_2(\kappa, t) = \beta s_1(\kappa, t), \tag{5.1}$$

where β is a scalar relating the gain of the two signals. Let $s_1(\kappa, t) = p_1 e^{j(\omega_0 t + \vartheta(\kappa))}$ and $s_2(\kappa, t) = p_2 e^{j(\omega_0 t + \vartheta(\kappa))}$ where $p_2 = \beta p_1$. The two signals have a randomly changing phase $\vartheta(\kappa)$, constant amplitude and an operating frequency of ω_0.

The signals $s_1(., t)$ and $s_2(., t)$ have the same phase and frequency. The phase difference between the two signals is a constant, in this case zero, i.e., $\vartheta(\kappa) - \vartheta(\kappa) = 0$, hence they are phase-coherent. Using Equation 4.2 it can be shown that when two signals are phase-coherent the degree of coherence is equal to 1 [74]:

$$\begin{aligned}
\rho &= \frac{E\{s_1(., t)s_2^*(., t)\}}{\sqrt{E\{|s_1(., t)|^2\}E\{|s_2(., t)|^2\}}} \\
&= \frac{p_1 p_2 e^{j(\omega_0 - \omega_0)t} E\{e^{j(\vartheta(.) - \vartheta(.))}\}}{\sqrt{E\{|p_1 e^{j(\omega_0 t + \vartheta(.))}|^2\}E\{|p_2 e^{j(\omega_0 t + \vartheta(.))}|^2\}}} \\
&= \frac{p_1 p_2}{\sqrt{p_1^2 p_2^2}} \\
&= 1.
\end{aligned} \tag{5.2}$$

Therefore $s_1(., t)$ and $s_2(., t)$ are 100% correlated or simply coherent.

5.2 Coherent Covariance Matrix Derivation

Assume a DOA estimation problem where the two coherent signals $s_1(., t)$ and $s_2(., t)$ described in Section 5.1 impinge on a 3-element ULA. The signals are arriving from the directions γ_1 and γ_2 respectively and the array elements are separated by a distance $d = \lambda/2$. The estimation problem assumes a noiseless case.

The two signals form a signal vector $\boldsymbol{s}(., t) = [s_1(., t) \quad s_2(., t)]^T$ and the signal covariance matrix denoted by $\boldsymbol{R}_{ss}$ is given as:

$$\begin{aligned}
\boldsymbol{R}_{ss} &= E\{\boldsymbol{s}(., t)\boldsymbol{s}^H(., t)\} \\
&= E\left\{\begin{bmatrix} s_1(., t) \\ s_2(., t) \end{bmatrix} \begin{bmatrix} s_1^*(., t) & s_2^*(., t) \end{bmatrix}\right\}
\end{aligned}$$

$$
\begin{aligned}
&= e^{j(\omega_0-\omega_0)t}\begin{bmatrix} p_1^2 E\{e^{j(\vartheta(.)-\vartheta(.))}\} & p_1p_2E\{e^{j(\vartheta(.)-\vartheta(.))}\} \\ p_1p_2E\{e^{j(\vartheta(.)-\vartheta(.))}\} & p_2^2E\{e^{j(\vartheta(.)-\vartheta(.))}\} \end{bmatrix} \\
&= \begin{bmatrix} p_1^2 & p_1p_2 \\ p_1p_2 & p_2^2 \end{bmatrix}. \qquad (5.3)
\end{aligned}
$$

A coherent array covariance matrix is derived for this problem and two Toeplitz matrices are reconstructed from the coherent covariance matrix using the CTOP and AVTOP decorrelation techniques. Based on the DOA estimation data model presented in Section 3.3, the array covariance matrix is given as

$$\boldsymbol{R} = \boldsymbol{A}\boldsymbol{R}_{ss}\boldsymbol{A}^H + \sigma^2\boldsymbol{I}, \qquad (5.4)$$

which reduces to

$$\boldsymbol{R} = \boldsymbol{A}\boldsymbol{R}_{ss}\boldsymbol{A}^H \qquad (5.5)$$

for a noiseless case. For the given case, the array steering matrix is a 3×2 matrix

$$\boldsymbol{A} = \begin{bmatrix} 1 & 1 \\ e^{-j\gamma_1} & e^{-j\gamma_2} \\ e^{-j2\gamma_1} & e^{-j2\gamma_2} \end{bmatrix}, \qquad (5.6)$$

where $\gamma_1 = \frac{2\pi d\sin(\theta_1)}{\lambda}$ and $\gamma_2 = \frac{2\pi d\sin(\theta_2)}{\lambda}$ are the electrical angles of $s_1(.,t)$ and $s_2(.,t)$ respectively. The angles θ_1 and θ_2 are the respective DOA (mechanical) angles. Substituting the expression for $\boldsymbol{R}_{ss}$ and $\boldsymbol{A}$ into Equation (5.5), the coherent array covariance matrix is obtained as follows

$$
\begin{aligned}
\boldsymbol{R}_C &= \boldsymbol{A}\boldsymbol{R}_{ss}\boldsymbol{A}^H \\
&= \begin{bmatrix} 1 & 1 \\ e^{-j\gamma_1} & e^{-j\gamma_2} \\ e^{-j2\gamma_1} & e^{-j2\gamma_2} \end{bmatrix} \begin{bmatrix} p_1^2 & p_1p_2 \\ p_1p_2 & p_2^2 \end{bmatrix} \begin{bmatrix} 1 & e^{j\gamma_1} & e^{j2\gamma_1} \\ 1 & e^{j\gamma_2} & e^{j2\gamma_2} \end{bmatrix} \qquad (5.7)
\end{aligned}
$$

where the subscript C denotes coherence. The final and simplified algebraic expression for $\boldsymbol{R}_C$ which was obtained through re-parameterisation of the original matrix is given as

$$\boldsymbol{R}_C =$$
$$\begin{bmatrix} \alpha+2\sigma & (\mu+\sigma)e^{j\gamma_1}+(\eta+\sigma)e^{j\gamma_2} & (\mu+\sigma)e^{j2\gamma_1}+(\eta+\sigma)e^{j2\gamma_2} \\ (\mu+\sigma)e^{-j\gamma_1}+(\eta+\sigma)e^{-j\gamma_2} & \alpha+\sigma\Theta & \mu e^{j\gamma_1}+\eta e^{j\gamma_2}+\sigma(e^{j\nu}+e^{j\upsilon}) \\ (\mu+\sigma)e^{-j2\gamma_1}+(\eta+\sigma)e^{-j2\gamma_2} & \mu e^{-j\gamma_1}+\eta e^{-j\gamma_2}+\sigma(e^{-j\upsilon}+e^{-j\nu}) & \alpha+\sigma\Phi \end{bmatrix}. \tag{5.8}$$

The significance of re-prameterising the variables of $\boldsymbol{R}_C$ is highlighted here.

5.2.1 Re-parameterisation

It is emphasised that, re-parameterisation of variables of the original expression of $\boldsymbol{R}_C$ was a very crucial step in this analysis. The process simplified the procedure of interpreting the structure of $\boldsymbol{R}_C$. Before re-parameterisation it was difficult to make any useful observation or interpretation from the original structure of $\boldsymbol{R}_C$. This is because its unsimplified expression is cumbersome and not manageable.

The re-parameterisation of matrix $\boldsymbol{R}_C$ was not just carried out by trial and error but based on the knowledge of the DOA estimation data model presented in Section 3.3. The objective of re-parameterisation was to isolate the complex exponentials $e^{j\gamma_1}, e^{j\gamma_2}, e^{j2\gamma_1}$ and $e^{j2\gamma_2}$ and their complex conjugates. These are the elements of the array steering matrix $\boldsymbol{A}$ which contains DOA information.

The parametric variables used to simplify the matrix $\boldsymbol{R}_C$ are defined as:

Electrical angles

(a) $\gamma = \frac{2\pi d}{\lambda}\sin(\theta)$

(b) $\Delta\gamma = \gamma_1 - \gamma_2$

(c) $\nu = 2\gamma_2 - \gamma_1, \quad \upsilon = 2\gamma_1 - \gamma_2$

Signal amplitudes

(a) $\mu = p_1^2, \quad \eta = p_2^2$

(b) $\alpha = \mu + \eta,\ \sigma = \sqrt{\mu\eta}$

(c) $q = 2\mu + \sigma\ , \quad r = 2\eta + \sigma$

Complex exponentials

(a) $\Theta = e^{j\Delta\gamma} + e^{-j\Delta\gamma}$

(b) $\Phi = e^{j2\Delta\gamma} + e^{-j2\Delta\gamma}$

5.2.2 Toeplitz matrix reconstruction

The CTOP and AVTOP decorrelation techniques were applied to the coherent array covariance matrix $\boldsymbol{R}_C$ to reconstruct two new decorrelated Toeplitz matrices. The decorrelation procedure of each Toeplitz technique is given in Section 4.5.

Let $\boldsymbol{R}_{CT}$ be the CTOP reconstructed Toeplitz matrix which is derived as:

$$\boldsymbol{R}_{CT} = \begin{bmatrix} \alpha+2\sigma & (\mu+\sigma)e^{j\gamma_1}+(\eta+\sigma)e^{j\gamma_2} & (\mu+\sigma)e^{j2\gamma_1}+(\eta+\sigma)e^{j2\gamma_2} \\ (\mu+\sigma)e^{-j\gamma_1}+(\eta+\sigma)e^{-j\gamma_2} & \alpha+2\sigma & (\mu+\sigma)e^{j\gamma_1}+(\eta+\sigma)e^{j\gamma_2} \\ (\mu+\sigma)e^{-j2\gamma_1}+(\eta+\sigma)e^{-j2\gamma_2} & (\mu+\sigma)e^{-j\gamma_1}+(\eta+\sigma)e^{-j\gamma_2} & \alpha+2\sigma \end{bmatrix}, \tag{5.9}$$

according to the CTOP reconstruction procedure and the AVTOP reconstructed Toeplitz matrix be $\boldsymbol{R}_{AVT}$, where:

$$\boldsymbol{R}_{AVT} = \begin{bmatrix} \frac{1}{3}[3\alpha+\sigma(2+\Theta+\Phi)] & \frac{1}{2}\left[qe^{-j\gamma_1}+re^{-j\gamma_2}+\sigma(e^{-j\nu}+e^{-j\upsilon})\right] & (\mu+\sigma)e^{-j2\gamma_1}+(\eta+\sigma)e^{-j2\gamma_2} \\ \frac{1}{2}\left[qe^{j\gamma_1}+re^{j\gamma_2}+\sigma(e^{j\nu}+e^{j\upsilon})\right] & \frac{1}{3}[3\alpha+\sigma(2+\Theta+\Phi)] & \frac{1}{2}\left[qe^{-j\gamma_1}+re^{-j\gamma_2}+\sigma(e^{-j\nu}+e^{-j\upsilon})\right] \\ (\mu+\sigma)e^{j2\gamma_1}+(\eta+\sigma)e^{j2\gamma_2} & \frac{1}{2}\left[qe^{j\gamma_1}+re^{j\gamma_2}+\sigma(e^{j\nu}+e^{j\upsilon})\right] & \frac{1}{3}[3\alpha+\sigma(2+\Theta+\Phi)] \end{bmatrix}. \tag{5.10}$$

The parametric variables contained in matrices $\boldsymbol{R}_{CT}$ and $\boldsymbol{R}_{AVT}$ are as defined in Section 5.2.1.

5.3 Investigation and Findings

The investigation of the derived matrices $\boldsymbol{R}_{C}$, $\boldsymbol{R}_{CT}$ and $\boldsymbol{R}_{AVT}$ focused on the distribution of complex exponentials $e^{j\gamma_1}$, $e^{j2\gamma_1}$, $e^{-j\gamma_1}$ and $e^{-j2\gamma_1}$ associated with source 1 steering vector as well as $e^{j\gamma_2}$, $e^{j2\gamma_2}$, $e^{-j\gamma_2}$ and $e^{-j2\gamma_2}$ associated with source 2 steering vector. These complex exponentials are treated as phasors (DOA phasors) that store DOA information.

5.3.1 Coherent array covariance matrix

As highlighted in the introduction of this chapter, the findings from this study provide an understanding as to why the CTOP decorrelation technique results in a more accurate DOA estimation and why the AVTOP decorrelation technique results in deviations from the true DOA. The following important observations were made by examining how the DOA phasors are organised in the entries of the rows and columns of $\boldsymbol{R}_{C}$.

Independent components

Each entry in the 1st row is made up of a sum of independent DOA phasors for sources $s_1(.,t)$ and $s_2(.,t)$. Note that the 1st column is a conjugate of the 1st row. Therefore, the same observation applies to its entries.

Figure 5.1 is a snapshot of the 1st row. Taking the first array element as a reference element, the first entry in this row is the autocorrelation of the reference element output. There are no DOA phasors present in this entry, thus all its terms are constants.

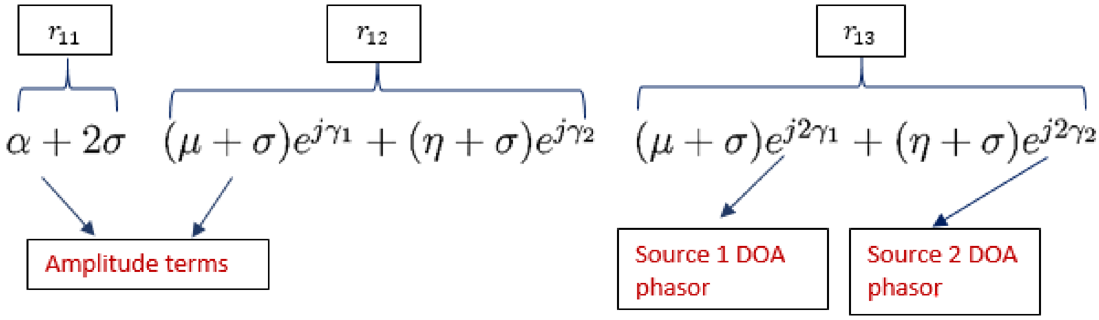

FIGURE 5.1: Row 1 observations.

The second entry is the correlation between the output of the second and the reference array elements and the third entry is the correlation between the output of the third and the reference array elements. The first row entries in expanded form are:

$$
\begin{aligned}
r_{11} &= \alpha + 2\sigma = p_1 + p_2 + 2p_1p_2, \\
r_{12} &= (\mu+\sigma)e^{j\gamma_1} + (\eta+\sigma)e^{j\gamma_2} = (p_1 + p_1p_2)e^{j\gamma_1} + (p_2 + p_1p_2)e^{j\gamma_2}, \\
r_{13} &= (\mu+\sigma)e^{j2\gamma_1} + (\eta+\sigma)e^{j2\gamma_2} = (p_1 + p_1p_2)e^{j2\gamma_1} + (p_2 + p_1p_2)e^{j2\gamma_2},
\end{aligned}
$$

where the amplitude of each DOA phasor is a linear combination of the source powers p_1 and p_2. It can be seen that in each entry of the first row (and column) the DOA phasors occur in a "*superposition*" form, that is, as independent sums.

Biased components

Apart from the 1st row and 1st column, every other column or row of $\boldsymbol{R}_C$ has an entry which is a sum of both independent DOA phasors and extra dependent terms. The extra terms are a result of the interaction or dependence between the two sources' DOA phasors. An example of this is entry r_{23} in the 2nd row and 3rd column, where

$$
\begin{aligned}
r_{23} &= \mu e^{j\gamma_1} + \eta e^{j\gamma_2} + \sigma(e^{j\nu} + e^{j\upsilon}) \\
&= p_1 e^{j\gamma_1} + p_2 e^{j\gamma_2} + p_1p_2(e^{j(2\gamma_2-\gamma_1)} + e^{j(2\gamma_1-\gamma_2)}).
\end{aligned}
$$

The terms $e^{j\nu} = e^{j(2\gamma_2-\gamma_1)}$ and $e^{j\upsilon} = e^{j(2\gamma_1-\gamma_2)}$ are referred to here as "*biased components*" because they are a result of an interaction between the DOA phasors $e^{-j\gamma_1}$, $e^{j2\gamma_1}$, $e^{-j\gamma_2}$ and $e^{j2\gamma_2}$ and are considered to cause bias in DOA information.

In a nutshell, a coherent array covariance matrix's first row and first column have entries in which DOA phasors occur in a superposition form without any biased components present. The remaining rows and columns have one entry, which is a linear combination of both independent and biased components.

The superposition claim

From the observations made on the algebraic structure of the coherent array covariance matrix, the following claim is made:

"The DOA information is preserved when the DOA phasors of the sources occur in a superposition form. That is, they occur as sums of the individual sources' information, in each of the off-diagonal entries of the array covariance matrix."

5.3.2 Toeplitz reconstructed matrices

It is evident that the CTOP reconstructed matrix contains undistorted DOA information due to the fact that it is constructed from the first row of $\boldsymbol{R}_C$. The first row contains the sum of DOA phasors in a superposition form, meaning there is no interaction between the DOA phasors. Thus, the reconstructed matrix's row space is equivalent to that of the ideal array covariance matrix. Recovering DOA information, free of interaction between the individual source information, is the principal behind successful decorrelation with the CTOP technique.

The problem of deviation in DOA estimation associated with the AVTOP technique is caused by the biased components in the information recovered during Toeplitz matrix reconstruction. Although the DOA information is recovered in a superposition form, extra dependent terms (biased components) are observed in the superdiagonals of matrix $\boldsymbol{R}_{AVT}$. This causes bias in the DOA information.

5.4 Verification of the Superposition Claim

In order to verify the "*superposition claim*", a multiple sources DOA estimation scenario is assumed. The array covariance matrices due to each source are derived independently and then summed. The noise is added in order to obtain the overall array covariance matrix.

The overall array covariance matrix is therefore given as a sum of the individual source array covariance matrices and the noise covariance matrix. Let the overall array covariance matrix be denoted by $\boldsymbol{R}_{OV}$ which is given as:

$$\boldsymbol{R}_{OV} = \sum_{i=1}^{N} \boldsymbol{R}_i + \sigma^2 \boldsymbol{I}, \tag{5.11}$$

where $\boldsymbol{R}_i$ is the array covariance matrix due to the ith source and $\sigma^2 \boldsymbol{I}$ is the noise covariance matrix. The verification was done using three DOA estimation scenarios described in Table 5.1.

TABLE 5.1: DOA estimation scenarios

Scenario	No. of array elements	No. of sources
1	3	2
2	4	2
3	4	3

For this purpose, consider three narrowband signal sources $s_i(\kappa, t) = e^{j(\omega_0 t + \vartheta_i(\kappa))}$ $(i = 1, 2, 3)$, each with a unity amplitude and a randomly changing phase $\vartheta(\kappa)$. The noise is assumed to be AWGN with a variance of σ^2. In each of the scenarios, the matrix $\boldsymbol{R}_{OV}$ is derived according to Equation (5.11).

The derivation of the individual source array covariance matrices (i.e. $\boldsymbol{R}_i = \boldsymbol{A}\boldsymbol{R}_{ss_i}\boldsymbol{A}^H, i = 1, 2, 3$) follow the same procedure as in Section 3.5, where an array covariance matrix based on a single source scenario was derived. For each scenario, the MUSIC algorithm is applied analytically as demonstrated in Section 3.5. In order to estimate the DOAs of the multiple sources, derivation and minimisation of a cost function need to be done.

Scenario 1: Three elements ULA and two sources

For scenario 1, the overall array covariance matrix is derived as

$$\begin{aligned}
\boldsymbol{R}_{OV} &= \boldsymbol{R}_1 + \boldsymbol{R}_2 + \sigma^2 \boldsymbol{I}_{3\times 3} \\
&= \boldsymbol{A}_1 \boldsymbol{R}_{ss_1} \boldsymbol{A}_1^H + \boldsymbol{A}_2 \boldsymbol{R}_{ss_2} \boldsymbol{A}_2^H + \sigma^2 \boldsymbol{I}_{3\times 3} \\
&= \begin{bmatrix} 1 & e^{j\gamma_1} & e^{j2\gamma_1} \\ e^{-j\gamma_1} & 1 & e^{j\gamma_1} \\ e^{-j2\gamma_1} & e^{-j\gamma_1} & 1 \end{bmatrix} + \begin{bmatrix} 1 & e^{j\gamma_2} & e^{j2\gamma_2} \\ e^{-j\gamma_2} & 1 & e^{j\gamma_2} \\ e^{-j2\gamma_2} & e^{-j\gamma_2} & 1 \end{bmatrix} + \sigma^2 \boldsymbol{I}_{3\times 3} \\
&= \begin{bmatrix} 2+\sigma^2 & e^{j\gamma_1} + e^{j\gamma_2} & e^{j2\gamma_1} + e^{j2\gamma_2} \\ e^{-j\gamma_1} + e^{-j\gamma_2} & 2+\sigma^2 & e^{j\gamma_1} + e^{j\gamma_2} \\ e^{-j2\gamma_1} + e^{-j2\gamma_2} & e^{-j\gamma_1} + e^{-j\gamma_2} & 2+\sigma^2 \end{bmatrix},
\end{aligned}$$

where $\boldsymbol{R}_1$ and $\boldsymbol{R}_2$ are the individual array covariance matrices for sources 1 and 2 respectively and $\boldsymbol{A}_i = [1, e^{-j\gamma_i}, e^{-j2\gamma_i}]^T$ (for $i = 1, 2$).

The derived noise eigenvalue-eigenvector pair for $\boldsymbol{R}$ is as given below

$$\lambda = \sigma^2, \quad \boldsymbol{v} = \begin{bmatrix} e^{j\gamma_1} e^{j\gamma_2} \\ -e^{j\gamma_1} - e^{j\gamma_2} \\ 1 \end{bmatrix}.$$

The matrix $\boldsymbol{V}_{\mathrm{n}}(\boldsymbol{\gamma})$ has one column formed by the noise eigenvector $\boldsymbol{v}$. Take note that in this case $\boldsymbol{\gamma} = [\gamma_1, \;\; \gamma_2]$.

Based on $\boldsymbol{V}_{\mathrm{n}}(\boldsymbol{\gamma})$ and the vector $\boldsymbol{w}(\phi) = \begin{bmatrix}1, & e^{-j\phi}, & e^{-j2\phi}\end{bmatrix}^T$, the cost function for this scenario is derived as:

$$\begin{aligned}
J_{32}(\phi, \boldsymbol{\gamma}) &= \boldsymbol{w}^H(\phi)\boldsymbol{V}_{\mathrm{n}}(\boldsymbol{\gamma})\boldsymbol{V}_{\mathrm{n}}^H(\boldsymbol{\gamma})\boldsymbol{w}(\phi) \\
&= (e^{j(\gamma_1+\gamma_2)} - e^{j(\gamma_1+\phi)} - e^{j(\gamma_2+\phi)} + e^{j2\phi})(e^{-j(\gamma_1+\gamma_2)} - e^{-j(\gamma_1+\phi)} - e^{-j(\gamma_2+\phi)} \\
&+ e^{-j2\phi}) \\
&= 4 - 4\cos(\gamma_1 - \phi) - 4\cos(\gamma_2 - \phi) + 2\cos(\gamma_1 + \gamma_2 - 2\phi) + 2\cos(\gamma_1 - \gamma_2)
\end{aligned} \tag{5.12}$$

and the minimisation of $J_{32}(\phi, \boldsymbol{\gamma})$ yields

$$\begin{aligned}
&\frac{\partial}{\partial\phi}J_{32}(\phi, \boldsymbol{\gamma}) = 4\sin(\gamma_1 + \gamma_2 - 2\phi) - 4\sin(\gamma_1 - \phi) - 4\sin(\gamma_2 - \phi) \\
&4\sin(\gamma_1 + \gamma_2 - 2\phi) - 4\sin(\gamma_1 - \phi) - 4\sin(\gamma_2 - \phi) = 0.
\end{aligned} \tag{5.13}$$

Equation (5.13) is satisfied when ϕ is equal to any of the target directions γ_1 and γ_2. This confirms that the cost function $J_{32}(\phi, \boldsymbol{\gamma})$ has two global minima, one at $\phi = \gamma_1$ and the other at $\phi = \gamma_2$. Assume that $\gamma_1 = 0.6981$ radians and $\gamma_2 = 2.6180$ radians, the cost function and its derivative are plotted in Figure 5.2.

In Figure 5.3 the cost function $J_{32}(\phi, \boldsymbol{\gamma})$ is plotted as a surface using contours, where source 1 direction traverses the whole angular space and source 2 direction is held constant at $\gamma_2 = 2.6180$ radians.

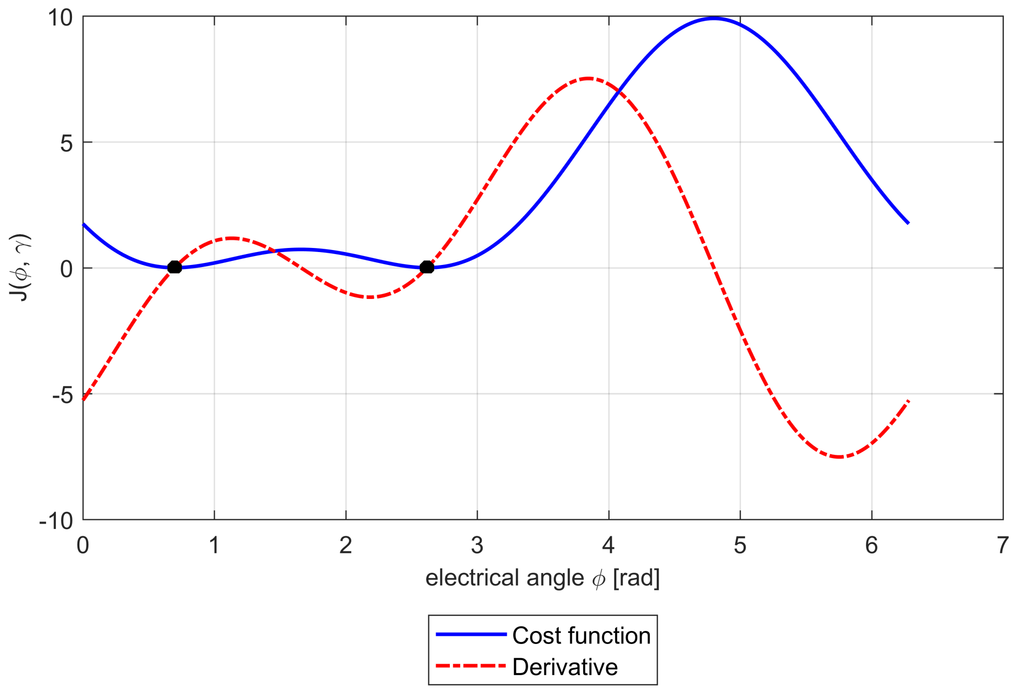

FIGURE 5.2: Two sources and three elements ULA.

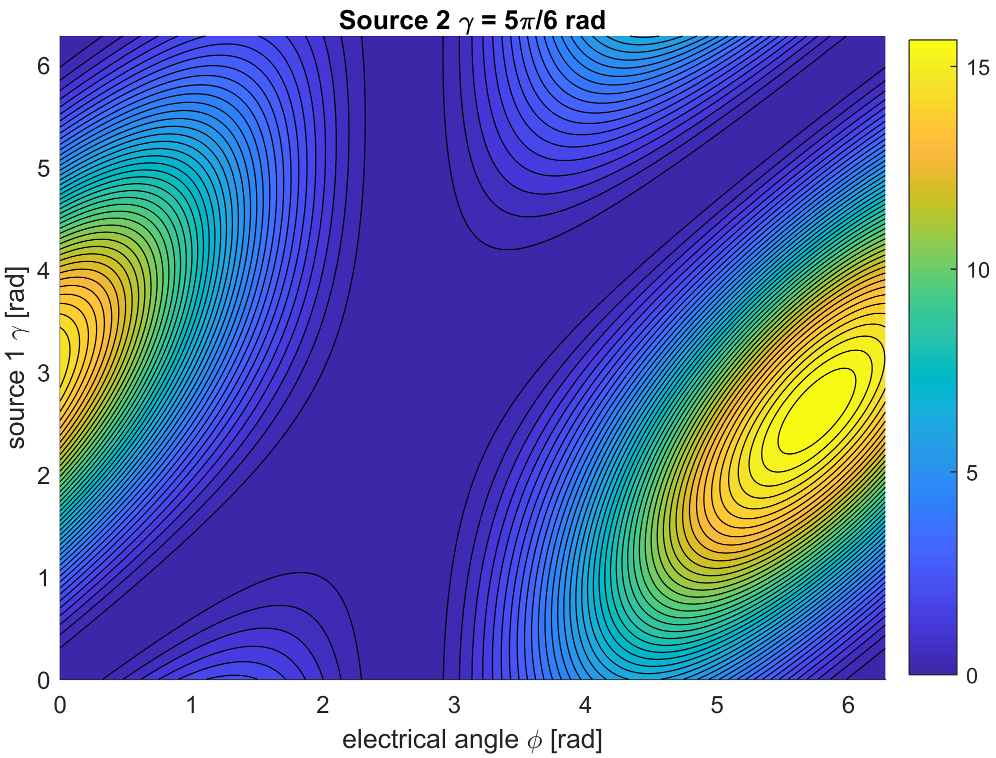

FIGURE 5.3: $J_{32}(\phi, \gamma)$ surface plot.

Scenario 2: Four elements ULA and two sources

The algebraic expression for $\boldsymbol{R}_{OV}$ is derived as

$$\begin{aligned}
\boldsymbol{R}_{OV} &= \boldsymbol{R}_1 + \boldsymbol{R}_2 + \sigma^2 \boldsymbol{I}_{4\times4} \\
&= \boldsymbol{A}_1 \boldsymbol{R}_{ss_1} \boldsymbol{A}_1^H + \boldsymbol{A}_2 \boldsymbol{R}_{ss_2} \boldsymbol{A}_2^H + \sigma^2 \boldsymbol{I}_{4\times4} \\
&= \begin{bmatrix} 1 & e^{j\gamma_1} & e^{j2\gamma_1} & e^{j3\gamma_1} \\ e^{-j\gamma_1} & 1 & e^{j\gamma_1} & e^{j2\gamma_1} \\ e^{-j2\gamma_1} & e^{-j\gamma_1} & 1 & e^{j\gamma_1} \\ e^{-j3\gamma_1} & e^{-j2\gamma_1} & e^{-j\gamma_1} & 1 \end{bmatrix} + \begin{bmatrix} 1 & e^{j\gamma_2} & e^{j2\gamma_2} & e^{j3\gamma_2} \\ e^{-j\gamma_2} & 1 & e^{j\gamma_2} & e^{j2\gamma_2} \\ e^{-j2\gamma_2} & e^{-j\gamma_2} & 1 & e^{j\gamma_2} \\ e^{-j3\gamma_2} & e^{-j2\gamma_2} & e^{-j\gamma_2} & 1 \end{bmatrix} + \sigma^2 \boldsymbol{I}_{4\times4} \\
&= \begin{bmatrix} 2+\sigma^2 & e^{j\gamma_1}+e^{j\gamma_2} & e^{j2\gamma_1}+e^{j2\gamma_2} & e^{j3\gamma_1}+e^{j3\gamma_2} \\ e^{-j\gamma_1}+e^{-j\gamma_2} & 2+\sigma^2 & e^{j\gamma_1}+e^{j\gamma_2} & e^{j2\gamma_1}+e^{j2\gamma_2} \\ e^{-j2\gamma_1}+e^{-j2\gamma_2} & e^{-j\gamma_1}+e^{-j\gamma_2} & 2+\sigma^2 & e^{j\gamma_1}+e^{j\gamma_2} \\ e^{-j3\gamma_1}+e^{-j3\gamma_2} & e^{-j2\gamma_1}+e^{-j2\gamma_2} & e^{-j\gamma_1}+e^{-j\gamma_2} & 2+\sigma^2 \end{bmatrix}
\end{aligned}$$

where $\boldsymbol{A}_i = [1, e^{-j\gamma_i}, e^{-j2\gamma_i}, e^{-j3\gamma_i}]^T$ (for $i = 1, 2$).

The derived noise eigenvalues and eigenvectors for the matrix $\boldsymbol{R}_{OV}$ are as follow

$$\lambda_1 = \sigma^2, \quad \boldsymbol{v}_1 = \begin{bmatrix} e^{j\gamma_1} e^{j\gamma_2} \\ -e^{j\gamma_1} - e^{j\gamma_2} \\ 1 \\ 0 \end{bmatrix}$$

$$\lambda_2 = \sigma^2, \quad \boldsymbol{v}_2 = \begin{bmatrix} e^{j\gamma_1} e^{j2\gamma_2} + e^{j2\gamma_1} e^{j\gamma_2} \\ -e^{j2\gamma_1} - e^{j2\gamma_2} - e^{j\gamma_1} e^{j\gamma_2} \\ 0 \\ 1 \end{bmatrix}.$$

The matrix $\boldsymbol{V}_n(\boldsymbol{\gamma})$, in this case is a 4×2 matrix whose columns are the noise eigenvectors $\boldsymbol{v}_1$ and $\boldsymbol{v}_2$ as shown below

$$\boldsymbol{V}_{\mathrm{n}}(\boldsymbol{\gamma}) = \begin{bmatrix} e^{j\gamma_1}e^{j\gamma_2} & e^{j\gamma_1}e^{j2\gamma_2} + e^{j2\gamma_1}e^{j\gamma_2} \\ -e^{j\gamma_1} - e^{j\gamma_2} & -e^{j2\gamma_1} - e^{j2\gamma_2} - e^{j\gamma_1}e^{j\gamma_2} \\ 1 & 0 \\ 0 & 1 \end{bmatrix}$$

where $\boldsymbol{\gamma} = [\gamma_1, \ \ \gamma_2]$. The cost function is derived using $\boldsymbol{w}(\phi) = \left[1, \ e^{-j\phi}, \ e^{-j2\phi}, \ e^{-j3\phi}\right]^T$ and $\boldsymbol{V}_{\mathrm{n}}(\boldsymbol{\gamma})$ as shown below

$$\begin{aligned} J_{42}(\phi, \boldsymbol{\gamma}) =& \boldsymbol{w}^H(\phi)\boldsymbol{V}_{\mathrm{n}}(\gamma)\boldsymbol{V}_{\mathrm{n}}^H(\gamma)\boldsymbol{w}(\phi) \\ =&(e^{j(\gamma_1+\gamma_2)} - e^{j(\gamma_1+\phi)} - e^{j(\gamma_2+\phi)} + e^{j2\phi})(e^{-j(\gamma_1+\gamma_2)} - e^{-j(\gamma_1+\phi)} - e^{-j(\gamma_2+\phi)} \\ &+ e^{-j2\phi})(e^{j(\gamma_1+2\gamma_2)} + e^{j(2\gamma_1+\gamma_2)} - e^{j(2\gamma_1+\phi)} - e^{j(2\gamma_2+\phi)} - e^{j(\gamma_1+\gamma_2+\phi)} + e^{j3\phi}) \\ &(e^{-j(\gamma_1+2\gamma_2)} + e^{-j(2\gamma_1+\gamma_2)} - e^{-j(2\gamma_1+\phi)} - e^{-j(2\gamma_2+\phi)} - e^{-j(\gamma_1+\gamma_2+\phi)} + e^{-j3\phi}) \\ =&10 - 8\cos(\gamma_1 - \phi) - 8\cos(\gamma_2 - \phi) - 2\cos\left[2(\gamma_1 - \phi)\right] - 2\cos\left[2(\gamma_2 - \phi)\right] \\ &- 2\cos(2\gamma_1 - \gamma_2 - \phi) - 2\cos(2\gamma_2 - \gamma_1 - \phi) + 2\cos(2\gamma_2 + \gamma_1 - 3\phi) + \\ &2\cos(2\gamma_1 + \gamma_2 - 3\phi) + 2\cos\left[2(\gamma_1 - \gamma_2)\right] + 8\cos(\gamma_1 - \gamma_2) \end{aligned} \tag{5.14}$$

The minimisation of $J_{42}(\phi, \boldsymbol{\gamma})$ yields

$$\begin{aligned} &\frac{\partial}{\partial\phi}J(\phi, \boldsymbol{\gamma}) = 6\sin(2\gamma_1 + \gamma_2 - 3\phi) + 6\sin(2\gamma_2 + \gamma_1 - 3\phi) - 8\sin(\gamma_1 - \phi) \\ &- 8\sin(\gamma_2 - \phi) - 4\sin\left[2(\gamma_1 - \phi)\right] - 4\sin\left[2(\gamma_2 - \phi)\right] - 2\sin(2\gamma_1 - \gamma_2 - \phi) \\ &- 2\sin(2\gamma_2 - \gamma_1 - \phi) \end{aligned}$$

$$\begin{aligned} &6\sin(2\gamma_1 + \gamma_2 - 3\phi) + 6\sin(2\gamma_2 + \gamma_1 - 3\phi) - 8\sin(\gamma_1 - \phi) - 8\sin(\gamma_2 - \phi) \\ &- 4\sin\left[2(\gamma_1 - \phi)\right] - 4\sin\left[2(\gamma_2 - \phi)\right] - 2\sin(2\gamma_1 - \gamma_2 - \phi) \\ &- 2\sin(2\gamma_2 - \gamma_1 - \phi) = 0 \end{aligned} \tag{5.15}$$

It is observed that substituting γ_1 or γ_2 for ϕ in Equation (5.15), the result is zero. This confirms that $J_{42}(\phi, \boldsymbol{\gamma})$ has two global minima at $\phi = \gamma_1$ and $\phi = \gamma_2$. Again assuming that $\gamma_1 = 0.6981$ radians and $\gamma_2 = 2.6180$ radians (as in scenario 1), the cost function and its derivative are plotted and the two global minima can be seen at the target directions indicated by the dots in Figure 5.4. The cost function $J_{42}(\phi, \boldsymbol{\gamma})$ has also been plotted as a surface, with source 1 direction scanning through the entire angular space and source 2 held constant at $\gamma_2 = 2.6180$ radians as shown in Figure 5.5.

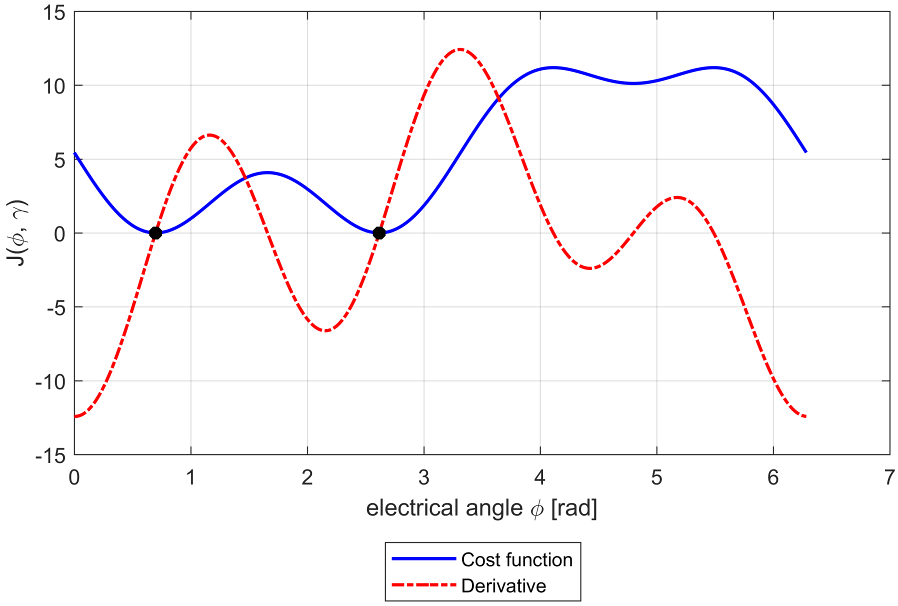

FIGURE 5.4: Two sources and four elements ULA.

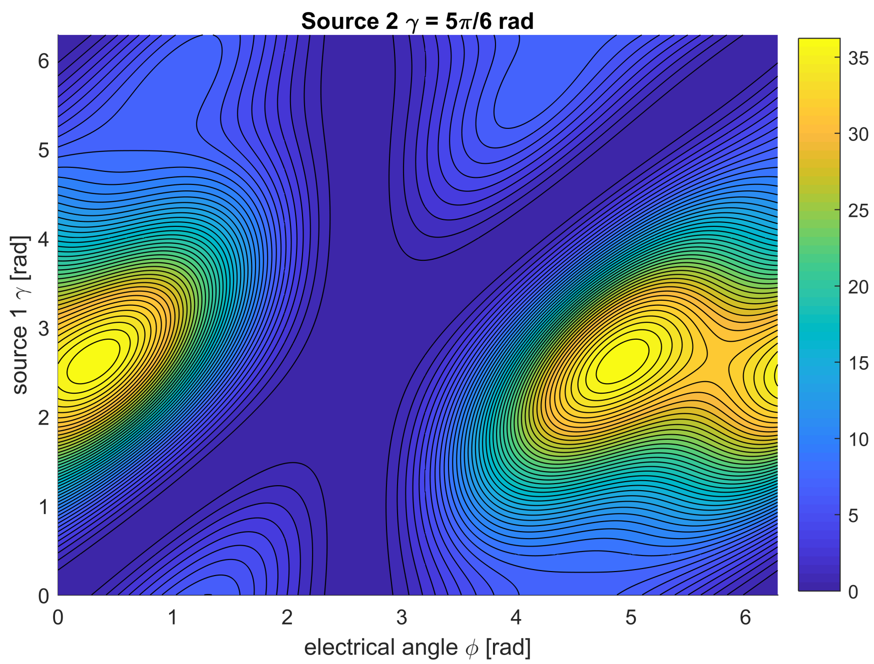

FIGURE 5.5: $J_{42}(\phi, \boldsymbol{\gamma})$ surface plot.

Scenario 3: Four elements ULA and three sources

The expression for the array covariance matrix for this scenario is derived as

$$\begin{aligned}
\boldsymbol{R}_{OV} &= \boldsymbol{R}_1 + \boldsymbol{R}_2 + \boldsymbol{R}_3 + \sigma^2 \boldsymbol{I}_{4\times4} \\
&= \boldsymbol{A}_1 \boldsymbol{R}_{ss_1} \boldsymbol{A}_1^H + \boldsymbol{A}_2 \boldsymbol{R}_{ss_2} \boldsymbol{A}_2^H + \boldsymbol{A}_3 \boldsymbol{R}_{ss_3} \boldsymbol{A}_3^H + \sigma^2 \boldsymbol{I}_{4\times4} \\
&= \begin{bmatrix} 1 & e^{j\gamma_1} & e^{j2\gamma_1} & e^{j3\gamma_1} \\ e^{-j\gamma_1} & 1 & e^{j\gamma_1} & e^{j2\gamma_1} \\ e^{-j2\gamma_1} & e^{-j\gamma_1} & 1 & e^{j\gamma_1} \\ e^{-j3\gamma_1} & e^{-j2\gamma_1} & e^{-j\gamma_1} & 1 \end{bmatrix} + \begin{bmatrix} 1 & e^{j\gamma_2} & e^{j2\gamma_2} & e^{j3\gamma_2} \\ e^{-j\gamma_2} & 1 & e^{j\gamma_2} & e^{j2\gamma_2} \\ e^{-j2\gamma_2} & e^{-j\gamma_2} & 1 & e^{j\gamma_2} \\ e^{-j3\gamma_2} & e^{-j2\gamma_2} & e^{-j\gamma_2} & 1 \end{bmatrix} \\
&+ \begin{bmatrix} 1 & e^{j\gamma_3} & e^{j2\gamma_3} & e^{j3\gamma_3} \\ e^{-j\gamma_3} & 1 & e^{j\gamma_3} & e^{j2\gamma_3} \\ e^{-j2\gamma_3} & e^{-j\gamma_3} & 1 & e^{j\gamma_3} \\ e^{-j3\gamma_3} & e^{-j2\gamma_3} & e^{-j\gamma_3} & 1 \end{bmatrix} + \sigma^2 \boldsymbol{I}_{4\times4} \\
&= \begin{bmatrix} 3+\sigma^2 & e^{j\gamma_1}+e^{j\gamma_2}+e^{j\gamma_3} & e^{j2\gamma_1}+e^{j2\gamma_2}+e^{j2\gamma_3} & e^{j3\gamma_1}+e^{j3\gamma_2}+e^{j3\gamma_3} \\ e^{-j\gamma_1}+e^{-j\gamma_2}+e^{-j\gamma_3} & 3+\sigma^2 & e^{j\gamma_1}+e^{j\gamma_2}+e^{j\gamma_3} & e^{j2\gamma_1}+e^{j2\gamma_2}+e^{j2\gamma_3} \\ e^{-j2\gamma_1}+e^{-j2\gamma_2}+e^{-j2\gamma_3} & e^{-j\gamma_1}+e^{-j\gamma_2}+e^{-j\gamma_3} & 3+\sigma^2 & e^{j\gamma_1}+e^{j\gamma_2}+e^{j\gamma_3} \\ e^{-j3\gamma_1}+e^{-j3\gamma_2}+e^{-j3\gamma_3} & e^{-j2\gamma_1}+e^{-j2\gamma_2}+e^{-j2\gamma_3} & e^{-j\gamma_1}+e^{-j\gamma_2}+e^{-j\gamma_3} & 3+\sigma^2 \end{bmatrix}
\end{aligned}$$

where $\boldsymbol{A}_i = [1, e^{-j\gamma_i}, e^{-j2\gamma_i}, e^{-j3\gamma_i}]^T$ (for $i = 1, 2, 3$) are the array steering matrices for each source.

The derived noise eigenvalue and eigenvector pair is given below. The noise eigenvector has an algebraic multiplicity of one. As a result, there is one corresponding noise eigenvector.

$$\lambda = \sigma^2, \quad \boldsymbol{v} = \begin{bmatrix} -e^{j\gamma_1} e^{j\gamma_2} e^{j\gamma_3} \\ e^{j\gamma_1} e^{j\gamma_2} + e^{j\gamma_1} e^{j\gamma_3} + e^{j\gamma_2} e^{j\gamma_3} \\ -e^{j\gamma_1} - e^{j\gamma_2} - e^{j\gamma_3} \\ 1 \end{bmatrix}.$$

The eigenvector $\boldsymbol{v}$ forms the matrix $\boldsymbol{V}_{\mathrm{n}}(\boldsymbol{\gamma})$ where in this case $\boldsymbol{\gamma} = [\gamma_1,\ \gamma_2,\ \gamma_3]$. Using the vector $\boldsymbol{w}(\phi)$ (same expression as used in scenario 2) and $\boldsymbol{V}_{\mathrm{n}}(\boldsymbol{\gamma})$ the cost function is derived as follows:

$$
\begin{aligned}
&J_{43}(\phi,\boldsymbol{\gamma}) = \boldsymbol{w}^H(\phi)\boldsymbol{V}_\mathrm{n}(\boldsymbol{\gamma})\boldsymbol{V}_\mathrm{n}^H(\boldsymbol{\gamma})\boldsymbol{w}(\phi)\\
&= (e^{-j3\phi} + e^{-j\phi}(e^{-j(\gamma_1+\gamma_2)} + e^{-j(\gamma_1+\gamma_3)} + e^{-j(\gamma_2+\gamma_3)}) - e^{-j2\phi}(e^{-j\gamma_1} + e^{-j\gamma_2} + e^{-j\gamma_3})\\
&- e^{-j\gamma_1}e^{-j\gamma_2}e^{-j\gamma_3})(e^{j3\phi} + e^{j\phi}(e^{j(\gamma_1+\gamma_2)} + e^{j(\gamma_1+\gamma_3)} + e^{j(\gamma_2+\gamma_3)})\\
&- e^{j2\phi}(e^{j\gamma_1} + e^{j\gamma_2} + e^{j\gamma_3}) - e^{j\gamma_1}e^{j\gamma_2}e^{j\gamma_3})\\
&= 8 - 8\cos(\gamma_1-\phi) - 8\cos(\gamma_2-\phi) - 8\cos(\gamma_3-\phi) + 4\cos(\gamma_1+\gamma_2-2\phi)\\
&+ 4\cos(\gamma_1+\gamma_3-2\phi) + 4\cos(\gamma_2+\gamma_3-2\phi) - 2\cos(\gamma_1+\gamma_2+\gamma_3-3\phi)\\
&- 2\cos(\gamma_1+\gamma_2-\gamma_3-\phi) - 2\cos(\gamma_1+\gamma_3-\gamma_2-\phi) - 2\cos(\gamma_2+\gamma_3-\gamma_1-\phi)\\
&+ 4\cos(\gamma_1-\gamma_2) + 4\cos(\gamma_1-\gamma_3) + 4\cos(\gamma_2-\gamma_3)
\end{aligned}
\tag{5.16}
$$

The cost function is minimised by taking taking a partial derivative with respect to ϕ and equating the result to zero as shown below:

$$
\begin{aligned}
&\frac{\partial}{\partial\phi}J_{43}(\phi,\boldsymbol{\gamma}) = 8\sin(\gamma_1+\gamma_2-2\phi) + 8\sin(\gamma_1+\gamma_3-2\phi) + 8\sin(\gamma_2+\gamma_3-2\phi)\\
&- 8\sin(\gamma_1-\phi) - 8\sin(\gamma_2-\phi) - 8\sin(\gamma_3-\phi) - 2\sin(\gamma_1+\gamma_2-\gamma_3-\phi)\\
&- 2\sin(\gamma_1+\gamma_3-\gamma_2-\phi) - 2\sin(\gamma_2+\gamma_3-\gamma_1-\phi) - 6\sin(\gamma_1+\gamma_2+\gamma_3-3\phi)
\end{aligned}
$$

$$
\begin{aligned}
&8\sin(\gamma_1+\gamma_2-2\phi) + 8\sin(\gamma_1+\gamma_3-2\phi) + 8\sin(\gamma_2+\gamma_3-2\phi)\\
&- 8\sin(\gamma_1-\phi) - 8\sin(\gamma_2-\phi) - 8\sin(\gamma_3-\phi) - 2\sin(\gamma_1+\gamma_2-\gamma_3-\phi)\\
&- 2\sin(\gamma_1+\gamma_3-\gamma_2-\phi) - 2\sin(\gamma_2+\gamma_3-\gamma_1-\phi) - 6\sin(\gamma_1+\gamma_2+\gamma_3-3\phi) = 0.
\end{aligned}
\tag{5.17}
$$

It has been confirmed that $J_{43}(\phi,\boldsymbol{\gamma})$ has three global minima at ϕ equal to the electrical angles γ_1, γ_2 and γ_3. Assuming the three sources have electrical angles $\gamma_1 = 0.6981$ radians, $\gamma_2 = 2.6180$ radians and $\gamma_3 = 4.3633$ radians, the plot of $J_{43}(\phi,\boldsymbol{\gamma})$ and its derivative is generated in Figure 5.6.

Using contours, the cost function is plotted as a surface in Figure 5.7. In this case sources 2 and 3 directions are held constant at $\gamma_2 = 2.6180$ radians and $\gamma_3 = 4.3633$ radians respectively while source 1 direction traverse the whole angular space.

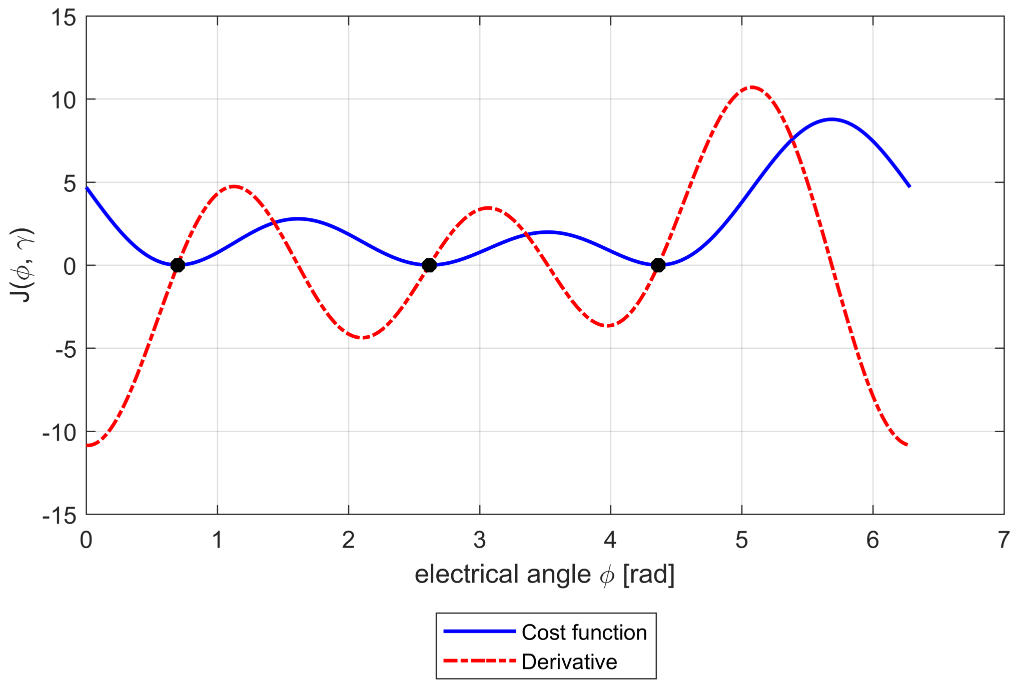

FIGURE 5.6: Three sources and four elements ULA.

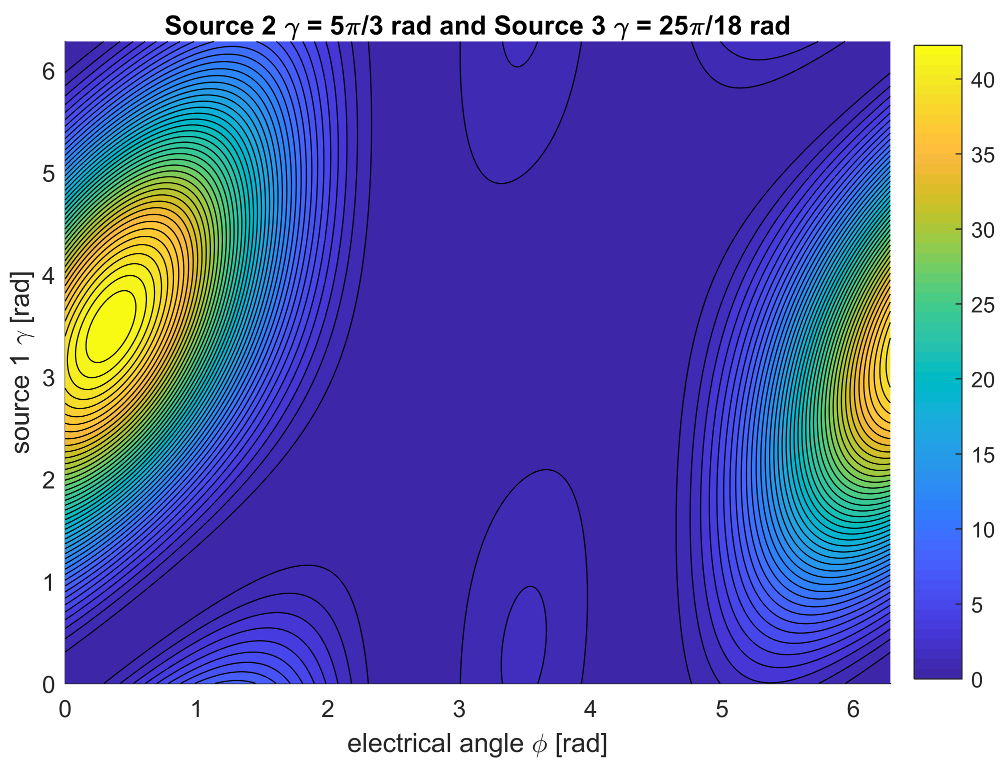

FIGURE 5.7: $J_{43}(\phi, \gamma)$ contour plot.

5.5 Discussion

From the scenarios studied above it has been verified that when the signal sources' DOA information is stored in a superposition form, their directions are independent of each other and can be estimated without any deviation from the true direction. Further observations made from the plots of cost functions and their derivatives presented in Figures 5.2 to 5.7 and from the derived expressions are discussed.

5.5.1 Line plots observations

(a) Global minima

In general, it has been observed that the cost function in each scenario has a unique solution at $\phi = \gamma$. It is unique in a sense that the cost function is only equal to zero i.e. $J(\boldsymbol{\gamma}, \phi) = 0$, at $\phi = \gamma$ and has a global minimum at this point and not anywhere else.

In Figures 5.2 and 5.4, each cost function has two global minima, one at $\phi = \gamma_1$ and the other at $\phi = \gamma_2$, which are the electrical angles for sources 1 and 2 respectively. The cost function in Figure 5.6 has three global minima at ϕ equal to the electrical angles $\gamma_1 = 0.6981$ radians, $\gamma_2 = 2.6180$ radians and $\gamma_3 = 4.3633$ radians for the three signal sources.

At each global minimum both the cost functions and their respective derivatives have a value of zero. As mentioned earlier, $J(\boldsymbol{\gamma}, \phi) = 0$ at ϕ equal to the electrical angle due to the orthogonality between the matrix $\boldsymbol{V}_{\mathrm{n}}(\gamma)$ and the vector $\boldsymbol{w}(\phi)$.

(b) Local minima

The cost functions in Figures 5.2 and 5.6 have no local minima. In Figure 5.4, which represents a scenario of two signal sources and an array of four elements, the cost function has one local minimum. In the case of multiple signal sources, the number of local minima may be equal to the maximum number of possible local minima or less depending on the direction γ of each source and the angle of separation between the sources.

In scenario 3, if the local minimum is present, it is either on one side or sandwiched by the two global minima. If it is sandwiched by the two global minima it was found that it always occurs at

$$\phi = \frac{\gamma_1 + \gamma_2}{2} \tag{5.18}$$

and if the local minimum is on one side as shown in Figure 5.4, the position of the local minimum is given by

$$\phi = 1.53\pi. \tag{5.19}$$

5.5.2 Contour plots observations

In each contour plot the axes represent the parameters γ and ϕ of the cost functions. On the y-axis of each plot the source 1 direction γ_1 is varied from 0 to 2π and on the x-axis the parameter ϕ which represents all the possible source directions is also varied from 0 to 2π. The sources 2 and 3 directions are held constant at 2.6180 radians and 4.3633 radians respectively.

It can be seen that all the contour plots confirm the existence of unique global minima at all values of ϕ corresponding to the true DOAs of the sources. Take note that in this case a global minimum is not a single point but a narrow plane stretching across the entire plot. Each global minimum traverses the contour plot along a straight line going through the points where ϕ and γ are equal and the global minimum is also symmetric about this line.

The global minima are shaded with a violet colour on each contour plot and are at a zero elevation as indicated on the colour bars. This confirms the observation that the cost functions have a unique value of zero at the global minima and not anywhere else.

(a) Diagonally traversing global minima

In each of the Figures 5.3, 5.5 and 5.7 a global minimum traverses along the diagonal of the contour plot. This global minimum is a narrow plane symmetric about a straight line $\gamma_1 = \phi$ which is joining the points $(0, 0)$ and $(2\pi, 2\pi)$. Take note that for each point on this line the values of γ_1 and ϕ are equal.

(b) Vertically traversing global minima

Each of the contour plots in Figures 5.3 and 5.5 has one vertically traversing global minimum. This global minimum is a narrow plane that vertically traverses along the vertical line $\phi = 2.6180$ corresponding to the direction of source 2. The contour plot in Figure 5.7 has two vertically traversing global minima one along the vertical line $\phi = 2.6180$ and another one along the vertical line $\phi = 4.3633$ corresponding to the sources 2 and 3 directions.

(c) The merger of global minima

A very insightful observation from all three contour plots is that, when two or more sources are closely spaced, their global minima merge. In a practical sense this would result in a DOA estimator being unable to resolve the DOA of the sources and these sources may be identified as a single source.

A good scenario is in Figure 5.7 where there are two vertically traversing global minima corresponding to the sources 2 and 3 directions. If the two sources are moved any further towards each other the two global minima will completely merge. The MUSIC estimator would detect them as a single source with a direction $\gamma = \frac{\gamma_1+\gamma_2}{2}$ radians, where γ_1 and γ_2 are the individual sources directions.

(d) Peaks and Saddles

The yellowish peaks on the contour plots represent the global maxima of the cost functions and do not provide any useful or relevant information to this analysis. However, what is worth noticing is a saddle sandwiched by two peaks as appearing in Figure 5.5. The saddle is a local minimum which would correspond to a secondary (false) peak in the MUSIC spatial spectrum.

5.5.3 Noise influence on DOA

Through the analytic application of the MUSIC algorithm, it has been observed that if the exact array covariance matrix is known and the noise at the ULA is additive white Gaussian noise, the noise has no influence on the directions of the sources. This has been deduced from the fact that, the noise eigenvector expressions, which are crucial in the derivation of the MUSIC spectrum function do not contain any noise component.

5.6 Summary

This chapter explained the principle behind the performance of the CTOP and AVTOP decorrelation techniques. The findings show that the accuracy of the CTOP technique is attributed to retaining the source DOA information in a superposition form. The deviation in DOA estimation associated with the AVTOP technique is a result of retaining biased DOA information. The superposition form claim was verified using specific DOA estimation scenarios where the MUSIC algorithm was applied analytically in order to estimate the DOA of the sources based on each scenario.

CHAPTER 6

Numerical Simulations

In this chapter, the performance of the CTOP and AVTOP decorrelation techniques applied with the MUSIC algorithm is investigated through numerical simulations for DOA estimation of coherent and non-coherent sources. The performance of the classic MUSIC algorithm is also investigated for benchmarking purposes. In the first section, the simulations' background information is given. The second section presents the simulation results for the performance of each technique. The performance is evaluated in terms of spatial spectrum, average standard deviation, probability of success (POS) and the Root Mean Square Error (RMSE) in DOA estimation. The performance metrics were computed for different levels of SNR and number of array elements. In the last section, the spatial spectra of the CTOP MUSIC derived from different rows of the coherent covariance matrix are investigated.

6.1 Simulations Background

The simulations were conducted in order to assess the performance of the CTOP and AVTOP decorrelation techniques. Each technique was applied in conjunction with the classic MUSIC algorithm to estimate the DOA of two sources for both coherent and non-coherent scenarios. The performance of the classic MUSIC algorithm was also evaluated for the same conditions in order to provide a baseline for comparison.

After combining each decorrelation technique with MUSIC, the resultant algorithms were referred to as

(a) AVTOP MUSIC: the classic MUSIC algorithm applied with the AVTOP decorrelation technique.

(b) CTOP MUSIC: the classic MUSIC algorithm applied with the CTOP decorrelation technique.

The simulations were implemented and run in MATLAB based on a ULA DOA estimation data model described in Section 3.3.

Coherent scenario

In order to emulate coherence of the signal sources, a multipath propagation scenario was assumed. For simplicity, consider a narrowband signal $s_1(t) = e^{j\omega_0 t}$ with unity amplitude and a DOA (mechanical angle) of $\theta_1 = -40°$ as a direct component and the reflected component as $s_2(t) = e^{j\omega_0 t}$ arriving from direction $\theta_2 = 30°$. The direct and reflected components have the operating frequency ω_0 and a phase of $0°$.

Non-coherent scenario

In the case of a non-coherent scenario, assume that the two narrowband signals $s_1(t)$ and $s_2(t)$ are emitted from different sources with different operating frequencies. The signal $s_1(t) = e^{j\omega_1 t}$ is arriving from direction $\theta_1 = -40°$ and signal $s_2(t) = e^{j\omega_2 t}$ is arriving from direction $\theta_2 = 30°$ and they are mutually independent.

The classic MUSIC, AVTOP MUSIC and CTOP MUSIC algorithms were applied for the estimation of sources $s_1(t)$ and $s_2(t)$ directions in the two scenarios. In comparison to the algebraic analysis where the exact array covariance matrix is known, in the numerical case a sample array covariance matrix is approximated by taking 1024 snapshots of the received data.

The following simulation parameters were fixed for all the simulations:

(a) Number of data snapshots $K = 1024$.

(b) Coherent scenario: operating frequency $\omega_0 = 800$ KHz.

(c) Non-coherent scenario: Operating frequencies $\omega_1 = 800$ KHz and $\omega_2 = 300$ KHz.

(d) Array element spacing $d = \frac{\lambda}{2}$.

6.2 Performance Results

The first part of the results presents the spectra of the CTOP MUSIC, AVTOP MUSIC and the classic MUSIC algorithms for the estimation of $s_1(t)$ and $s_2(t)$ DOAs. The second part presents the performance results of the three algorithms obtained by varying the number of sensors while the third part presents the performance results obtained by varying the SNR. The performance is evaluated in terms of Root Mean Square Error (RMSE), average standard deviation and probability of success (POS).

6.2.1 Performance metrics definition

The following are the definitions of the metrics used to evaluate the performance of the three algorithms.

The definition of RMSE is given by [21, 67, 78], defined as

$$RMSE = \sqrt{\frac{1}{T}\sum_{i=1}^{T}(\theta_i - \hat{\theta}_i)^2} \tag{6.1}$$

while the standard deviation in the estimates of each source is defined as

$$SD = \sqrt{\sum_{i=1}^{T} \frac{(\hat{\theta}_i - \hat{\theta}_{av})^2}{T}}, \tag{6.2}$$

and therefore the average standard deviation in the estimates of both sources is given by

$$average\ SD = \frac{SD_1 + SD_2}{2}. \tag{6.3}$$

In the case of the probability of success, an event is defined as a success if it satisfies the condition $max(|\hat{\theta}_i - \theta_i|) < \epsilon$, for $i = 1, ..., N$ [79]. For this study, ϵ was chosen to be 0.8 degrees for comparison versus SNR and the number of sensors. For a particular simulation trial or event, the absolute value of the difference between the DOA estimate and the actual DOA of each source is obtained. If the largest of these absolute values is less than 0.8 degrees, then that particular event is considered to be a success. The probability of success is therefore given as,

$$POS = \frac{number\ of\ times\ \text{``}success\text{''}\ happens}{T}. \tag{6.4}$$

The parameters used in Equations 6.1, 6.2, 6.3 and 6.4 are defined as

(a) θ = actual DOA,

(b) $\hat{\theta}$ = estimated DOA,

(c) $\hat{\theta}_{av}$ = mean estimate,

(d) T = number of independent trials,

(e) SD_1, SD_2 = standard deviation in sources 1 and 2 DOA estimates and

(f) N = number of sources.

6.2.2 Spatial spectrum

The spectra of the three algorithms were generated for a 4-element ULA in the presence of two coherent sources (due to a multipath propagation effect) and also in the presence of two non-coherent sources. The SNR was fixed at 10 dB and the other simulation parameters were as described in Section 6.1.

The CTOP MUSIC, AVTOP MUSIC and classic MUSIC spectra were plotted on the same plot as shown in Figures 6.1 and 6.2 below. The simulations were run ten times repeatedly and the spectra for each algorithm were generated and plotted on top of one another for both signal scenarios.

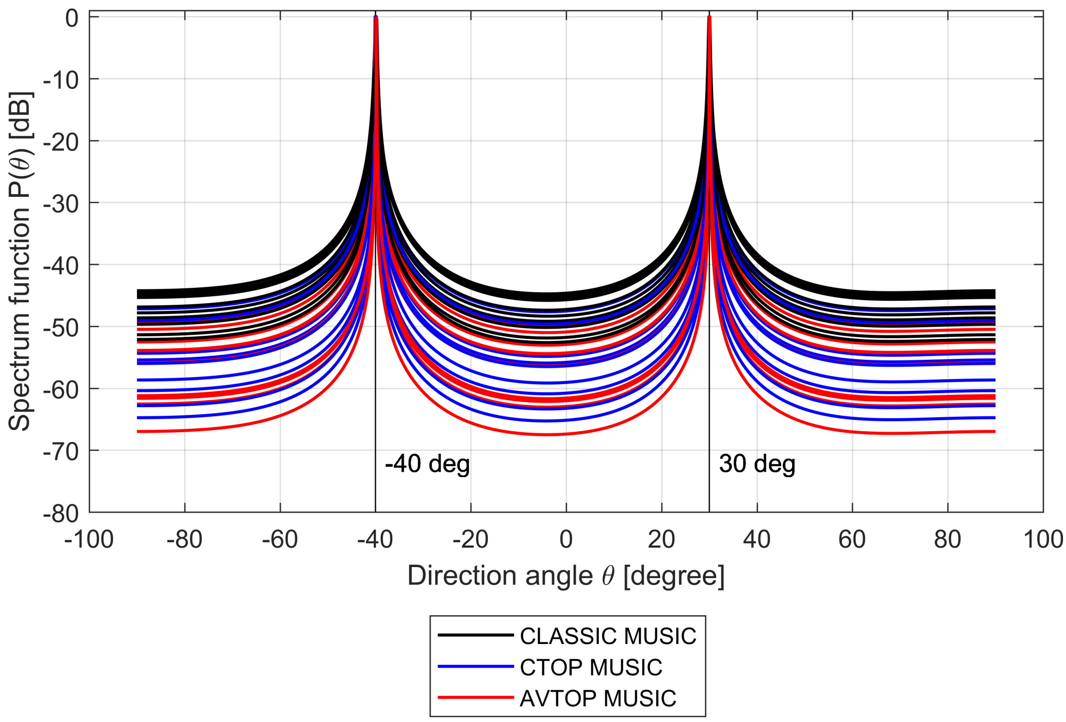

FIGURE 6.1: Typical spectra: non-coherent scenario.

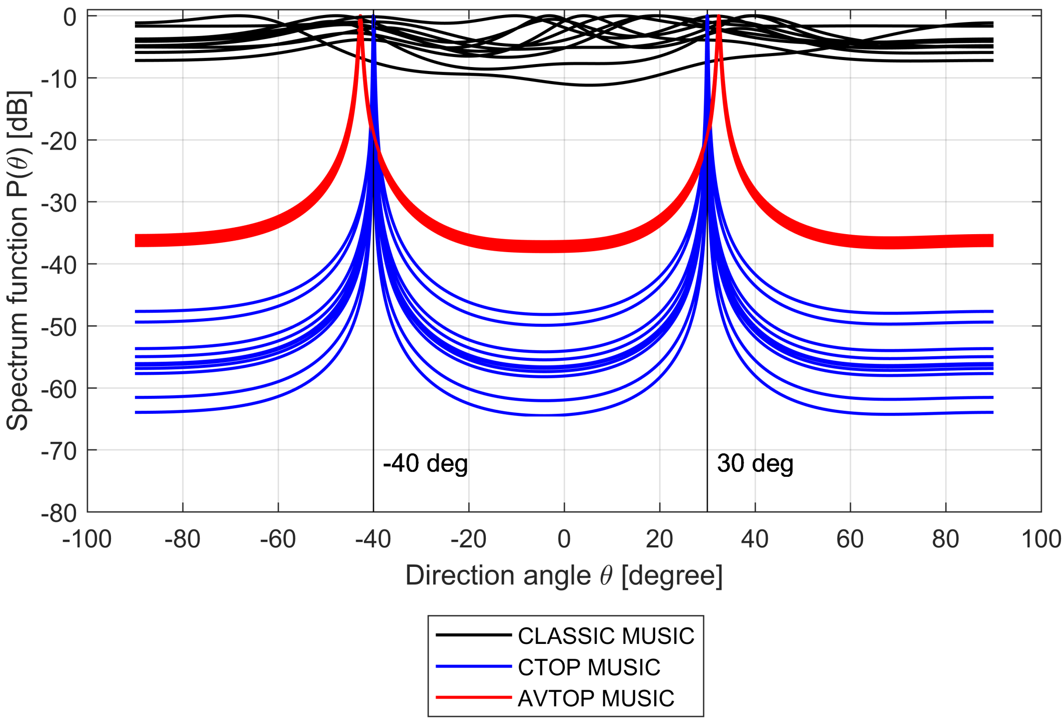

FIGURE 6.2: Typical spectra: coherent scenario.

Discussion

The results for the non-coherent scenario in Figure 6.1 show that when the two sources are mutually independent all the three algorithms are able to resolve the DOAs of the two sources. This is indicated by the sharp and narrow peaks at $-40°$ and $30°$ in the spatial spectrum of each algorithm. However the three algorithms have different levels of accuracy in estimation as investigated in later sections.

When the signals are coherent, the classic MUSIC algorithm completely fails to resolve DOAs of the two signals as shown in Figure 6.2. The results in the same figure also show that the CTOP and AVTOP MUSIC algorithms are able to resolve DOAs of coherent sources as indicated by the two peaks in the spectra of each algorithm. The peaks occur at around $30°$ and $-40°$, corresponding to DOA of the direct and reflected paths respectively.

The CTOP MUSIC yields nearly accurate estimates of the incident angles compared to the AVTOP MUSIC, confirming the conclusion drawn by Bai et al. in [23].

By observing the position of the peaks, it is clear that the AVTOP MUSIC DOA estimates greatly deviate from the true DOA of both the direct and reflected components. This agrees with the findings of the algebraic analysis in Section 5.3, where it was found that the cause of the deviation in estimation was due to the biased components which are a result of the interaction between the two sources' DOA information.

The CTOP MUSIC has high accuracy in estimation because during Toeplitz decorrelation, the DOA information of the coherent sources is retained as independent sums without any interaction between the individual sources information, as observed from the algebraic analysis. It was shown via applying MUSIC analytically (Section 5.4) that if the DOA information is retained as independent sums or simply in a superposition form (the case of CTOP decorrelation), then accurate DOA of the coherent sources can be obtained regardless of coherence.

Sections 6.2.3 and 6.2.4 present the performance evaluation results for the three algorithms at different number of sensors and different levels of SNR. The RMSE, average standard deviation and the probability of success (POS) values were computed for each scenario. In order to compute each performance metric value, 200 independent trial simulations were run.

6.2.3 Performance at different number of sensors

In this test, the SNR was fixed at 2 dB and the number of sensors was varied from 3 to 13 sensors at an interval of one. The performance results obtained for each signal scenario are presented in Figures 6.3 to 6.8 below.

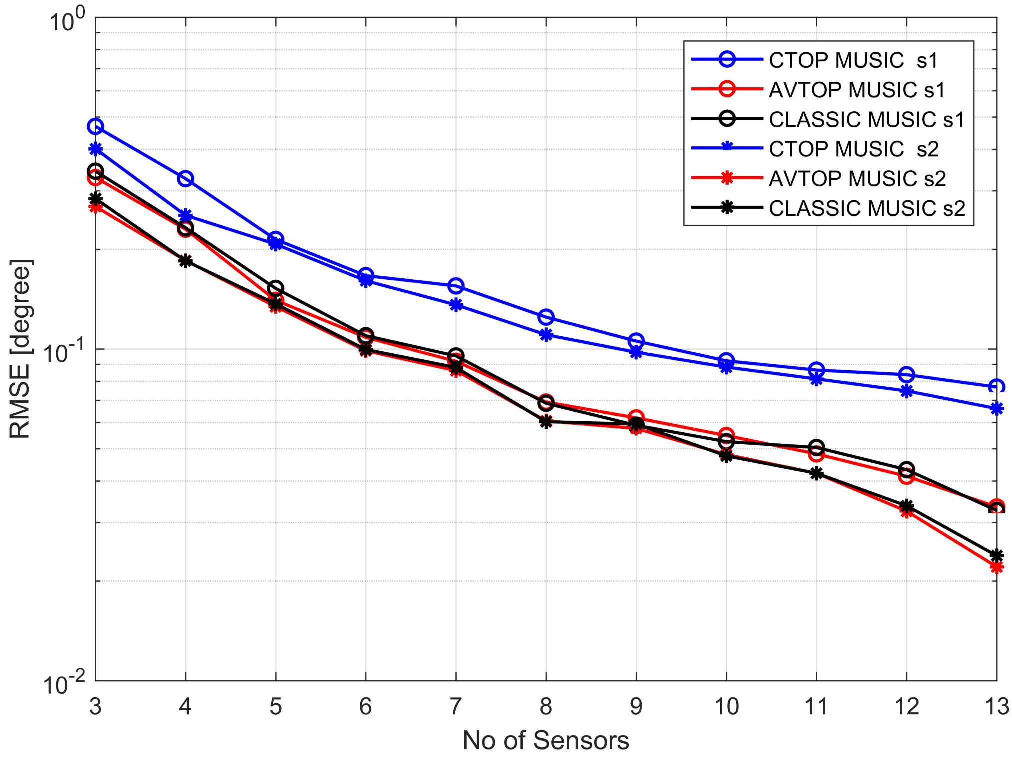

FIGURE 6.3: RMSE at different numbers of sensors: non-coherent scenario.

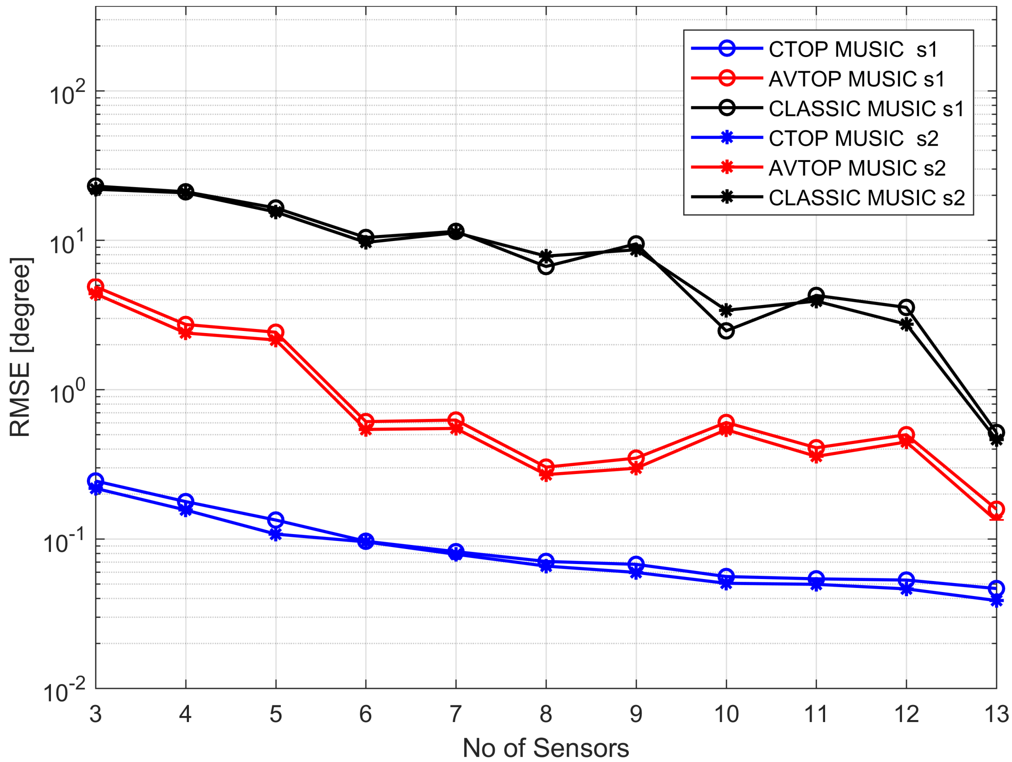

FIGURE 6.4: RMSE at different numbers of sensors: coherent scenario.

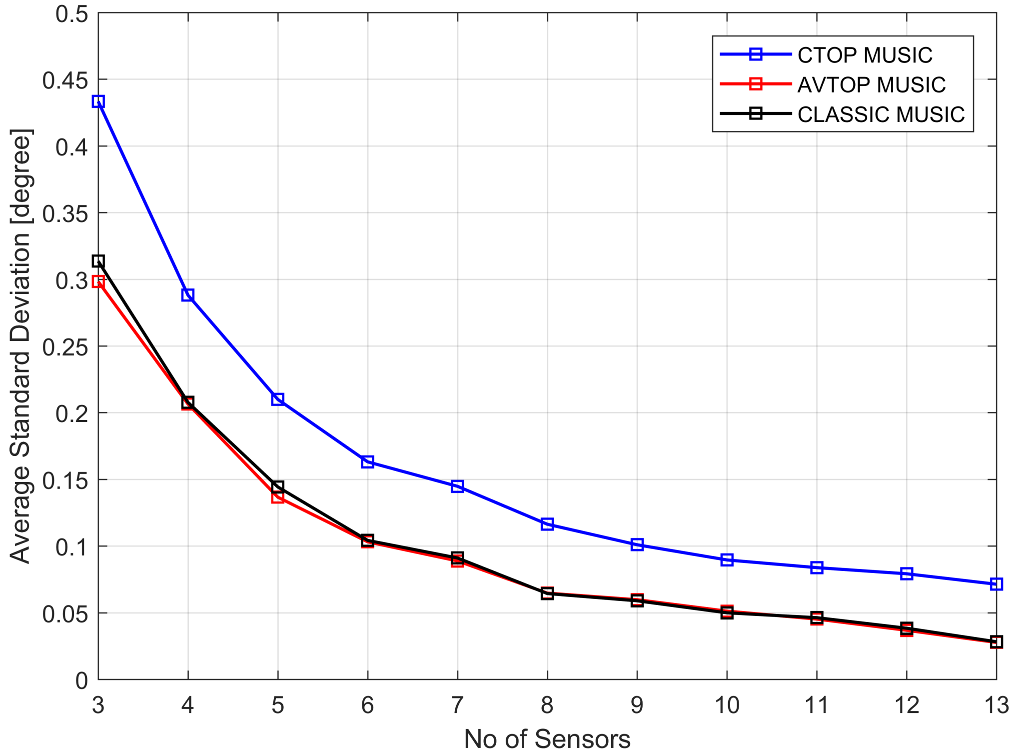

FIGURE 6.5: Spread in DOA estimates at different numbers of sensors: non-coherent case.

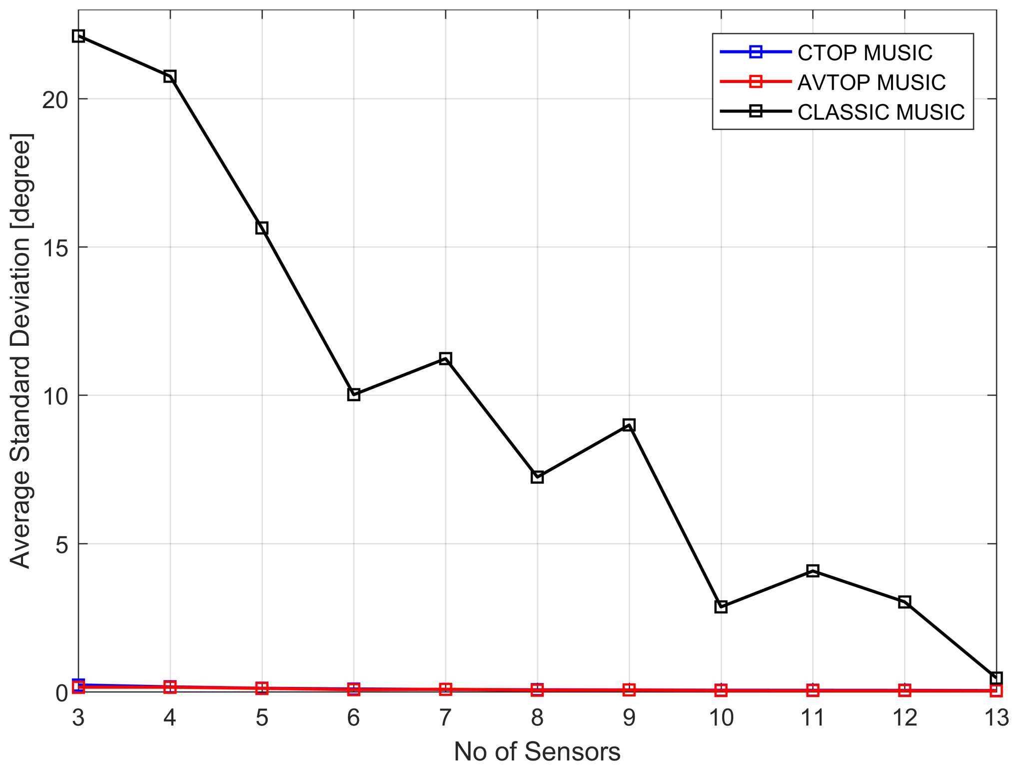

FIGURE 6.6: Spread in DOA estimates at different numbers of sensors: coherent case.

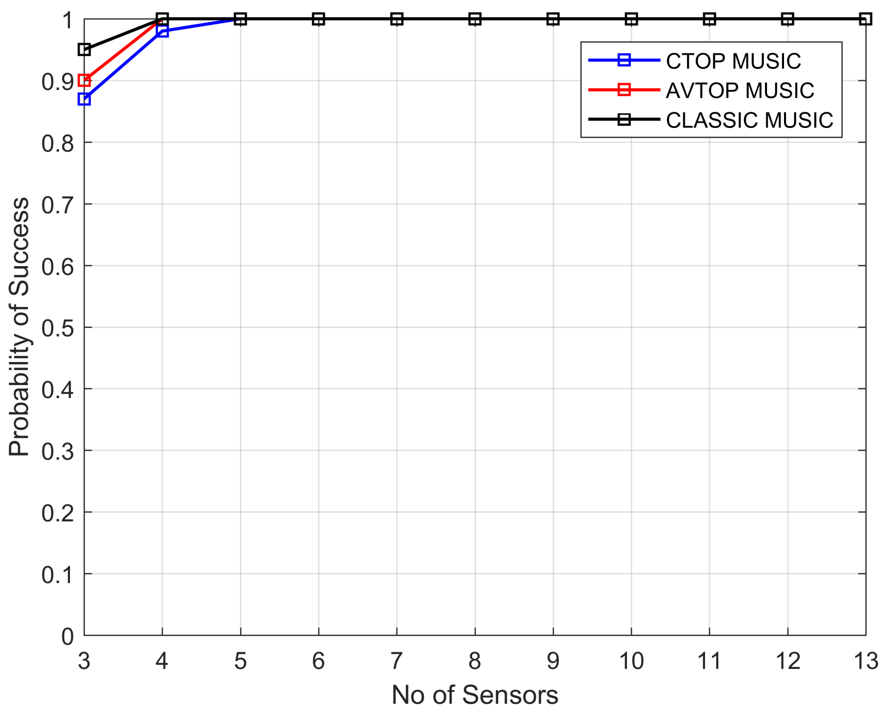

FIGURE 6.7: POS at different numbers of sensors: non-coherent case.

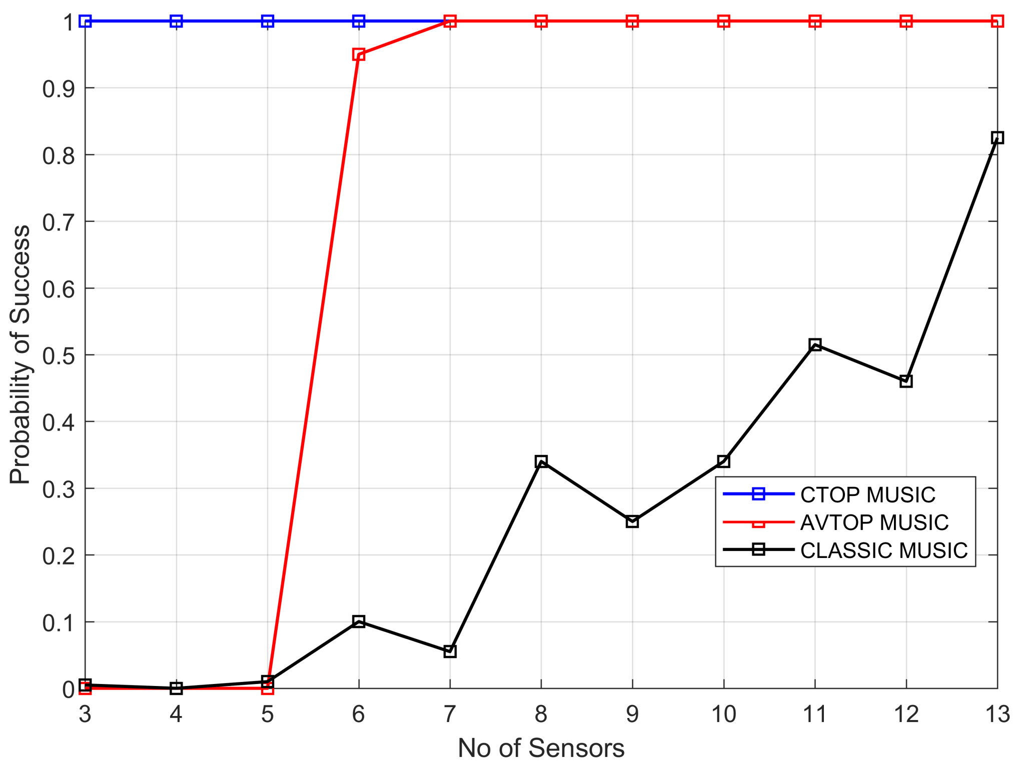

FIGURE 6.8: POS at different numbers of sensors: coherent case.

Discussion

RMSE: Figures 6.3 and 6.4 show the RMSE in DOA estimation versus the number of sensors for individual sources and algorithms.

The results for the non-coherent scenario presented in Figure 6.3 show that all the three algorithms exhibit a low RMSE in DOA estimation. The highest recorded RMSE value is 0.47 degrees at 3 sensors with the CTOP MUSIC algorithm. While the AVTOP and classic MUSIC algorithms have the RMSE values of 0.33 degrees and 0.34 degrees respectively at the same number of sensors. In general, the RMSE for all the algorithms tend to decrease with increase in the number of sensors.

It can be seen that there is a low RMSE in the DOA estimates for source 1 throughout, in comparison to source 2 for each algorithm. This phenomenon requires a thorough investigation in order to get an insight of why this happens.

The performance results for the coherent scenario shown in Figure 6.4 confirm the superiority of the CTOP MUSIC algorithm over the AVTOP and classic MUSIC algorithms in resolving the directions of coherent sources. The CTOP MUSIC algorithm is superior because during the decorrelation stage, the CTOP technique retains superimposed DOA information of coherent sources. Which according to the "*superposition claim*" made in Chapter 5, is the reason behind recovering DOA information of coherent sources without any spurious information.

With the least number of sensors, 3, the CTOP MUSIC algorithm has a RMSE of approximately 0.2 degrees, while the AVTOP MUSIC has a RMSE of about 5 degrees and the classic MUSIC has the highest RMSE of approximately 23 degrees. The RMSE for all the three algorithms slowly drops with increase in the number of sensors. Take note that these results were obtained at SNR=2 dB. This means that the CTOP MUSIC algorithm yields nearly accurate estimates even under low SNR conditions and minimum number of sensors, making it a more robust algorithm.

The high RMSE in the AVTOP MUSIC estimates is attributed to retaining of biased DOA information during decorrelation as it was found in the algebraic analysis, which leads to deviations from the true DOA. The classic MUSIC algorithm has the highest RMSE because its performance and resolution severely degrade in a coherent source environment due to the rank deficiency of the signal covariance matrix.

Although the RMSE for the classic MUSIC algorithm is decreasing with an increase in the number of sensors, the resolution is very poor as shown in Figures 6.9 to 6.12 below. The spectra for the classic MUSIC algorithm do not have high and sharp pointed peaks as in the case of the CTOP and AVTOP MUSIC algorithms. As the number of sensors increases, the classic MUSIC spectra peaks become more definite but still dome shaped (blunt) and with low power.

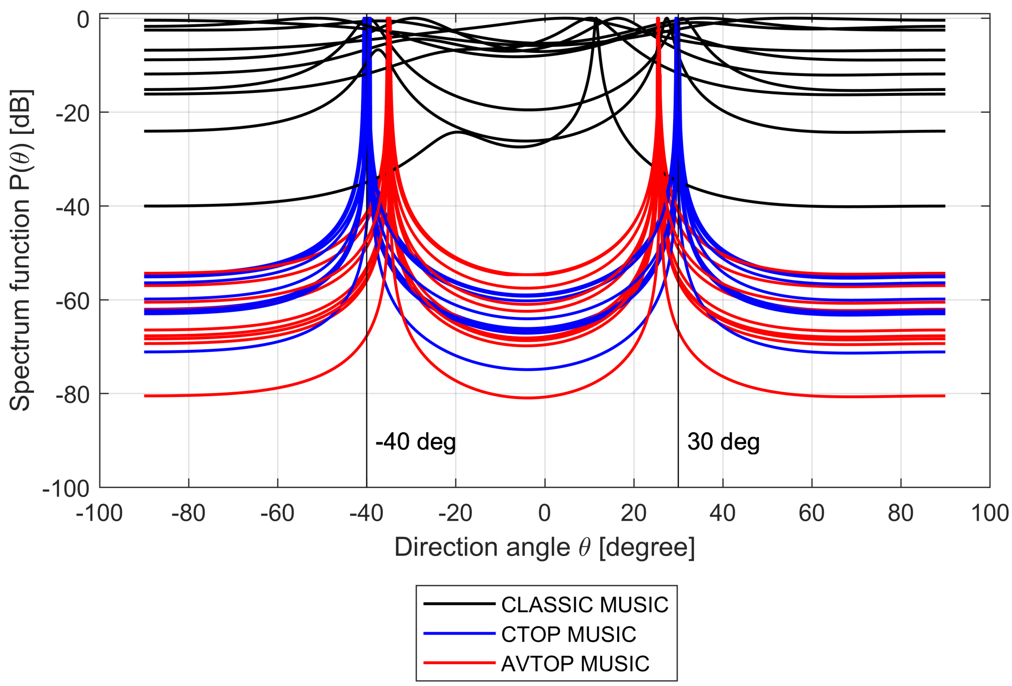

Figure 6.9: CTOP, AVTOP and classic MUSIC spectra at 3 sensors.

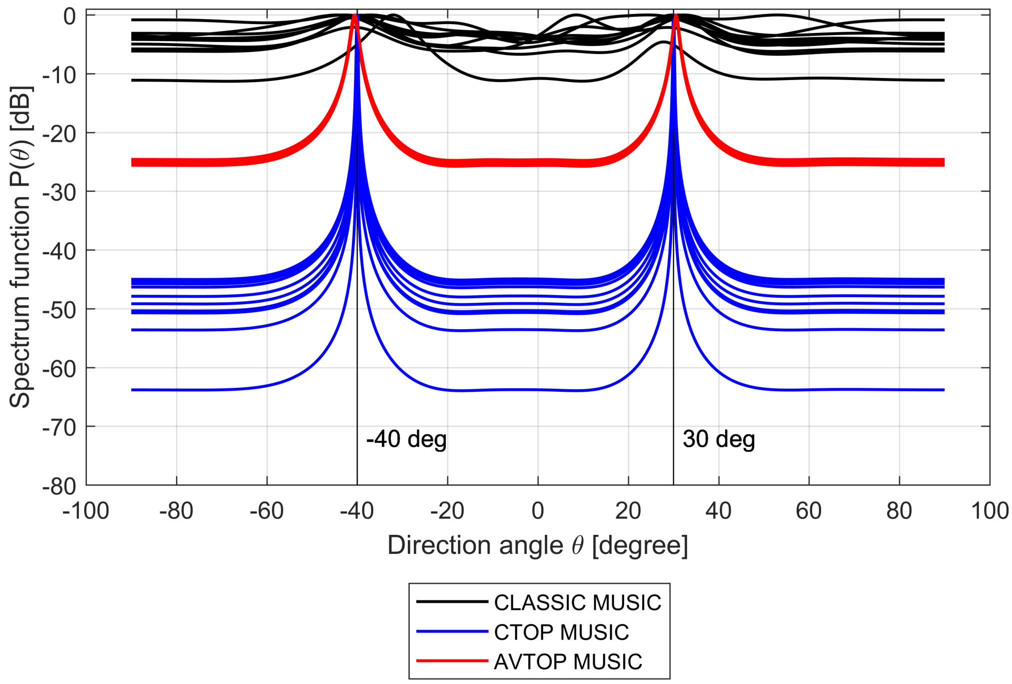

FIGURE 6.10: CTOP, AVTOP and classic MUSIC spectra at 6 sensors.

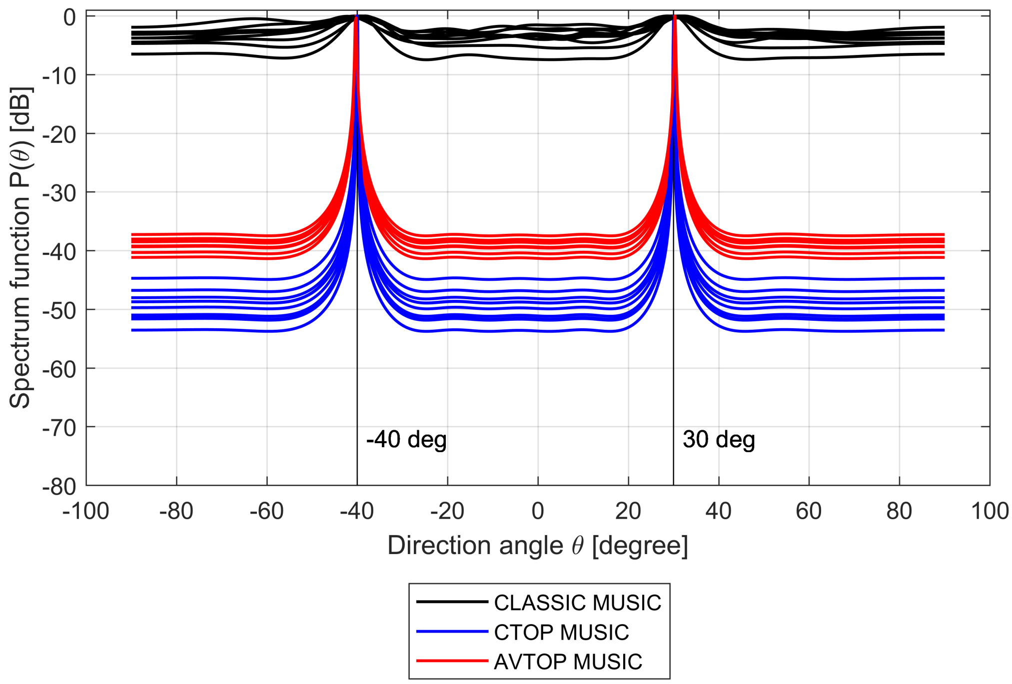

FIGURE 6.11: CTOP, AVTOP and classic MUSIC spectra at 9 sensors.

Spread: The plots in Figures 6.5 and 6.6 present the spread among the DOA estimates of each algorithm by means of average standard deviation versus the

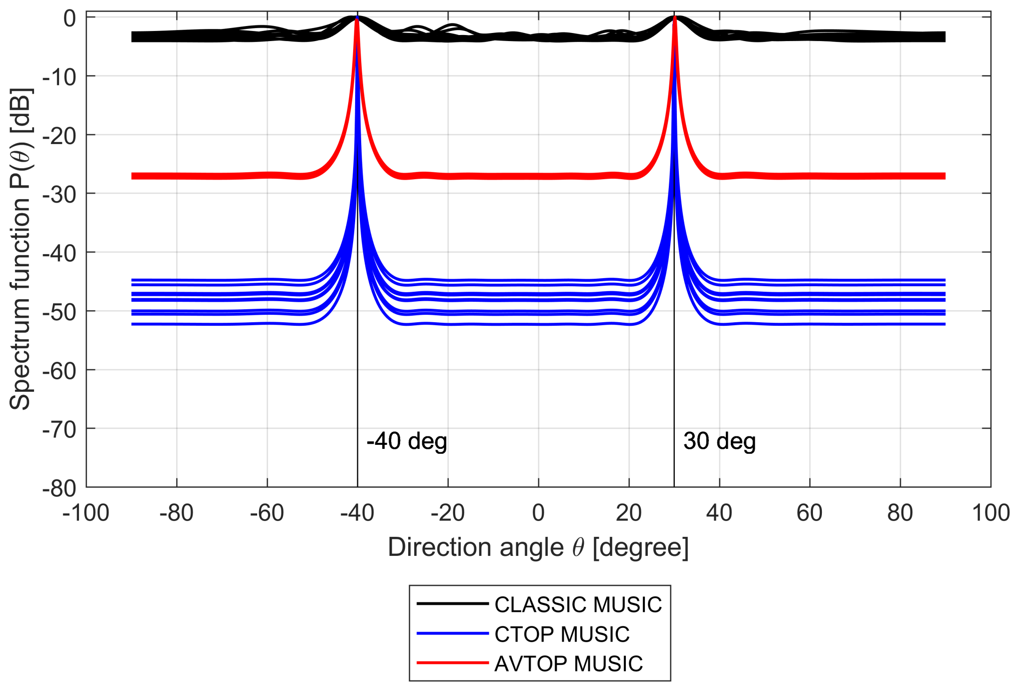

FIGURE 6.12: CTOP, AVTOP and classic MUSIC spectra at 13 sensors.

number of sensors.

In a non-coherent scenario all the three algorithms have a very low spread in the DOA estimates as shown in Figure 6.5. At 3 sensors an average standard deviation of 0.43, 0.30 and 0.31 degrees has been recorded for the CTOP, AVTOP and classic MUSIC algorithms respectively. After 8 sensors the average standard deviation in the DOA estimates of all the algorithms dropped to below 0.15 degrees and remained almost constant throughout. It can be seen that in a non-coherent scenario the average standard deviation for the CTOP MUSIC algorithm remained approximately 0.1 degrees higher than that of the AVTOP and classic MUSIC algorithms.

In the coherent scenario (Figure 6.6) the classic MUSIC algorithm has a very high spread in DOA estimation. An average standard deviation of 22 degrees was obtained at 3 sensors and sharply dropped to 10 degrees at 6 sensors. After 6 sensors the average standard deviation for the classic MUSIC algorithm gradually dropped with increase in the number of sensors in a rise and fall pattern. The observed pattern in the results is due to the inconsistency or randomness in the position of peaks in the spectra of the classic MUSIC algorithm when the incident sources are coherent.

At a small number of sensors, a few random peaks positioned away from the true DOA can be observed in the classic MUSIC spectra as shown in the results in Figures 6.9 and 6.10, leading to a high spread from the mean DOA estimate. The spread in the CTOP and AVTOP MUSIC DOA estimates is very low and close zero degrees as in the case of a non-coherent scenario. Figure 6.13 gives a magnified view of the graphs at the bottom of the plot in Figure 6.6. The graphs are for the CTOP and AVTOP MUSIC algorithms results.

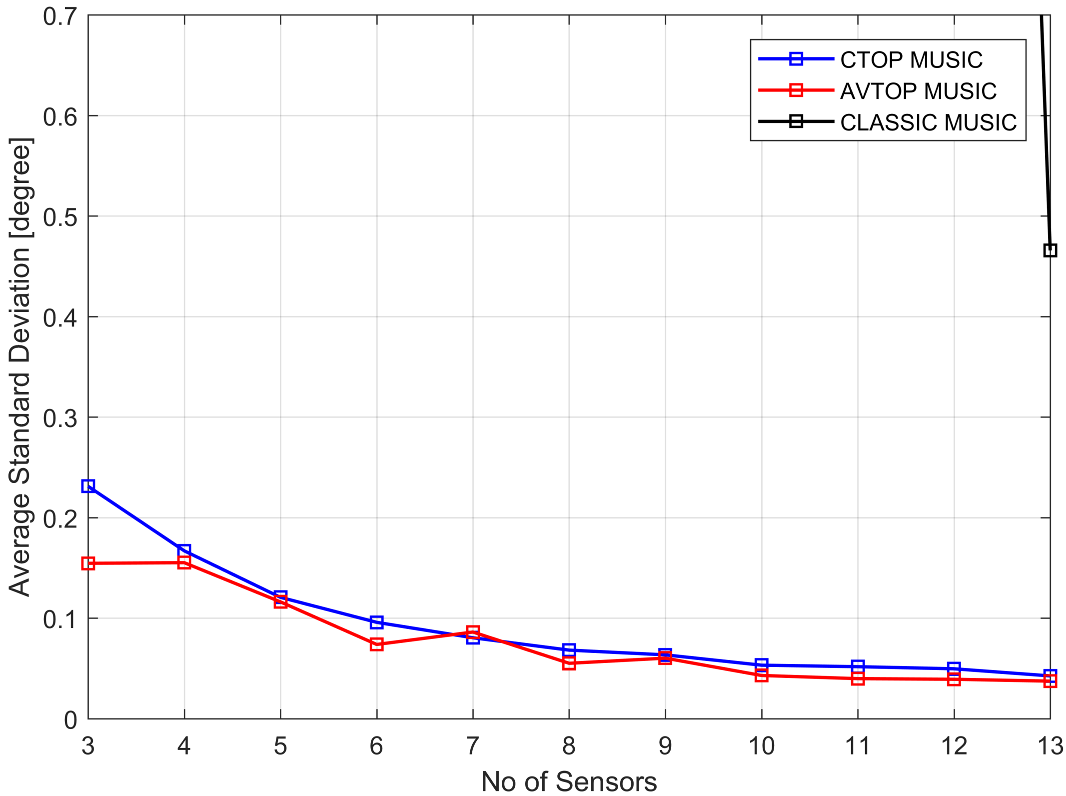

FIGURE 6.13: Magnified view.

Probability of success: The Figures 6.7 and 6.8 show the results of the probability of success versus the number of sensors. The knowledge of the definition of probability of success given in Section 6.2.1 is required in order to understand the interpretation of these results.

The non-coherent scenario results presented in Figure 6.7 show that all the algorithms attained a probability of success of 1 after 5 sensors. This means that after 5 sensors for each simulation trial, the highest of the absolute values of the difference between the DOA estimates and the corresponding actual DOAs for the two sources is less than 0.8 degrees. According to the criteria defined in Section 6.2.1, this indicates that all the algorithms have a high probability of detection when the sources are independent.

The coherent scenario results in Figure 6.8 show that the CTOP MUSIC algorithm has a probability of success of 1 throughout. The AVTOP MUSIC algorithm attained a probability of success of 1 at 7 sensors. At 5 sensors and lower, it has a probability of success of 0, this is due to a great deviation from the true DOA at a lower number of sensors associated with the AVTOP MUSIC as shown by the spatial spectra plot in Figure 6.9.

Figure 6.8 shows that the probability of success for the classic MUSIC algorithm is approximately 0 at 5 sensors and below. After 5 sensors it gradually increased with increase in the number of sensors to until 0.8 at 13 sensors. However the increase is not monotonic, as indicated by the rise and fall pattern in the curve. The rise and fall pattern in the curve is due to the inaccuracies in the estimates as a result of coherence among the sources.

6.2.4 Performance at different levels of SNR

In this set of results the performance of each algorithm was evaluated at different levels of SNR. The number of sensors was fixed at 4 and the SNR was varied from -25 dB to 25 dB at an increment of 5 dB. The performance results are presented in Figures 6.14 to 6.19 below.

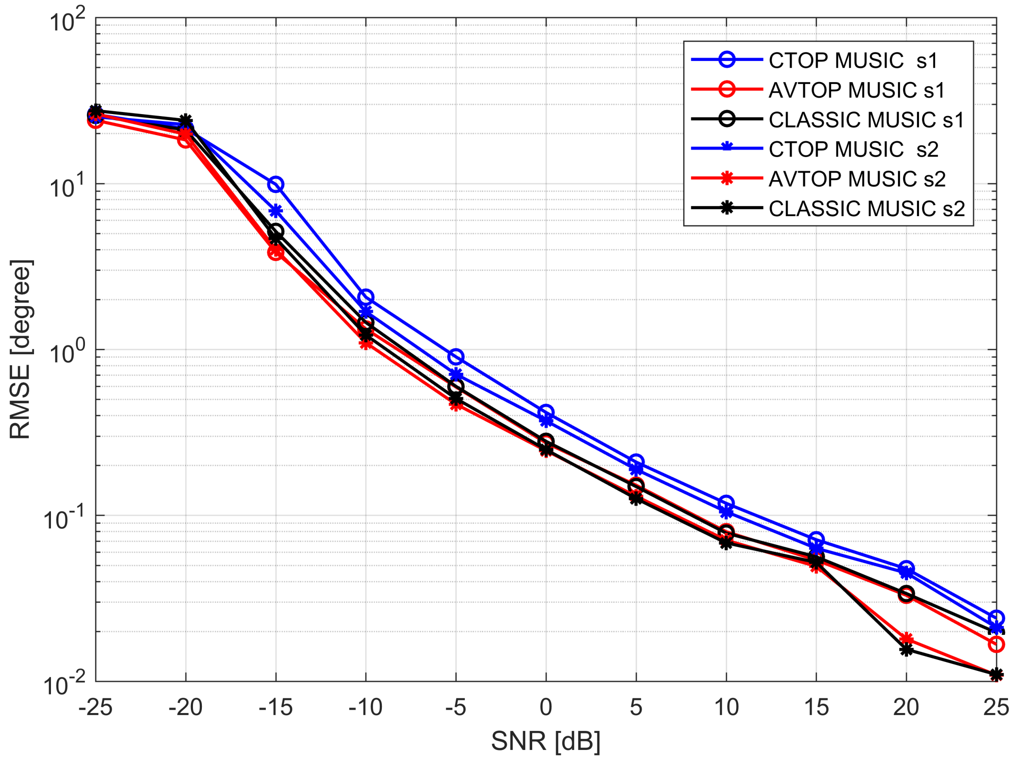

FIGURE 6.14: RMSE at different levels of SNR: non-coherent case.

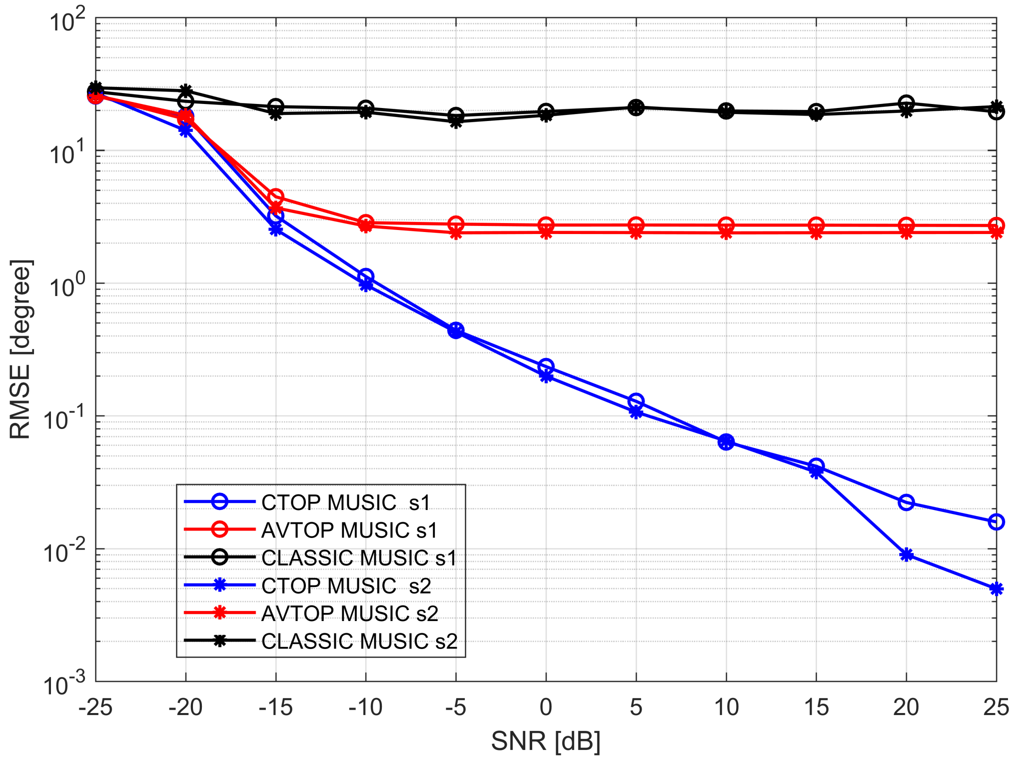

FIGURE 6.15: RMSE at different levels of SNR: coherent case.

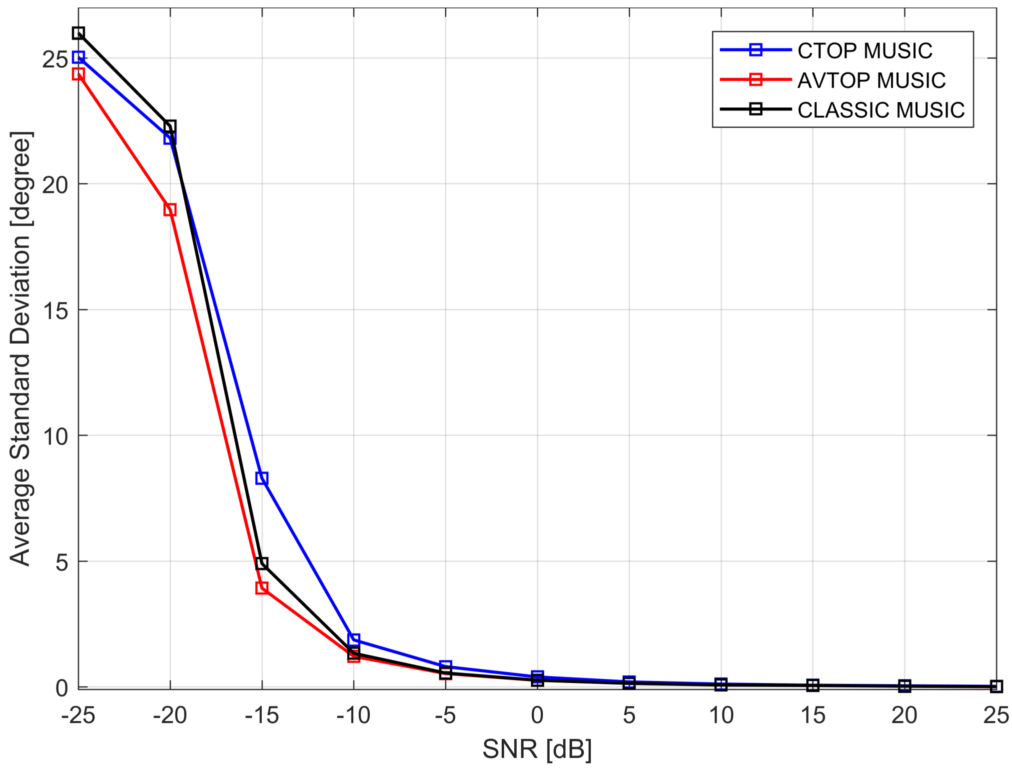

FIGURE 6.16: Spread in DOA estimates at different levels of SNR: non-coherent scenario.

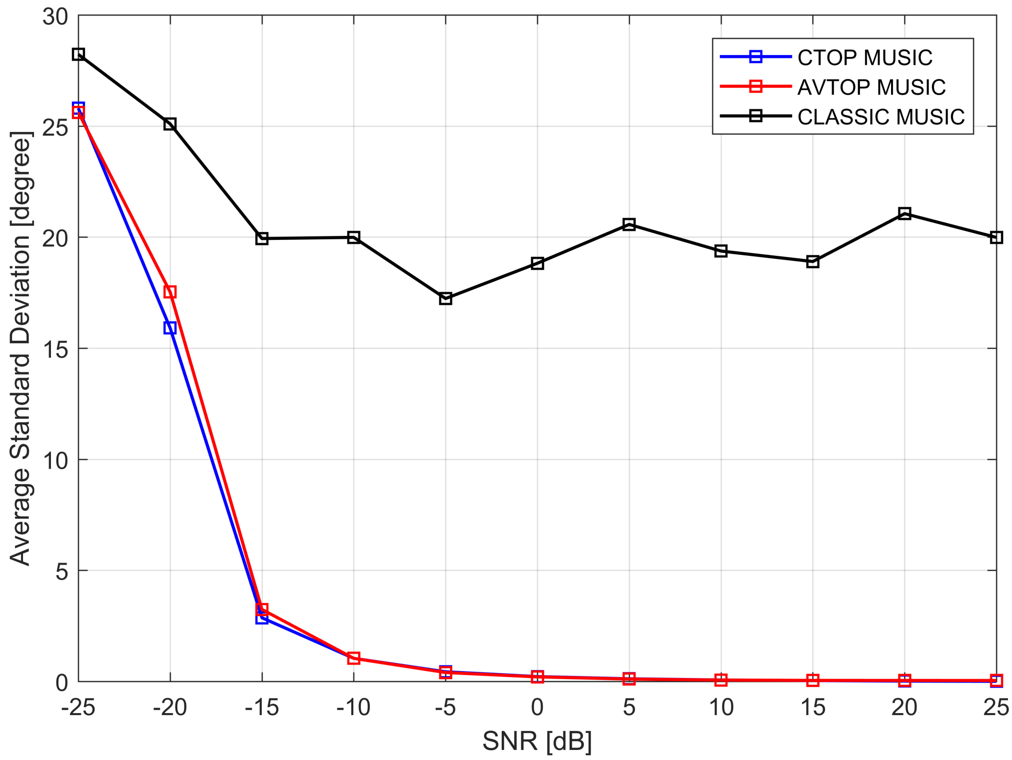

FIGURE 6.17: Spread in DOA estimates at different levels of SNR: coherent scenario.

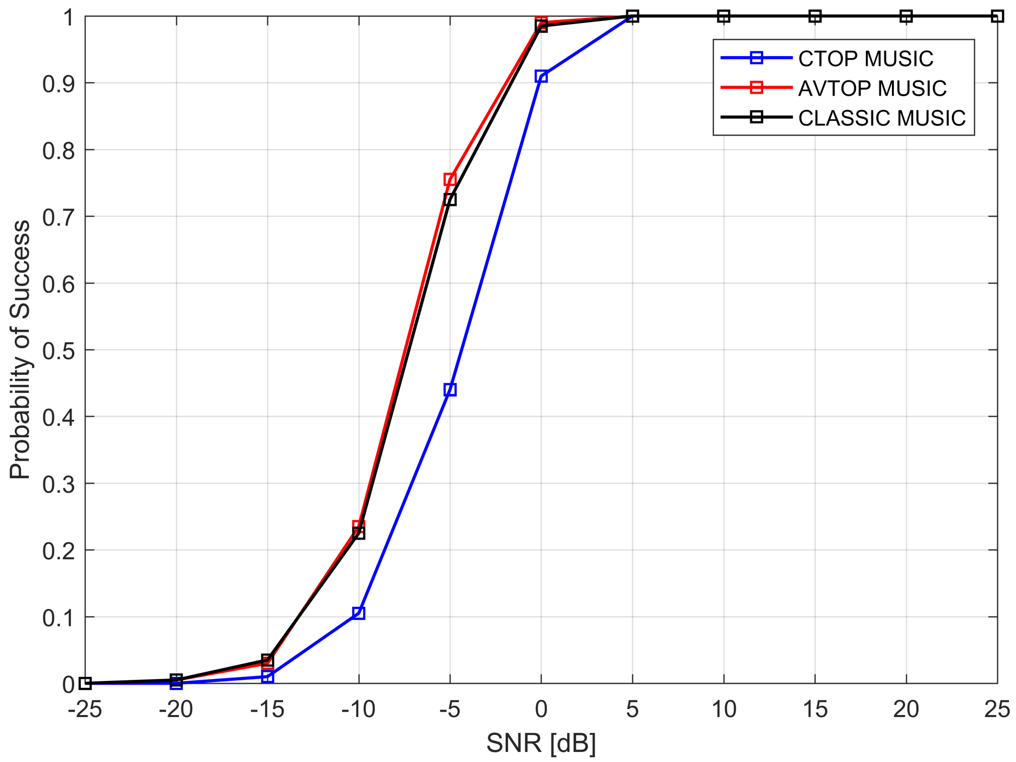

FIGURE 6.18: POS at different levels of SNR: non-coherent case.

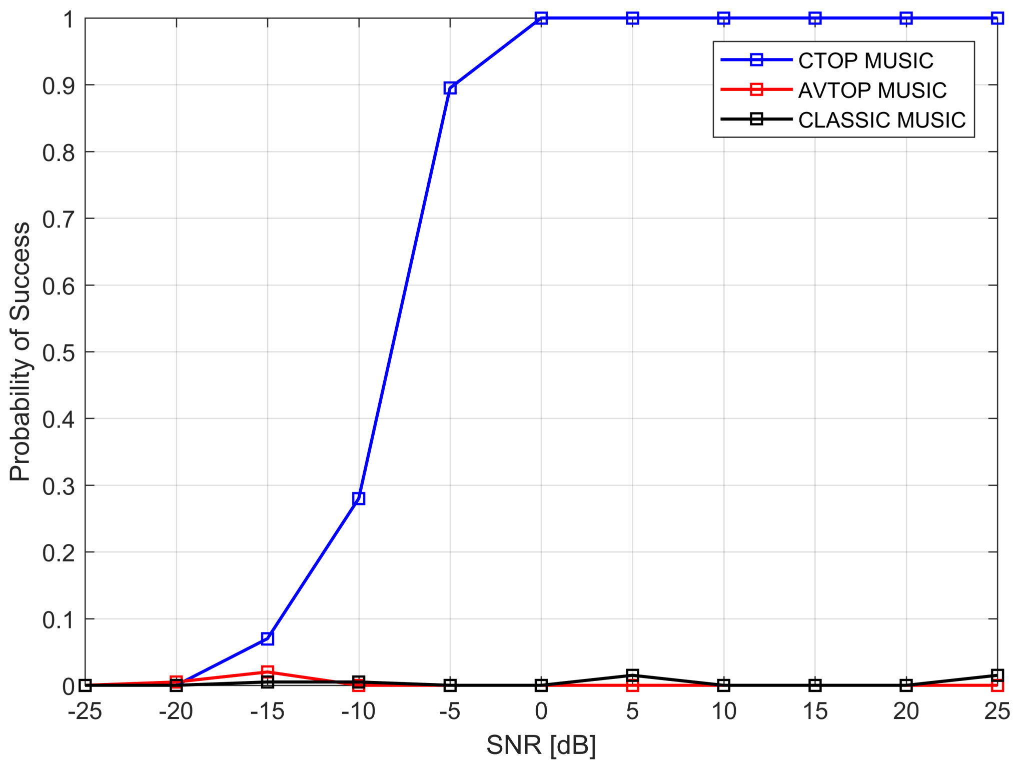

FIGURE 6.19: POS at different levels of SNR: coherent case.

Discussion

RMSE: The results in Figures 6.14 and 6.15 show the extreme case where the noise power is significantly higher than the signal power. In a non-coherent scenario, at the SNR of -25 dB the algorithms have a RMSE between 24 and 27 degrees. As the SNR increases, the RMSE for all the algorithms gradually drops almost at the same rate to below 1 degrees after -5 dB as shown in Figure 6.14.

The results for a coherent scenario presented in Figure 6.15 show that at -25 dB, the RMSE values of approximately 26, 25 and 29 degrees were obtained for the CTOP, AVTOP and classic MUSIC algorithms respectively. After -15 dB the RMSE in the CTOP MUSIC estimates gradually dropped with increase in the level of SNR to below 0.2 degrees after 0 dB.

The RMSE for the AVTOP MUSIC algorithm remained constant at around 3 degrees after -15 dB irregardless of the increase in the level of SNR. This means that 4 array sensors are not sufficient for an improved accuracy with the AVTOP MUSIC algorithm. Hence, to achieve a better accuracy both the SNR and number of sensors should be high enough. The RMSE associated with the classic MUSIC algorithm dropped to about 20 degrees at -15 dB and remained constant throughout. The high RMSE in the classic MUSIC algorithm estimates is due to the degraded performance as a result of coherence among the incident sources.

Spread: As the SNR increases the spread in DOA estimates of the CTOP and AVTOP MUSIC algorithms exponentially drops at almost the same rate to approximately 0 degrees after 0 dB in both the coherent and non-coherent scenarios. There is minimal variability in the position of the peaks in the CTOP and AVTOP MUSIC spectra as it be seen in Figures 6.9 to 6.12, hence the low spread in the DOA estimates.

The classic MUSIC algorithm has the same performance as the CTOP and AVTOP MUSIC algorithms in a non-coherent scenario. However, in a coherent scenario it exhibits a very high spread in DOA estimation which does not tend to improve with the increase in SNR. On average the average standard deviation in the DOA estimates fluctuates around 20 degrees after −15 dB. The high standard deviation is due to the inconsistency in the DOA estimates of the classic MUSIC algorithm when subjected to coherent sources.

It has been observed that in a non-coherent scenario the average standard deviation curves flatten out for the SNR values above 0 dB as it appear in Figure 6.16. In the coherent scenario the same is only true for the curves of the CTOP and AVTOP MUSIC algorithms as shown in Figure 6.17. The average standard deviation goes to 0 degrees after 0 dB. This is because for the SNR values high than 0 dB, the incident signals have more power than the noise. As a result the effect of noise power on the signals is minimal hence there is less spread or error in the DOA estimates.

Probability of success: The results of the probability of success at different levels of SNR are shown in Figures 6.18 and 6.19 for the coherent and non-coherent scenarios respectively. In a non-coherent scenario the probability of success of each algorithm exponentially increases with increase in SNR. All the three algorithms attained a probability of success of 1 at 5 dB as shown in Figure 6.18. In a coherent scenario (Figure 6.19) the same trend is only true for the CTOP MUSIC algorithm where the probability of success of 1 was attained 0 dB.

The AVTOP and classic MUSIC algorithms have a probability of success of approximately 0 throughout. This is because with a number of 4 array sensors, regardless of the level of SNR the deviation in DOA estimation associated with the AVTOP MUSIC algorithm is significantly high. Hence the DOA estimates merely satisfies the probability of success criteria given in Section 6.2.1. The classic MUSIC algorithm too has a poor probability of success due to a high RMSE and spread in the DOA estimates of the classic MUSIC algorithm in a coherent source environment.

6.3 CTOP from Different Rows

It has been stated in [50] that any row of the coherent covariance matrix can be used to construct a new Toeplitz matrix for decorrelation of coherent sources. It is shown here that although any row can be used, it is only from the first row that one can accurately decorrelate coherent sources and achieve a better accuracy in DOA estimation.

Based on the coherent scenario and simulation parameters described in Section 6.1, a simulation was done to generate different CTOP MUSIC spectra. The spectra were obtained by carrying out CTOP decorrelation using different rows of the coherent covariance matrix. The SNR was fixed at 10 dB and the number of sensors was 4.

Figure 6.20 shows four CTOP MUSIC spectra generated based on CTOP decorrelation using each row of a 4×4 coherent array covariance matrix. The two sources have DOAs of $-40°$ and $30°$.

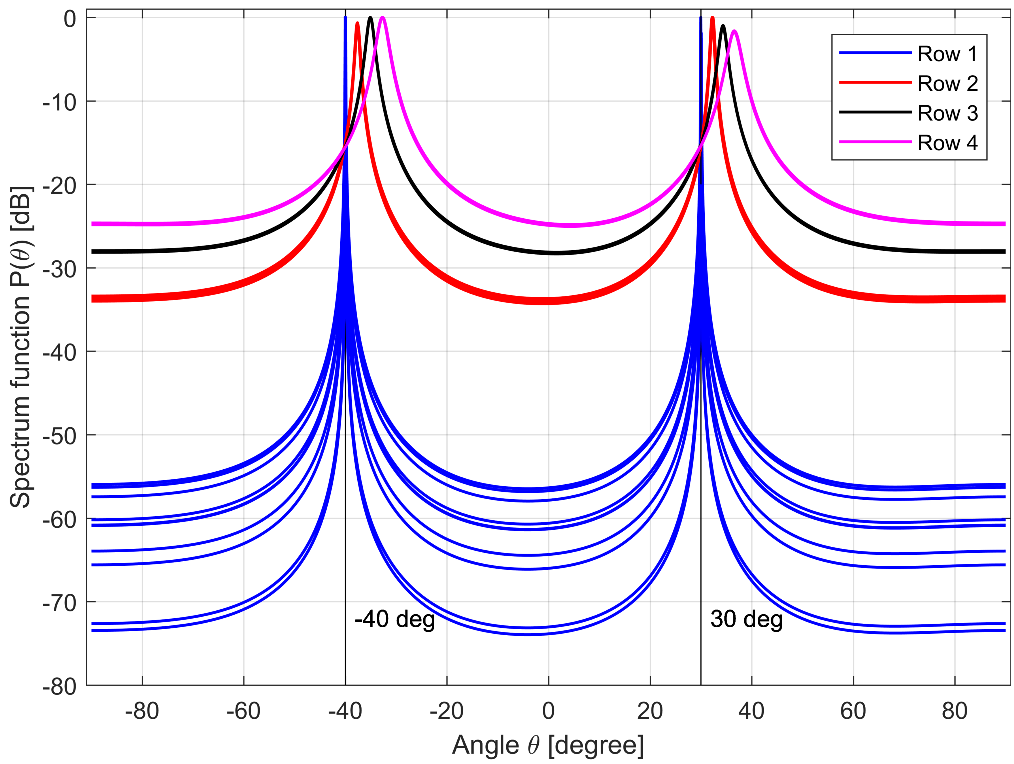

FIGURE 6.20: CTOP MUSIC-using different rows.

The results in Figure 6.20 show that decorrelation based on the first row yields more accurate estimation compared to other rows of the coherent covariance matrix. Decorrelation based on the first row also yields high power spectra with sharp pointed peaks. In this particular case, row 4 resulted in the most deviation from the true DOA. Again, these results confirm the findings and observations from Section 5.3 of the algebraic analysis.

6.4 Summary

The numerical simulations conducted have confirmed the robustness and accuracy in the DOA estimates of the CTOP MUSIC algorithm for coherent sources. The performance evaluation results have shown that the CTOP, AVTOP and classic MUSIC have high accuracy in DOA estimation of non-coherent sources, however only the CTOP MUSIC algorithm maintains the same level of accuracy in a coherent scenario. It is again emphasised here that CTOP decorrelation using the first row of the coherent covariance matrix yields more accurate DOA estimates in comparison to using other rows. This is because, the first row has DOA information of the individual sources organised as independent sums in each entry of the row. This independence is the key to preserving DOA information in a coherent scenario.

CHAPTER 7

Conclusion and Future Work

In this chapter, the conclusions and recommendations of this study are given. The research objectives and the analysis approach taken to answer the research question are summarised. The chapter also highlights the major findings of the algebraic analysis as well as the performance evaluation of the two decorrelation techniques that the study focused on. The recommendations for future works are given at the end of the chapter.

7.1 Conclusion

The direction of Arrival estimation of coherent sources has been widely studied in literature. The existence of coherent sources results in a rank deficiency of the received signals covariance matrix, causing failure of the subspace-based methods such as MUSIC. A pre-processing technique is applied on the coherent data in order to alleviate the effect of coherence. Techniques based on Toeplitz matrix reconstruction offer a promising solution, however, the studies that employ Toeplitz techniques do not provide more information on the working principles behind these techniques.

Therefore, the main objective of this study was to carry out an algebraic analysis in order to develop an understanding of the working principle behind the selected Toeplitz decorrelation techniques, namely the correlation Toeplitz (CTOP) and averaging Toeplitz (AVTOP) techniques. It has been stated in the literature review that the CTOP technique has better accuracy than the AVTOP technique, and that the AVTOP technique has deviation in DOA estimation. In order to meet this objective, an algebraic analysis approach was taken. Firstly, a coherent array covariance matrix was derived based on a scenario of a 3-element ULA and two coherent sinusoidal narrowband sources in a noiseless environment. The two sources corresponds to a direct and reflected components of a multipath propagation effect. The CTOP and AVTOP decorrelation techniques were then applied to reconstruct two new decorrelated Toeplitz matrices from the coherent array covariance matrix.

The analysis focused on investigating the algebraic structure of the coherent and the Toeplitz reconstructed matrices. Knowing that the signals DOA information is contained in the array steering matrix elements, referred to as the "*DOA phasors*" in the study, the analysis focused on the distribution and interaction between the DOA phasors in the derived matrices. The following is a summary of the most important observations made from the structure of the derived matrices:

(a) Coherent covariance matrix: In each entry of the first row or column of the coherent matrix, the DOA phasors occur in a "*superposition form*" (as independent sums). Every other row or column has one entry which is a sum of independent DOA phasors and extra "*biased*" (dependent) terms, which are a result of the interaction between the two sources DOA phasors.

(b) CTOP reconstructed matrix: All the off diagonal entries are a sum of independent DOA phasors without any biased term.

(c) AVTOP reconstructed matrix: The superdiagonal entries are a sum of the independent DOA terms and biased terms. This means that every column or row has one entry containing biased terms.

It is concluded that the accuracy of the CTOP decorrelation technique is attributed to retaining the DOA information in a superposition form. This is because the CTOP technique reconstructs a Toeplitz matrix from the first row of the coherent covariance matrix, where there are no interactions between the DOA phasors. This is referred to as the "*superposition claim*" in the study. The deviation in DOA estimation associated with the AVTOP technique is a result of additional biased terms in the superdiagonal entries of the reconstructed Toeplitz matrix.

In order to verify the "*superposition claim*" the MUSIC algorithm was applied analytically, taking noise into consideration. It was confirmed that if the DOA information is organised in a superposition form in the array covariance matrix, the "*exact*" angle of arrival information of the sources can be obtained using the MUSIC algorithm. It was also found that if the exact data covariance matrix is known, the AWGN has no influence on the source direction's information. Further analysis of the symbolic MUSIC results have shown that the MUSIC spectrum can have secondary peaks around the main peaks (peaks at the source directions) depending on the scenario and the positions of these secondary peaks are deterministic.

Numerical simulations were also carried out to verify the robustness of the CTOP MUSIC algorithm over the AVTOP MUSIC in both coherent and non-coherent scenarios. The performance of the classic MUSIC algorithm was also evaluated to provide a baseline for comparison. The results have shown that the CTOP MUSIC has more accurate estimation performance compared to the AVTOP MUSIC even under low SNR conditions and minimum number of sensors. The CTOP MUSIC algorithm maintains its accurate estimation performance irregardless of whether the sources are coherent or non-coherent.

The AVTOP and classic MUSIC algorithms can only match the performance of the CTOP MUSIC when the incident sources are not coherent. In a coherent scenario, although the AVTOP MUSIC has a low spread in DOA estimation, the method is less accurate and has a poor probability of success due to deviations from the true DOA. The estimation performance of the classic MUSIC algorithm is severely affected by the coherence among the sources. The peaks in the classic MUSIC spectra are dome shaped and have a very low power in comparison to high power and sharp pointed peaks associated with the CTOP and AVTOP MUSIC spectra. This is an indication of a poor resolution in DOA estimation.

Further simulations were also done to verify that CTOP decorrelation based on the first row of the coherent covariance matrix results in a more accurate estimation compared to the decorrelation based on using other rows.

7.2 Future Work

This study recommends the following:

(a) The noise model was assumed to be AWGN and it was found that it does not have an influence on the source directions provided that the exact data covariance matrix is known. The same analysis should be carried out using other noise models such as colored noise to investigate how it influences the directions of the sources.

(b) The analytic MUSIC approach was only studied for up to a maximum of four elements ULA due to the algebraic limitation that polynomials of degrees of five or higher cannot be solved. The study recommends that the analytic MUSIC results for a 2×2, 3×3 and 4×4 array covariance matrices should be used to generalise the analytic MUSIC approach in order to enable analysis of ULAs of sizes lager than four elements.

(c) Future studies could also investigate the impact of array covariance matrix approximation on the peak heights in the MUSIC spectrum and as well as on the target directions (peak positions).

Appendix A

Background Theory

In this appendix, basic definitions and properties of Toeplitz and covariance matrices are given after which the spectral theorem of Hermitian matrices is presented. These concepts are very important for understanding the full derivation of the MUSIC algorithm presented in the last section of this appendix.

A.1 Special Matrices

A.1.1 Toeplitz matrix

A Toeplitz matrix is a matrix with a specific characteristic that is, all elements in each of its diagonals are equal. Let $\boldsymbol{T}$ represents a $(N+1) \times (N+1)$ Toeplitz matrix, which is modelled as [21],

$$\boldsymbol{T} = \begin{bmatrix} t_0 & t_1 & t_2 & \cdots & t_N \\ t_{-1} & t_0 & t_1 & \cdots & t_{N-1} \\ t_{-2} & t_{-1} & t_0 & \ddots & \vdots \\ \vdots & \vdots & \ddots & \ddots & t_1 \\ t_{-N} & t_{-N+1} & \cdots & t_{-1} & t_0 \end{bmatrix}. \tag{A.1}$$

If the Toeplitz matrix is conjugate symmetric, it is called Hermite Toeplitz matrix and has the form

$$\boldsymbol{T}_0 = \begin{bmatrix} t_0 & t_1^* & t_2^* & \cdots & t_N^* \\ t_1 & t_0 & t_1^* & \cdots & t_{N-1}^* \\ t_2 & t_1 & t_0 & \ddots & \vdots \\ \vdots & \vdots & \ddots & \ddots & t_1^* \\ t_N & t_{N-1} & \cdots & t_1 & t_0 \end{bmatrix}. \tag{A.2}$$

A.1.2 Covariance matrix

Given that DOA estimation with subspace-based methods is solely dependent on utilising the eigenstructure of the array data covariance matrix, it is worth noting the following important properties of covariance and correlation matrices in general as discussed in [80].

Definition: Let a stationary discrete-time stochastic process be represented by an observation vector $\boldsymbol{x}(n)$ of size $M \times 1$ where M is the total number of observations. Vector $\boldsymbol{x}(n)$ is composed of zero-mean time series elements $x(n), x(n-1), .., x(n-M+1)$ as given by

$$\boldsymbol{x}(n) = [x(n), x(n-1), ..., x(n-M+1)]^H. \tag{A.3}$$

The expectation of the outer product of the observation vector $\boldsymbol{x}(n)$ with itself generates what is called the covariance matrix. Let $\boldsymbol{R}$ represent the $M \times M$ covariance matrix which is given by

$$\boldsymbol{R} = E[\boldsymbol{x}(n)\boldsymbol{x}^H(n)]. \tag{A.4}$$

Substituting Equation (A.3) into Equation (A.4) the expanded form of the covariance matrix is given as follows

$$\boldsymbol{R} = \begin{bmatrix} r(0) & r(1) & \cdots & r(M-1) \\ r(-1) & r(0) & \cdots & r(M-2) \\ \vdots & \vdots & \ddots & \vdots \\ r(-M+1) & r(-M+2) & \cdots & r(0) \end{bmatrix}. \tag{A.5}$$

The main diagonal element $r(0)$ is always real. In a case where the vector $\boldsymbol{x}(n)$ is complex-valued, $\boldsymbol{R}$ has complex off diagonal elements.

Properties of Covariance Matrices

The following are properties of the covariance matrix $\boldsymbol{R}$:

(a) Hermitian

The covariance matrix is equal to its conjugate transpose also known as Hermitian transpose. Complex-valued matrices of this nature are called Hermitian matrices. The Hermitian property is expressed as $\boldsymbol{R} = \boldsymbol{R}^H$.

(b) Toeplitz

The structure of the covariance matrix $\boldsymbol{R}$ in Equation (A.5) is such that the main diagonal has all of its elements equal and each of the diagonals below or above the main diagonal also has equal elements. Hence the wide-sense discrete time stochastic process has a covariance matrix of a Toeplitz structure.

(c) Almost always positive definite and always nonnegative definite

Assume a complex-valued nonzero vector $\boldsymbol{a}$. The expression $\boldsymbol{a}^H\boldsymbol{R}\boldsymbol{a}$ is called Hermitian form. If the Hermitian form satisfies the condition $\boldsymbol{a}^H\boldsymbol{R}\boldsymbol{a} \geq 0$ then $\boldsymbol{R}$ is *nonnegative definite* and $\boldsymbol{R}$ is *positive definite* if $\boldsymbol{a}^H\boldsymbol{R}\boldsymbol{a} > 0$.

(d) Nonsingular

The covariance matrix of a wide-sense stationary process is nonsingular, i.e. $\det(\boldsymbol{R}) \neq 0$, due to the presence of additive noise which cannot be avoided.

(e) Equivalence of backward rearrangement and transposition

If $\boldsymbol{x}(n)$ is an observation vector of a stationary discrete-time stochastic process, transposition of the covariance matrix of $\boldsymbol{x}(n)$ is equivalent to backward rearrangement of the elements of $\boldsymbol{x}(n)$.

(f) Concatenation

The covariance matrices $\boldsymbol{R}_M$ and $\boldsymbol{R}_{M+1}$ of a discrete-time stochastic process for M and $M+1$ observations respectively, are related by

$$\boldsymbol{R}_{M+1} = \left[\begin{array}{c:c} r(0) & \boldsymbol{r}^H \\ \hdashline \boldsymbol{r} & \boldsymbol{R}_M \end{array}\right] \tag{A.6}$$

where $r(0)$ is the autocovariance of the process for lag of zero and $\boldsymbol{r}^H = [r(1), r(2), ..., r(M)]$.

A.2 Spectral Decomposition

The following definition of the Spectral theorem is taken from [81]. If $\boldsymbol{R} \in \mathbb{C}^{M\times M}$ is a Hermitian matrix, there exists a unitary matrix $\boldsymbol{U} \in \mathbb{C}^{M\times M}$ and a diagonal matrix $\boldsymbol{\Lambda} \in \mathbb{R}^{M\times M}$ such that

$$\boldsymbol{\Lambda} = \boldsymbol{U}^H \boldsymbol{R} \boldsymbol{U}, \tag{A.7}$$

where the columns of $\boldsymbol{U}$ are the eigenvectors and the main-diagonal entries of $\boldsymbol{\Lambda}$ are eigenvalues $\boldsymbol{R}$. From this theorem, the spectral decomposition of $\boldsymbol{R}$ is therefore given by

$$\boldsymbol{R} = \boldsymbol{U}^H \boldsymbol{\Lambda} \boldsymbol{U}. \tag{A.8}$$

The eigenvectors of $\boldsymbol{R}$ are orthonormal and linearly independent, and the associated eigenvalues are real. Let $\boldsymbol{u}$ and λ be the eigenvector and corresponding eigenvalue of $\boldsymbol{R}$ respectively. If one multiplies columns by rows in Equation (A.8), then $\boldsymbol{R}$ can be written as a combination of one-dimensional projections, which are special matrices $\boldsymbol{u}\boldsymbol{u}^H$ of rank 1 multiplied by λ [82]:

$$\boldsymbol{R} = \sum_{i=1}^{M} \lambda_i \boldsymbol{u}_i \boldsymbol{u}_i^H = \lambda_1 \boldsymbol{u}_1 \boldsymbol{u}_1^H + \lambda_2 \boldsymbol{u}_2 \boldsymbol{u}_2^H + ... + \lambda_M \boldsymbol{u}_M \boldsymbol{u}_M^H \tag{A.9}$$

A.3 Derivation of the MUSIC Algorithm

Assume the data model presented in Section 3.3, where a ULA of M elements is used to capture data from N incoming signals and the data captured by individual array elements is linearly combined to give a vector $\boldsymbol{x}(t)$ where additive noise is assumed to be of Gaussian distribution and is uniform at all array elements. As given earlier in Equation (3.7) $\boldsymbol{x}(t)$ has a covariance matrix

$$\boldsymbol{R} = \boldsymbol{A}\boldsymbol{R}_{ss}\boldsymbol{A}^H + \sigma_{\mathrm{n}}^2 \boldsymbol{I}, \tag{A.10}$$

where the equation parameters are as described in Section 3.3. The main principle of the MUSIC algorithm is based on exploiting the eigenstructure of the covariance matrix $\boldsymbol{R}$. The following derivation of the MUSIC algorithm is borrowed from [4].

Eigendecomposition of R

Let $\lambda_1, \lambda_2, ..., \lambda_M$ be the eigenvalues of the $M \times M$ matrix $\boldsymbol{R}$ such that

$$|\boldsymbol{R} - \lambda_i \boldsymbol{I}| = 0 \quad \text{for} \ (1 \leq i \leq M). \tag{A.11}$$

Using Equation (A.10), Equation (A.11) can be rewritten as

$$|\boldsymbol{A}\boldsymbol{R}_{ss}\boldsymbol{A}^H + \sigma_{\mathrm{n}}^2\boldsymbol{I} - \lambda_i\boldsymbol{I}| = |\boldsymbol{A}\boldsymbol{R}_{ss}\boldsymbol{A}^H - (\lambda_i - \sigma_{\mathrm{n}}^2)\boldsymbol{I}| = 0. \tag{A.12}$$

Consequently, it can be seen that the eigenvalues of $\boldsymbol{A}\boldsymbol{R}_{ss}\boldsymbol{A}^H$ are

$$\psi_i = \lambda_i - \sigma_{\mathrm{n}}^2. \tag{A.13}$$

Matrix $\boldsymbol{A}$ has a full column rank since it is composed of linearly independent steering vectors and the signal covariance matrix $\boldsymbol{R}_{ss}$ is non-singular matrix as long as the incoming signals are not coherent. This guarantees that if the number of sources is fewer than the number of elements in the array, that is $N < M$, then the rank of the $M \times M$ matrix $\boldsymbol{A}\boldsymbol{R}_{ss}\boldsymbol{A}^H$ is equal to N, which is a positive semidefinite matrix. Since $\boldsymbol{A}\boldsymbol{R}_{ss}\boldsymbol{A}^H$ is of M dimension this creates a null space in the eigen-spectrum.

From linear algebra it is clear that $M - N$ of the eigenvalues, ψ_i, of $\boldsymbol{A}\boldsymbol{R}_{ss}\boldsymbol{A}^H$, are equal to zero, that is

$$\begin{aligned}\psi_i &= \chi_i + 0 \;\text{ for }\; i = 1, ..., M \\ &= \begin{cases} \chi_i + 0, & \text{for } \; i = 1, ..., N \\ 0, & \text{for } \; i = N+1, ..., M \end{cases}.\end{aligned} \tag{A.14}$$

From Equations (A.10) and (A.11), this too implies that $\boldsymbol{R}$ has $M - N$ eigenvalues identical to the noise variance σ_{n}^2, that is

$$\begin{aligned}\lambda_i &= \psi_i + \sigma_{\mathrm{n}}^2 \;\text{ for }\; i = 1, ..., M \\ &= \begin{cases} \psi_i + \sigma_{\mathrm{n}}^2, & \text{for } \; i = 1, ..., N \\ \sigma_{\mathrm{n}}^2, & \text{for } \; i = N+1, ..., M \end{cases}.\end{aligned} \tag{A.15}$$

If the eigenvalues of $\boldsymbol{R}$ are sorted in a descending order such that λ_1 is the largest eigenvalue and λ_M is the smallest eigenvalue, then the following holds

$$\lambda_{N+1}, ..., \lambda_M = \sigma_{\mathrm{n}}^2. \tag{A.16}$$

Estimation of number of incoming signals

Practically, the covariance matrix $\boldsymbol{R}$ is approximated by taking samples of the input data vector (see Equation (3.8)), this means that not all the $M - N$ eigenvalues corresponding to noise variance are exactly similar. Instead they occur as a closely spaced cluster where their spread has a variance that decreases with the increase in the number of samples taken. By using the multiplicity K of the smallest eigenvalue and the relation $M = N + K$, an estimate of the number of incident signals, $\hat{N}$, can be given by

$$\hat{N} = M - K. \tag{A.17}$$

Orthogonality of subspaces

The eigenvalue λ_i has a corresponding eigenvector $\boldsymbol{v}_i$ such that

$$(\boldsymbol{R} - \lambda_i \boldsymbol{I})\boldsymbol{v}_i = 0. \tag{A.18}$$

For the eigenvectors corresponding to $M-N$ smallest eigenvalues in Equation (A.16), Equation (A.18) becomes

$$(\boldsymbol{R} - \lambda_i \boldsymbol{I})\boldsymbol{v}_i = \boldsymbol{A}\boldsymbol{R}_{ss}\boldsymbol{A}^H\boldsymbol{v}_i + (\sigma_n^2\boldsymbol{I} - \sigma_n^2\boldsymbol{I})\boldsymbol{v}_i = 0, \tag{A.19}$$

hence

$$\boldsymbol{A}\boldsymbol{R}_{ss}\boldsymbol{A}^H\boldsymbol{v}_i = 0. \tag{A.20}$$

Since $\boldsymbol{A}$ is full rank and $\boldsymbol{R}_{ss}$ is nonsingular, the product $\boldsymbol{A}\boldsymbol{R}_{ss}$ cannot be equal to zero, for Equation (A.20) to be equal to zero it implies that

$$\boldsymbol{A}^H \boldsymbol{v}_i = 0 \tag{A.21a}$$

$$\begin{bmatrix} \boldsymbol{a}^H(\theta_1)\boldsymbol{v}_i \\ \boldsymbol{a}^H(\theta_2)\boldsymbol{v}_i \\ \vdots \\ \boldsymbol{a}^H(\theta_N)\boldsymbol{v}_i \end{bmatrix} = \begin{bmatrix} 0 \\ 0 \\ \vdots \\ 0 \end{bmatrix}. \tag{A.21b}$$

From Equation (A.21) it can be seen that the N steering vectors of matrix $\boldsymbol{A}$ are orthogonal to the eigenvectors corresponding to the $M-N$ smallest eigenvalues,

$$\{\boldsymbol{a}(\theta_1), ..., \boldsymbol{a}(\theta_N)\} \perp \{\boldsymbol{v}_{N+1}, ..., \boldsymbol{v}_M\}. \tag{A.22}$$

Important Observation

This means that the steering vectors associated with the incoming sources can be estimated by identifying steering vectors that are almost orthogonal to the eigenvectors corresponding to the eigenvalues of $\boldsymbol{R}$ which are nearly equivalent to σ_n^2.

From the above analysis, it can be seen that the eigenvectors of $\boldsymbol{R}$ belongs to either of the two orthogonal subspaces: these are the non-principal eigen subspace (*noise subspace*) and the principal eigen subspace (*signal subspace*). The DOA steering vectors form part of the signal subspace thus orthogonal to the noise subspace. An alternative proof is presented by Van Wyk in [83].

Search function and DOA estimation

The DOAs of the incoming signals are determined by locating steering vectors that are orthogonal to the noise subspace in a continuum of all possible steering vectors. Let the matrix containing the noise eigenvectors be

$$\boldsymbol{V}_{\mathrm{n}} = [\boldsymbol{v}_{N+1} \boldsymbol{v}_{N+2}, ..., \boldsymbol{v}_M] \tag{A.23}$$

Because the steering vectors corresponding to the DOAs of the incident signals are perpendicular to the noise subspace, then

$$\boldsymbol{a}^H(\theta)\boldsymbol{V}_{\mathrm{n}}\boldsymbol{V}_{\mathrm{n}}^H\boldsymbol{a}(\theta) = 0, \tag{A.24}$$

this is true for all θ corresponding to DOA of the incident signals. The θs are obtained by finding $\hat{N}$ largest peaks in the MUSIC spatial spectrum which is given by

$$P_{MUSIC}(\theta) = \frac{1}{\boldsymbol{a}^H(\theta)\boldsymbol{V}_{\mathrm{n}}\boldsymbol{V}_{\mathrm{n}}^H\boldsymbol{a}(\theta)} \tag{A.25}$$

or, alternatively

$$P_{MUSIC}(\theta) = \frac{\boldsymbol{a}^H(\theta)\boldsymbol{a}(\theta)}{\boldsymbol{a}^H(\theta)\boldsymbol{V}_{\mathrm{n}}\boldsymbol{V}_{\mathrm{n}}^H\boldsymbol{a}(\theta)}. \tag{A.26}$$

The peaks in the spectrum are generated as a result of the orthogonality between $\boldsymbol{a}(\theta)$ and $\boldsymbol{V}_n$ as indicated in Equation(A.24), which minimizes the denominator of the spatial spectrum.

Appendix B

MATLAB Codes

The following are MATLAB codes used in generating numerical simulation results presented in chapter 6.

```
%UNIVERSITY OF THE WITWATERSRAND, JOHANNESBURG SOUTH AFRICA
%Name: Frans Shiwovanhu Shafuda
%MSc in Engineering (field: Sensor Array Signal Processing)
%Date first created: 12 February 2017
% In this program we simulate CTOP and AVTOP decorrelation
    techniques with MUSIC for DOA estimation  of highly correlated (
    coherent) sources
close all
clc;
clear variables;
iteration=10;
for loop=1:iteration
%%%%%%%%%%% OBTAIN DATA COVARIANCE MATRIX %%%%%%%%%%%%%%%%%%%%
doa=[-40 30]/180*pi; %Direction of Arrival of incident signals
N=1024;%Number of Snapshots
f=[800000  800000]'; %Frequency Hz
w=2*pi*f; %frequency in radians
M=4; %Number of array elements
c=3e8; %speed of light in m/s
D=length(w); %The number of incident signal
lambda=c/max(w);%Compute average wavelength: Wavelength = c/w
```

```
d=lambda/2; %Element spacing, half of wavelength
snr=10; %Signal to Noise Ratio
A=zeros(D,M); %Form a matrix with D rows and M columns
for h=1:D
A(h,:)=exp(-1i*2*pi*d*sin(doa(h))/lambda*(0:M-1)); %steering matrix
end
A=A'; % MxD Array Steering Matrix
s=1*exp(1i*(w*(1:N))); %Simulate signal
xx=A*s;
xn=awgn(xx,snr);%add AWGN to data
Rxx=(xn*xn')/N; % MxM covarivance matrix of xn
%%%%%%%%%%%%%%%%%%%%%%%%%%%%%%%%%%%%%%%%%%%%%%%%%%%%%%%%%%%%%%%

%%%%%%%%%%%%%%%%%%% CLASSIC MUSIC ALGORITHM %%%%
[V0,Dia0]=eig(Rxx); %Find the eigenvalues and eigenvectors of  Rxx
[Dia0,Index0]=sort(diag(Dia0),1,'descend');%Sort the eigen values in descending order
V0=V0(:,Index0);%Sort the eigenvectors
V0s =V0(:,1:D);%Get signal eigenvectors
V0n=V0(:,D+1:M);%Get noise eigenvectors(associated with M-D smallest eigenvalues)
%%%%%%%%%%%%%%%%%%%%%%%%%%%%%%%%%%%%%%%%%%%%%%%%%%%%%%%%%

%%%%%CORRELATION TOEPLITZ (CTOP) MATRIX RECONSTRUCTION %%%
rc= Rxx(1,:);%row one of covariance matrix
RT= toeplitz(rc);%reconstructed Toeplitz matrix
[V1,Dia1]=eig(RT); %Find the eigenvalues and eigenvectors of  RT
[Dia1,Index1]=sort(diag(Dia1),1,'descend');%Sort the eigen values in descending order
V1=V1(:,Index1);%Sort the eigenvectors
V1s =V1(:,1:D);%Get signal eigenvectors
```

```
V1n=V1(:,D+1:M); %Get noise eigenvectors(associated with M-D smallest eigenvalues)
%%%%%%%%%%%%%%%%%%%%%%%%%%%%%%%%%%%%%%%%%%%%%%%%%%%%%%%%%%%%%%%

%%LOWER TRIANGLE AVERAGE TOEPLITZ (AVTOP) MATRIX RECONSTRUCTION %%
m=1;
k=1;
r= zeros(1,M); %Allocate size of vector to store averages of elements in each diagonal
for i =1:M
    m=i-k;
  r(i)=sum(diag(Rxx,m))/(max(size(diag(Rxx,m))));
  k=k+2;
end
% CONSTRUCT NEW TOEPLITZ MATRIX USING r
 RTav= toeplitz(r);
 RTr1=flip(RTav,1); %flip rows of RTav
 RTav1=flip(RTr1,2); %flip columns of RTav
[V2,Dia2]=eig(RTav1); %Find the eigenvalues and eigenvectors  RTav1
[Dia2,Index2]=sort(diag(Dia2),1,'descend');%Sort the eigen values in descending order
V2=V2(:,Index2);%Sort the eigenvectors to put signal eigenvectors first
V2s =V2(:,1:D);%Get signal eigenvectors
V2n=V2(:,D+1:M); %Get noise eigenvectors(associated with M-D smallest eigenvalues)
%%%%%%%%%%%%%%%%%%%%%%%%%%%%%%%%%%%%%%%%%%%%%%%%%%%%%%%%%%%%

theta=-90:90/1000:90; %Peak search
%GENERATE SPECTRUM SEARCH FOR CLASSIC MUSIC
Pmusic_spec0=zeros(length(theta),1);
```

```
for zz=1:length(theta)
Svec=zeros(1,length(M));%Create a steering vector to multiply the noise subspace
for yy=0:M-1
%Create a DOA search vector(continuum of all possible DOA)
Svec(1+yy)=exp(-1i*2*yy*pi*d*sin(theta(zz)/180*pi)/lambda);
end
Po0=Svec*(V0n*V0n')*Svec';%A single point in the spectrum
Pmusic_spec0(zz)=abs(1/ Po0);
end
%GENERATE SPECTRUM SEARCH FOR CTOP MUSIC
Pmusic_spec1=zeros(length(theta),1);
for zz=1:length(theta)
Svec=zeros(1,length(M));
for yy=0:M-1
%Create a DOA search vector(continuum of all possible DOA)
Svec(1+yy)=exp(-1i*2*yy*pi*d*sin(theta(zz)/180*pi)/lambda);
end
Po1=Svec*(V1n*V1n')*Svec';%A single point in the spectrum
Pmusic_spec1(zz)=abs(1/ Po1);
end
%GENERATE SPECTRUM SEARCH FOR AVTOP MUSIC
Pmusic_spec2=zeros(length(theta),1);
for zz=1:length(theta)
Svec=zeros(1,length(M));
for yy=0:M-1
%Create a DOA search vector(continuum of all possible DOA)
Svec(1+yy)=exp(-1i*2*yy*pi*d*sin(theta(zz)/180*pi)/lambda);
end
Po2=Svec*(V2n*V2n')*Svec';%A single point in the spectrum
Pmusic_spec2(zz)=abs(1/ Po2);
```

```
end
%Normalised Spatial spectrum function
Pmusic_spec0=(10*log10(Pmusic_spec0/max(Pmusic_spec0))); %CLASSIC
    MUSIC
Pmusic_spec1=(10*log10(Pmusic_spec1/max(Pmusic_spec1))); %CTOP MUSIC
Pmusic_spec2=(10*log10(Pmusic_spec2/max(Pmusic_spec2))); %AVTOP
    MUSIC
%Plot the spectra
axis([-100 100 -80 1])
plot(theta,Pmusic_spec0,'-k','linewidth',1.2)
hold on
plot(theta,Pmusic_spec1,'-b','linewidth',1.2)
hold on
plot(theta,Pmusic_spec2,'-r','linewidth',1.2)
ylabel('Spectrum function P(\theta) /dB')
xlabel('Angle \theta/degree')
title('Spatial Spectrum estimation-CTOP, AVTOP and CLASSIC MUSIC')
legend('CLASSIC MUSIC','CTOP MUSIC','AVTOP MUSIC','Location','
    SouthOutside')
grid on
end
```

References

[1] E. M. Al-Ardi, R. M. Shubair, and M. E. Al-Mualla, “Performance evaluation of direction finding algorithms for adapative antenna arrays,” in *Proceedings of the IEEE International Conference on Electronics, Circuits, and Systems*, vol. 2, 2003, pp. 735–738.

[2] P. Gupta and S. P. Kar, “MUSIC and improved MUSIC algorithm to estimate direction of arrival,” in *International Conference on Communication and Signal Processing (ICCSP)*, 2015, pp. 757–761.

[3] X. Yang, X. Wu, S. Li, and T. K. Sarkar, “A Fast and Robust DOA Estimation Method Based on JSVD for Co-Prime Array,” *IEEE Access*, vol. 6, pp. 41 697–41 705, 2018.

[4] J. C. Liberti and T. S. Rappaport, *Smart Antennas for Wireless Communications: IS-95 and Third Generation CDMA Applications*, illustrate ed. Prentice Hall PTR, 1999.

[5] R. Schmidt, “Multiple emitter location and signal parameter estimation,” *IEEE Transactions on Antennas and Propagation*, vol. 34, no. 3, pp. 276–280, 1986.

[6] A. J. Barabell, “Improving the resolution performance of eigenstructure-based direction-finding algorithms,” in *ICASSP ’83. IEEE International Conference on Acoustics, Speech, and Signal Processing*, vol. 8, 1983, pp. 336 – 339.

[7] R. Roy and T. Kailath, “ESPRIT-Estimation of signal parameters via rotational invariance techniques,” *EEE Transactions on Acoustics, Speech, and Signal Processing*, vol. 37, no. 7, pp. 984–995, 1989.

[8] J. Capon, "High resolution frequency-wavenumber spectrum analysis," in *Proc. of the IEEE*, vol. 57, no. 8, 1969, pp. 1408–1418.

[9] Y. Liao, A. Abouzaid, and R. April, "Resolution Improvement for MUSIC and ROOT MUSIC Algorithms," *Journal of Information Hiding and Multimedia Signal Processing*, vol. 6, no. 2, pp. 189–197, 2015.

[10] Y. Sun, Y. Kan, and W. Zhao, "Robust DOA estimation for coherent signals based on modified MUSIC algorithm," in *ICICIP 2012 - 3rd International Conference on Intelligent Control and Information Processing*, 2012, pp. 31–35.

[11] C. Sun and Y.-x. Yang, "On beampattern design for beamspace music," *Acoustical Science and Technology*, vol. 25, no. 1, pp. 2–8, 2004.

[12] A. Govinda Raj and J. H. McClellan, "Single Snapshot Super-Resolution DOA Estimation for Arbitrary Array Geometries," *IEEE Signal Processing Letters*, vol. 26, no. 1, pp. 119–123, 2018.

[13] C. Qian, L. Huang, W. J. Zeng, and H. C. So, "Direction-of-arrival estimation for coherent signals without knowledge of source number," *IEEE Sensors Journal*, vol. 14, no. 9, pp. 3267–3273, 2014.

[14] Y. Yang, C. Wan, C. Sun, and Q. Wang, "DOA estimation for coherent sources in beamspace using spatial smoothing," in *ICICS-PCM 2003 - Proceedings of the 2003 Joint Conference of the 4th International Conference on Information, Communications and Signal Processing and 4th Pacific-Rim Conference on Multimedia*, vol. 2, 2003, pp. 1028–1032.

[15] H. Li, Y. He, R. Yang, and J. Guan, "Beamspace based DOA estimation methods of coherent sources in the presence of impulsive noise," in *International Conference on Signal Processing Proceedings, ICSP*, vol. 4, 2006.

[16] Q. Chen and R. Liu, "On the explanation of spatial smoothing in MUSIC algorithm for coherent sources," in *International Conference on Information Science and Technology, ICIST 2011*, 2011, pp. 699–702.

[17] S. Changgan and L. Yumin, "An Improved Forward / backward Spatial Smoothing Root-MUSIC Algorithm Based on Signal Decorrelation," in *IEEE Workshop on Advanced Research and Technology in Industry Applications*, 2014, pp. 1252–1255.

[18] G. T. Pham, P. Loubaton, and P. Vallet, "Performance analysis of spatial smoothing schemes in the context of large arrays," *IEEE Transactions on Signal Processing*, vol. 64, no. 1, pp. 160–172, 2016.

[19] M. Wang and B. Xiao, "Separation of cogerent multi-path signals with improved MUSIC algorithm," in *Proceedings - 2011 International Conference on Computational and Information Sciences, ICCIS 2011*, 2011, pp. 992–995.

[20] X. Q. Hu, J. W. Chen, H. Chen, and Y. L. Wang, "Estimation DOAs of the coherent sources based on Toeplitz decorrelation," in *Proceedings - 1st International Congress on Image and Signal Processing, CISP 2008*, vol. 5, 2008, pp. 54–58.

[21] X. Zhang, X. Liu, H. Yu, and C. Liu, "Improved MUSIC algorithm for DOA estimation of coherent signals via Toeplitz and fourth-order-cumulants," *International Journal of Control and Automation*, vol. 8, no. 10, pp. 261–272, 2015.

[22] A. Goian, M. I. Alhajri, R. M. Shubair, L. Weruaga, A. R. Kulaib, R. Almemari, and M. Darweesh, "Fast detection of coherent signals using pre-conditioned root-MUSIC based on Toeplitz matrix reconstruction," in *2015 IEEE 11th International Conference on Wireless and Mobile Computing, Networking and Communications, WiMob 2015*, 2015, pp. 168–174.

[23] J. Bai, X. Shen, H. Wang, and Y. Liu, "Improved Toeplitz Algorithms to Coherent Sources DOA Estimation," in *2010 International Conference on Measuring Technology and Mechatronics Automation*, vol. 2, 2010, pp. 442–445.

[24] R. O. Schmidt, "A signal subspace approach to multiple emitter location and spectral estimation," Ph.D. dissertation, Stanford University, Stanford, CA, 1981.

[25] G. Bienvenu, "Influence of the Spatial Coherence of the Background Noise on," in *Proceedings of the International Conference on Acoustics, Speech, and Signal Processing*, vol. 4. Washington, DC: IEEE, 1979, pp. 306–309.

[26] A. Paulraj and T. Kailath, "Eigenstructure Methods for Direction of Arrival Estimation in the Presence of Unknown Noise Fields," *IEEE Transactions on Acoustics, Speech, and Signal Processing*, vol. 34, no. 1, pp. 13–20, 1986.

[27] A. Paulraj, B. Ottersten, R. Roy, A. Swindlehurst, G. X, and T. Kailath, "Subspace Methods for Directions-of-Arrival Estimation," *Handbook of Statistics*, vol. 10, pp. 693–739, 1993.

[28] W. A. Gardner, "Simplification of MUSIC and ESPRIT by Exploitation of Cyclostationarity," *Proceedings of the IEEE*, vol. 76, no. 7, pp. 845–847, 1988.

[29] D. W. Tufts and R. Kumaresan, "Estimating the angle of arrival of multiple plane waves," *IEEE Transactions on Aerospace and Electronic Systems*, vol. 19, no. 1, pp. 134–139, 1983.

[30] M. Zeytinoglu, J. Litva, and J. Qian, "High-resolution direction finding using circular arrays," in *1991 IEEE Int. Conf. Acoust., Speech, and Signal Process. (ICASSP)*, vol. 5, 1991, pp. 3341–3344.

[31] T. Huang and A. Mohan, "Effects of array mutual coupling on near-field DOA estimation," in *CCECE 2003 - Canadian Conference on Electrical and Computer Engineering. Toward a Caring and Humane Technology*, vol. 3, 2003, pp. 1881–1884.

[32] T. T. Zhang, Y. L. Lu, and H. T. Hui, "Compensation for the mutual coupling effect in uniform circular arrays for 2D DOA estimations employing the maximum likelihood technique," *IEEE Transactions on Aerospace and Electronic Systems*, vol. 44, no. 3, pp. 1215–1221, 2008.

[33] I. J. Gupta and A. A. Ksienski, “Effect of mutual coupling on the performance of adaptive arrays,” *Adaptive Antennas for Wireless Communications*, vol. 31, no. 5, pp. 785–791, 2009.

[34] A. M. Elbir, “Direction Finding in the Presence of Direction-Dependent Mutual Coupling,” *IEEE Antennas and Wireless Propagation Letters*, vol. 16, pp. 1541–1544, 2017.

[35] Z. Chen, G. Gokeda, and Y. Yu, *Introduction to Direction-of-arrival Estimation.* Norwood: Artech House, 2010.

[36] A. M. Elbir, “Direction finding in the presence of array imperfections, model mismatches and multipath,” Ph.D Dissertation, Middle East Technical University (METU), 2016.

[37] H. Shi, W. Leng, A. Wang, and T. Guo, “DOA estimation for mixed uncorrelated and coherent sources in multipath environment,” *International Journal of Antennas and Propagation*, vol. 2015, p. 8, 2015.

[38] E. M. Al-Ardi, R. M. Shubair, and M. E. Al-Mualla, “Direction of arrival estimation in a multipath environment: An overview and a new contribution,” *Applied Computational Electromagnetics Society Journal*, vol. 21, no. 3, pp. 226–238, 2006.

[39] J. E. Evans, J. R. Johnson, and D. F. Sun, “Applications of Advanced Signal Processing Techniques to Angle of Arrival Estimation in ATC Navigation and Surveillance System,” Lincoln Laboratory, MIT, Lexington, MA, Tech. Rep. June, 1982.

[40] T.-j. Shan, M. Wax, and T. Kailath, “On Spatial Smoothing for Direction-of-Arrival Estimation of Coherent Signals,” *IEEE Transactions on Acoustics, Speech, and Signal Processing*, vol. 33, no. 4, pp. 806–811, 1985.

[41] S. Unnikrishna Pillai and B. H. Kwon, “Forward/Backward Spatial Smoothing Techniques For Coherent Signal Identification,” *IEEE Transactions on Acoustics, Speech, and Signal Processing*, vol. 37, no. 1, pp. 8–15, 1989.

[42] A. Abu, “An improved spatial smoothing technique for DoA estimation of highly correlated signals,” *Engineering Letters*, vol. 19, no. 1, 2011.

[43] I. K. Rhee and H. S. Kim, “Improved DOA estimation of correlated signals in correlated antenna noises environment,” in *International Conference on Information Networking*, 2013, pp. 66–70.

[44] S.-W. Gao and Z. Bao, “Data-based matrix decomposition technique for high-resolution array processing of coherent signals,” *Electronics Letters*, vol. 23, no. 12, pp. 643–645, 1987.

[45] H. Sun, J. Guo, and L. Fang, “Improved Singular Value Decomposition (TopSVD) for Source Number Estimation of Low SNR in Blind Source Separation,” *IEEE Access*, vol. 5, pp. 26 460–26 465, 2017.

[46] L. Zhou and D. Huang, “A new ESPRIT algorithm based on Toeplitz method for coherent signals,” in *Proceedings 2011 International Conference on Transportation, Mechanical, and Electrical Engineering, TMEE 2011*, 2011, pp. 1521–1524.

[47] W. Xu, “Signal Directional-of-Arrival and Amplitude Estimation for Multiple-Row Bathymetric Sidescan Sonars,” Masters dissertation, Massachesetts Institute of Technology & Woods Hole Oceanographic Institution, 1998.

[48] M. A. Masnadi-Shirazi, C. De Moustier, P. Cervenka, and S. H. Zisk, “Differential Phase Estimation with the SeaMARC II Bathymetric Sidescan Sonar System,” *IEEE Journal of Oceanic Engineering*, vol. 17, no. 3, pp. 239–251, 1992.

[49] C. Hui, H. Benxiong, D. Bin, and H. Yaoqin, “A modified toeplitz algorithm for doa estimation of coherent signals,” in *2007 International Symposium on Intelligent Signal Processing and Communications Systems, ISPACS 2007 - Proceedings*, vol. 2, 2007, pp. 80–83.

[50] F. M. Han and X. D. Zhang, "An ESPRIT-like algorithm for coherent DOA estimation," *IEEE Antennas and Wireless Propagation Letters*, vol. 4, no. 1, pp. 443–446, 2005.

[51] H. Chen, C. P. Hou, Q. Wang, L. Huang, and W. Q. Yan, "Cumulants-based toeplitz matrices reconstruction method for 2-D coherent DOA estimation," *IEEE Sensors Journal*, vol. 14, no. 8, pp. 2824–2832, 2014.

[52] D. Li, C. Dong, and J. Huang, "A study on the application of Toeplitz Approximation Method on DOA estimation," in *2010 2nd International Conference on Signal Processing Systems*, vol. 3, 2010, pp. 215–218.

[53] Y. Han, B. Cao, W. Dong, Q. Fang, and W. Zhang, "An improved mode-music algorithm for DOA estimation of coherent sources based on hybrid array," in *International Conference on Signal Processing Proceedings, ICSP*, 2014, pp. 358–362.

[54] W. Si, X. Li, and N. Wu, "2-D DOA estimation of improved Toeplitz algorithms to coherent sources," in *Proceedings of the 2012 2nd International Conference on Instrumentation and Measurement, Computer, Communication and Control, IMCCC 2012*, 2012, pp. 1251–1254.

[55] X. Wu, W. P. Zhu, and J. Yan, "A Toeplitz Covariance Matrix Reconstruction Approach for Direction-of-Arrival Estimation," *IEEE Transactions on Vehicular Technology*, vol. 66, no. 9, pp. 8223–8237, 2017.

[56] S. U. Pillai and H. B. Kwon, "New resolution threshold results in three source scenes," in *Twenty-Third Asilomar Conference on Signals, Systems and Computers, 1989.*, vol. 2, 1989, pp. 772 – 776.

[57] B. Friedlander, "A Sensitivity Analysis of the MUSIC Algorithm," *IEEE Transactions on Acoustics, Speech, and Signal Processing*, vol. 38, no. 10, pp. 1740–1751, 1990.

[58] A. Ferréol, P. Larzabal, and M. Viberg, "On the asymptotic performance analysis of subspace DOA estimation in the presence of modeling errors: Case

of MUSIC," *IEEE Transactions on Signal Processing*, vol. 54, no. 3, pp. 907–920, 2006.

[59] J. D. Lin, W. H. Fang, and C. H. Lin, "Further results of the analysis of the MUSIC for closely spaced, non-equal power plane waves," in *ICASSP, IEEE International Conference on Acoustics, Speech and Signal Processing - Proceedings*, vol. 3, 2007, pp. 809–812.

[60] R. T. Suryaprakash and R. R. Nadakuditi, "Consistency and MSE Performance of MUSIC-Based DOA of a Single Source in White Noise With Randomly Missing Data," *IEEE Transactions on Signal Processing*, vol. 63, no. 18, pp. 4756–4770, 2015.

[61] J. Steinwandt, F. Roemer, and M. Haardt, "Second-Order Performance Analysis of Standard Esprit," in *Acoustics, Speech and Signal Processing (ICASSP), 2017 IEEE International Conference on*, 2017, pp. 3051–3055.

[62] W. Mianzhi and A. Nehorai, "Coarrays, MUSIC, and the Cram´er-Rao Bound," *IEEE Transactions on Signal Processing*, vol. 65, no. 4, pp. 933 – 946, 2017.

[63] A. J. Fenn, *Adaptive Antennas and Phased Arrays for Radar and Communications*, illustrate ed. Artech House, 2007.

[64] C. A. Balanis, *Antenna Theory: Analysis and Design*, illustrate ed. John Wiley & Sons, 2016.

[65] R. J. Mailloux, *Phased Array Antenna Handbook*, 2nd ed. Artech House, 2005.

[66] H. Tang, "DOA Estimation Based on Music Algorithm," Ph.D. dissertation, 2014.

[67] D. J. Yeom, S. H. Park, J. R. Kim, and M. J. Lee, "Performance analysis of beamspace MUSIC with beamforming angle," in *2014, 8th International Conference on Signal Processing and Communication Systems, (ICSPCS)-Proceedings*, 2014, pp. 1–5.

[68] D. Potts, M. Tasche, and T. Volkmer, "Efficient Spectral Estimation by MUSIC and ESPRIT with Application to Sparse FFT," *Frontiers in Applied Mathematics and Statistics*, vol. 2, no. 1, 2016.

[69] P. Stoica and R. Moses, *Spectral Analysis of Signals*. New Jersey: Prentice Hall, 2005.

[70] W. Liao and A. Fannjiang, "MUSIC for single-snapshot spectral estimation: Stability and super-resolution," *Applied and Computational Harmonic Analysis*, vol. 40, pp. 33–67, 2016.

[71] S. Marple and C. Marino, "Coherence in signal processing: a fundamental redefinition," in *Conference Record of the Thirty-Eighth Asilomar Conference on Signals, Systems and Computers*, vol. 1, 2004, pp. 1035–1038.

[72] W. A. Gardner, "A unifying view of coherence in signal processing," *Signal Processing*, vol. 29, no. 2, pp. 113–140, 1992.

[73] W. He, Z. Fan, Z. Li, and S. Li, "Study of improved multiple signal classification algorithm based on coherent signal sources," in *World Automation Congress Proceedings*. TSI Enterprise Inc (TSI Press), 2016, pp. 1–4.

[74] Agilent Technologies, "Signal Source Solutions for Coherent and Phase Stable Multi-Channel Systems Application Note," Agilent Technologies, Inc, Tech. Rep., 2010.

[75] G. V. Serebryakov, "Direction-of-Arrival Estimation of Correlated Sources by Adaptive Beamforming," *IEEE Transactions on Signal Processing*, vol. 43, no. 11, pp. 2782–2787, 1995.

[76] H. Jiang and S. Wang, "Fourth-order cyclic cumulant TLS-ESPRIT algorithm to estimate direction of cyclostationary coherent sources," in *Proceedings of 2003 International Conference on Neural Networks and Signal Processing, ICNNSP'03*, vol. 2, 2003, pp. 1330–1333.

[77] T.-J. Shan and T. Kailath, "Adaptive beamforming for coherent signals and interference," *IEEE Transactions on Acoustics, Speech, and Signal Processing*, vol. 33, no. 3, pp. 527–536, 1985.

[78] L. Wan, G. Han, L. Shu, S. Chan, and T. Zhu, "The Application of DOA Estimation Approach in Patient Tracking Systems with High Patient Density," *IEEE Transactions on Industrial Informatics*, vol. PP, no. 99, pp. 1–1, 2016.

[79] Q. Wang, H. Chen, G. Zhao, B. Chen, and P. Wang, "An improved direction finding algorithm based on toeplitz approximation," *Sensors*, vol. 13, pp. 746–757, 2013.

[80] S. S. Haykin, *Adaptive Filter Theory : International Edition*, 5th ed. Pearson Education Limited, 2014.

[81] D. S. Watkins, *Fundamentals of Matrix Computations*, 2nd ed. John Wiley & Sons, 2004.

[82] G. Strang, *Linear Algebra and its Applications*, 4th ed. Thomson, Brooks/-Cole, 2006.

[83] M. A. van Wyk, "Super-Resolution Techniques," Johannesburg, pp. 1–6.